LA-13721-T
Thesis

The Chain-Length Distribution in Subcritical Systems

Los Alamos
NATIONAL LABORATORY

Los Alamos National Laboratory is operated by the University of California for the United States Department of Energy under contract W-7405-ENG-36.

This thesis was accepted by the Department of Nuclear Engineering, Texas A & M University, College Station, Texas, in partial fulfillment of the requirements for the degree of Doctor of Philosophy. The text and illustrations are the independent work of the author and only the front matter has been edited by the CIC-1 Writing and Editing Staff to conform with Department of Energy and Los Alamos National Laboratory publication policies.

An Affirmative Action/Equal Opportunity Employer

LA-13721-T
Thesis

Issued: June 2000

The Chain-Length Distribution in Subcritical Systems

Steven Douglas Nolen

Los Alamos
NATIONAL LABORATORY
Los Alamos, New Mexico 87545

ACKNOWLEDGMENTS

This research reflects the efforts and impact of many individuals. The author would like to thank Dr. Theodore Parish for serving as the committee chair, and moreover, for his understanding, support, and constant encouragement throughout this research. The author would also like to express sincere appreciation to Dr. Gregory Spriggs of the Los Alamos National Laboratory for serving as the principal advisor to this dissertation. His infectious vision and vast experience with subcritical experiments at the LANL Pajarito site have made this research a continually rewarding and informative process. I would also like to thank the other members of my committee, Drs. Marvin Adams, Yassin Hassan, Dante DeBlassie and Paulette Beatty for their commitment of time and energy.

I would like to thank a number of people at Los Alamos National Laboratory who contributed to this dissertation. First, I would like to thank each of the many group leaders that have lent their support. I am profoundly grateful to Stephen Lee who first envisioned *MC++*, who taught me *C++*, and who encouraged me to take the long, hard road to a Ph.D. I am also grateful for the Monte Carlo knowledge obtained during numerous conversations with Dr. Art Forster and Dr. Forrest Brown. I would like to thank Julian Cummings and the Blanca code team for their advice and assistance in working out the technical details of a production code.

Dr. Bob Busch at the University of New Mexico also has my appreciation for providing access to their university's AGN reactor.

A special thanks goes to my colleagues and peers at the laboratory including Chris Gesh, Kelly Thompson, Jon Dahl, and David Court. In addition to their unswerving friendship and encouragement, I have benefited from their example proving that this graduate degree can be achieved.

I am truly grateful for the love and support of my entire family. My parents, Cecil and Lynette, have always stood by me, trusted me, and provided a home with unconditional love. My sister and brother-in-law, Cindy and Alan, have always had an open door for me even during the tough times. They were there many times with my nephew and niece, Jarrett and Connor, to give me a break and a smile. My brother, Greg, was probably my closest supporter and confidant. I can never thank him enough for running the numerous errands when I was away from campus and for the solid support I found in him. April's parents, Dick and Judy, provided some much needed financial support and some even more needed encouragement that comes from experience. My wife, April, I mention last though she has been through the most. Her ability to adapt and press on during these years still amazes me. In the midst of it all, she still found time to impact peoples' lives for Christ, and mine was not the least.

My final and most ardent thanks belongs to my Lord and Savior, Christ, who has been my comfort and compass.

TABLE OF CONTENTS

Page

CHAPTER Page

LIST OF FIGURES

FIGURE Page

FIGURE Page

FIGURE Page

LIST OF TABLES

ABSTRACT

The Chain-Length Distribution in Subcritical Systems. (May 2000)

Steven Douglas Nolen, B.S., Texas A&M University;

M.S., Texas A&M University

Chair of Advisory Committee: Dr. Theodore Parish

The individual fission chains that appear in any neutron multiplying system provide a means, via neutron noise analysis, to unlock a wealth of information regarding the nature of the system. This work begins by determining the probability density distributions for fission chain lengths in zero-dimensional systems over a range of prompt neutron multiplication constant (K) values. This section is followed by showing how the integral representation of the chain-length distribution can be used to obtain an estimate of the system's subcritical prompt multiplication (M_P). The lifetime of the chains is then used to provide a basis for determining whether a neutron noise analysis will be successful in assessing the neutron multiplication constant, k, of the system in the presence of a strong intrinsic source. A Monte Carlo transport code, *MC++*, is used to model the evolution of the individual fission chains and to determine how they are influenced by spatial effects. The dissertation concludes by demonstrating how experimental validation of certain global system parameters by neutron noise analysis may be precluded in situations in which the system K is relatively low and in which realistic detector efficiencies are simulated.

CHAPTER I

INTRODUCTION

Criticality safety is vitally important in the nuclear industry. If there were any doubts about this, these should have disappeared after the accident in Tokai-mura, Japan last year.[1] On September 30, 1999, three workers were seriously injured when they inadvertently created a super-critical configuration of uranyl nitrate solution at a fuel-reprocessing plant. As with any industrial process, there are always some associated risks in the nuclear industry, but these risks can be minimized with continued research and development in the area of operational safety. This assertion is particularly valid in the field of criticality safety where there has been an obvious need to develop accurate and reliable techniques to provide continuous monitoring of the subcriticality of nuclear processing and storage facilities. These types of monitoring systems differ from the current criticality alarm systems found in most plants that trip at setpoints that indicate that criticality has already occurred. Had a continuous monitoring system been in place in Tokai-mura rather than a criticality alarm system, this accident might have been averted.

Presently, there are several techniques for measuring the effective neutron multiplication constant, k, in reactor systems operating near delayed critical. However, as systems become more and more subcritical, only a few of these techniques are general enough that they can be adapted to perform *in-situ* subcriticality measurements in

[1] This dissertation follows the style and format of *Nuclear Science and Engineering*.

process and storage facilities. Of these techniques, neutron noise analysis is certainly an attractive option. For highly subcritical systems, however, the neutron noise signal becomes complex, and its interpretation becomes somewhat more difficult. Accordingly, a better understanding of neutron noise techniques and their relation to important system parameters, such as k, is needed to increase our ability to accurately unfold signals from subcritical systems. Armed with additional understanding, it may be possible to develop new monitoring systems that will provide nuclear workers with early warning systems if criticality safety limits are being approached.

Traditionally, two distinct research areas have carried the label *neutron noise analysis*. The first of these deals with observing fluctuations in a reactor's power level and correlating these changes with naturally occurring or mechanically induced physical disturbances occurring elsewhere in the reactor system. Examples of such disturbances include the growth and collapse of bubbles in the core of a boiling water reactor, the opening and closing of a relief valve, or the rotation of a special rod oscillator at some prescribed frequency. Unlike that due to the stochastic nature of individual prompt fission chains, this type of neutron noise is inherently deterministic with respect to the response of the neutron population. While it will not receive further attention here, there are a number of books on power reactor noise theory by Thie and others.[2,3]

The second type of research termed *neutron noise analysis* deals with the observation of individual prompt fission chains and the correlation of the resulting microscopic fluctuations of the neutron population with physical parameters of the system. This type of neutron noise analysis was first performed by researchers at the

Los Alamos National Laboratory (LANL) while experimenting with zero-power, critical-mass assemblies.[4-8] They noted that the neutron leakage flux exhibited larger-than-expected random fluctuations. Bruno Rossi proposed that these fluctuations corresponded to sharp changes in the neutron population as individual prompt fission chains spawned and then died-out on a time scale characterized by the neutron lifetime of the system.[8] In systems in which the mean time between source neutron births is significantly greater than the average life span of a prompt fission chain, the neutrons in the system appear in brief bursts, or *clumps*. As these clumps of neutrons die-out, the neutron population temporarily dips to zero until another prompt fission chain begins to spawn. The analysis of the observed statistical fluctuations in the neutron population has been explored by a number of researchers.[9-15] An example of the clumping phenomena is illustrated in Figure 1 which shows the neutron reaction rate as the number of observed events that occur within 0.125 μsec. wide intervals.

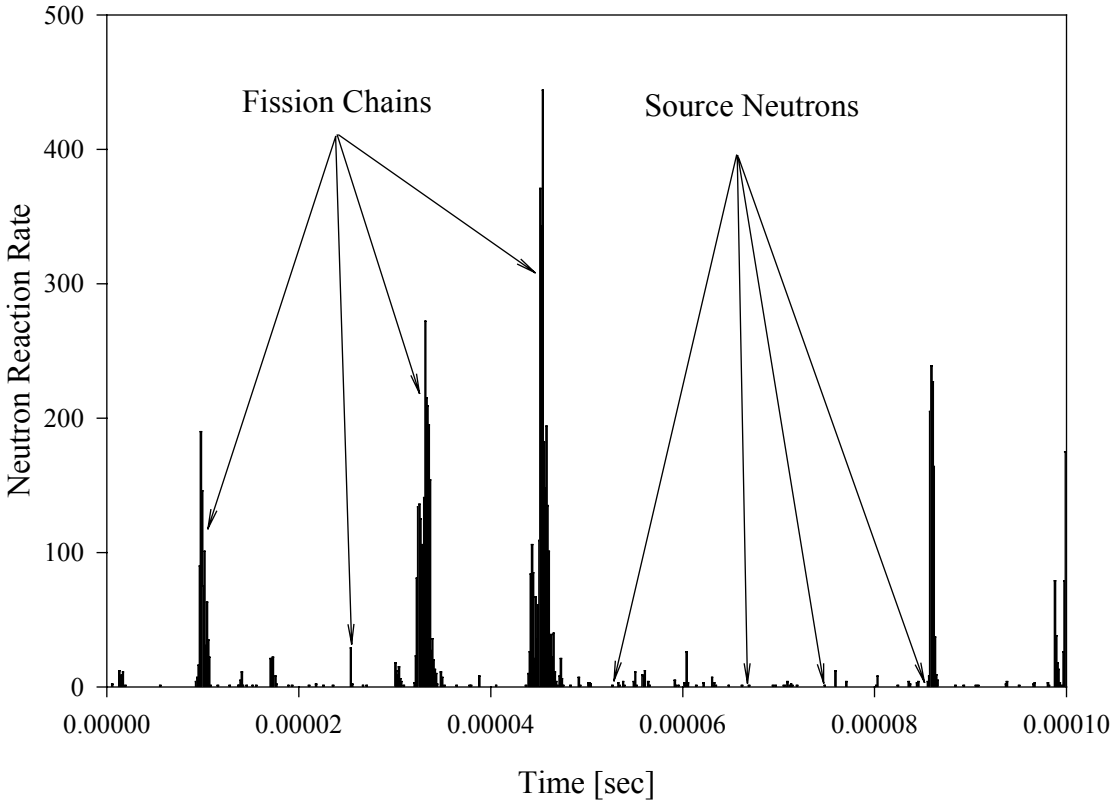

Figure 1. Example of prompt fission chains.

In this example, note that the neutron population is zero for a significant portion of the time. The exact length of time over which the population is zero depends highly on the strength of the driving source, the prompt neutron multiplication factor, K, and the prompt neutron lifetime, τ. The prompt neutron multiplication factor is defined as

$$K = k_{eff}\left(1-\beta_{eff}\right) \quad ,$$

where k_{eff} is the effective neutron multiplication factor and β_{eff} is the effective delayed neutron fraction. The zero-population intervals are quite evident in the bare, metal Godiva assembly because of its very short neutron lifetime. If the assembly is driven

only by its weak intrinsic neutron source (i.e. about 100 n/s) and is operating at 10 cents below delayed critical (i.e., $K=0.99274$), the neutron population in the assembly is zero for over 99.997% of the time. Even for thermal neutron systems operating under similar conditions, the percentage of time during which there are no neutrons in the system can be quite significant. For example, in an AGN reactor, which is driven by a weak intrinsic source of about 75 n/s, the probability of having zero neutrons in the system at any instant of time is 66% while operating at 10 cents subcritical.

The stochastic behavior of the fission chains gives rise to a wildly fluctuating neutron population that is clearly evident in subcritical or zero-power reactors, such as the Los Alamos Low Power Water Boiler (LOPO). In systems in which the neutron source rate is high relative to the neutron lifetime in the system, individual prompt fission chains cannot be readily observed since there are a large number of co-existing, or overlapping, chains.[16] In low-power or zero-power systems containing weak neutron sources, however, most individual prompt fission chains are separated in time and can be readily observed. This is the type of neutron noise that will be examined in this dissertation, using the chain-length distribution as the primary means of characterizing their impact.

In particular, the purpose of this dissertation is to investigate the basic underlying phenomenon of neutron noise in subcritical multiplying systems by examining the chain-length distribution of prompt fission chains. Numerical results are presented for this distribution based on both a highly idealized, one-energy, point reactor model as well as for a full energy-, angular-, and spatially-dependent Monte Carlo model. Some previous

work in this area has been preformed by Mihalczo et al. using KENO-NR in which they calculated the chain-length distribution for a BWR operating at a $k=0.9$.[17,18] The aim of this dissertation is to extend this work by increasing the resolution of the chain-length distribution and by examining a K range from 0.3 to 0.999. Results will also be present for the chain-length distributions produced by a variety of neutron source distributions and including various spatial effects that occur in single and multi-region systems. Moreover, the role of the overall detector efficiency in neutron noise measurements will be examined to demonstrate how low detector efficiencies can preclude the accurate estimation of system parameters when using neutron noise-based techniques in highly subcritical systems.

CHAPTER II

THEORY

In this chapter, the fundamental concepts of neutron noise theory are presented beginning with the definition of a fission chain and a demonstration of how it characterizes the behavior of a neutron multiplying system. Next, the chain-length distribution is introduced and a description is provided on how the neutron multiplicity and the source distribution determine its form. The introduction of the chain-length distribution concept is followed by a mathematical representation of the noise problem based on a point kinetics model. Finally, the chapter concludes by showing how neutron noise can be used to reveal some global parameters that characterize the subcritical neutron multiplying system.

A. Definition of a Fission Chain

The term *fission chain* refers to any neutrons that appear in a system that are related to a common ancestor or initiating source neutron. In determining the total number of neutrons in a chain, only the source neutron and the *prompt* fission neutrons are considered. In a multiplying system, the source neutrons originate in a variety of ways including: 1) external sources (i.e., special reactor components such as Pu-Be startup sources), 2) intrinsic sources, where the neutrons are emitted from spontaneous fission events occurring randomly throughout the nuclear fuel, and 3) delayed neutron sources that arise from the radioactive decay of certain fission products. Although delayed neutron precursors are generated from fission events that occur as a part of a

fission chain, the delayed neutrons are treated as a separate part of the total source since the time constants associated with their appearance are significantly greater than the average lifetime of a prompt neutron. For instance, the lifetime of a prompt neutron generally ranges from a few milliseconds to as long as few microseconds depending on the type of system. In contrast, the mean lifetimes of the delayed neutron precursors range from milliseconds to over a minute with the average being around 12 seconds. Within the context of the definition used here, fission chain neutrons are comprised entirely of fission neutrons that appear (for practical purposes) simultaneously with a fission event and that interact on a time scale characterized by the prompt neutron lifetime of the system.

In a very general sense, every fission chain is unique. In a neutron multiplying system, three factors contribute to this uniqueness. The first factor is the randomness associated with the specific number of neutrons emitted as a result of each fission event. This number can vary from 0 to 7 or more in accordance with a neutron number distribution, P_ν, for a given isotope. This distribution, or *multiplicity* as it is sometimes referred to, has been measured experimentally for many fissionable isotopes, and has been expressed in various empirical correlations.[19-27] The exact number of neutrons released in any fission event varies from fission to fission, even when the fissions occur under identical circumstances. Consequently, even fission chains that have the same number of fission events can have vastly different neutron productions.

Another factor that contributes to the randomness of the chain behavior is the neutron lifetime, τ. The neutron lifetime represents the average time that a neutron

exists before it undergoes some event that removes it from the system (i.e., an absorption or leakage). Similarly to the randomness in the number of neutrons emitted per fission, the actual time between removal events varies even for neutrons with identical starting conditions. The exact time of removal is distributed exponentially in time,

$$p(t)\,dt = e^{-\frac{t}{\tau}}\frac{dt}{\tau} \quad ,$$

where τ is the neutron removal lifetime, and $p(t)\,dt$ is the probability that a neutron will survive until time, *t*, and then be removed from the system in the time interval *dt* about *t*.

The final factor that contributes to the randomness of the chain behavior is the probability that an event of a particular type will occur. In any neutron multiplying system, a neutron can interact with surrounding medium by means of a large number of nuclear reactions. These include fission, parasitic absorption, elastic and inelastic scattering, leakage, and so forth. For this research, the probability for causing a fission event, P_f, is the most important.

Because of these three random factors, it is impossible to predict the exact behavior of any given fission chain. Nevertheless, when a large number of chains are sampled, the aggregate behavior of the fission chains becomes quite predictable. This situation is analogous to the rolling of a single die. It is impossible to predict which number will appear on any given roll, but, on an average, it is possible to show that each number has an equal probability of $1/6^{th}$ for appearing. Similarly, neutron noise theory is based on predicting the average behavior of a large number of individual, random chains.

To further understand the concept of a fission chain and its inherent randomness, a detector's response to a neutron multiplying system has been simulated for a small interval of time. These results are shown in Figure 2. The prompt neutron multiplication factor, *K*, for this system was 0.99, which in accordance with the source multiplication equation,

$$M_p = \frac{1}{1-K} \quad , \tag{II.1}$$

yields a prompt subcritical multiplication, M_p, of 100. For this simulation, 100 source neutrons were randomly put into the system at a rate of $5 \cdot 10^5 \, n/\text{sec}$. The source neutrons then spawned several fission chains producing a total of 6,934 fission neutrons over a simulated run time of about 0.2 msec. When divided into equal channel widths of 1 μsec, the average number of reactions appearing per channel was calculated to be 34.82. However, because of the tight groupings of the neutrons within the fission chains, most of the channels recorded zero events. In fact, the majority of the observed events (roughly 80% of the total counts over the counting interval) came from a single fission chain, which only lasted about ~13 μsec. This illustrates what the Los Alamos researchers observed as fluctuations in the neutron intensity.[4]

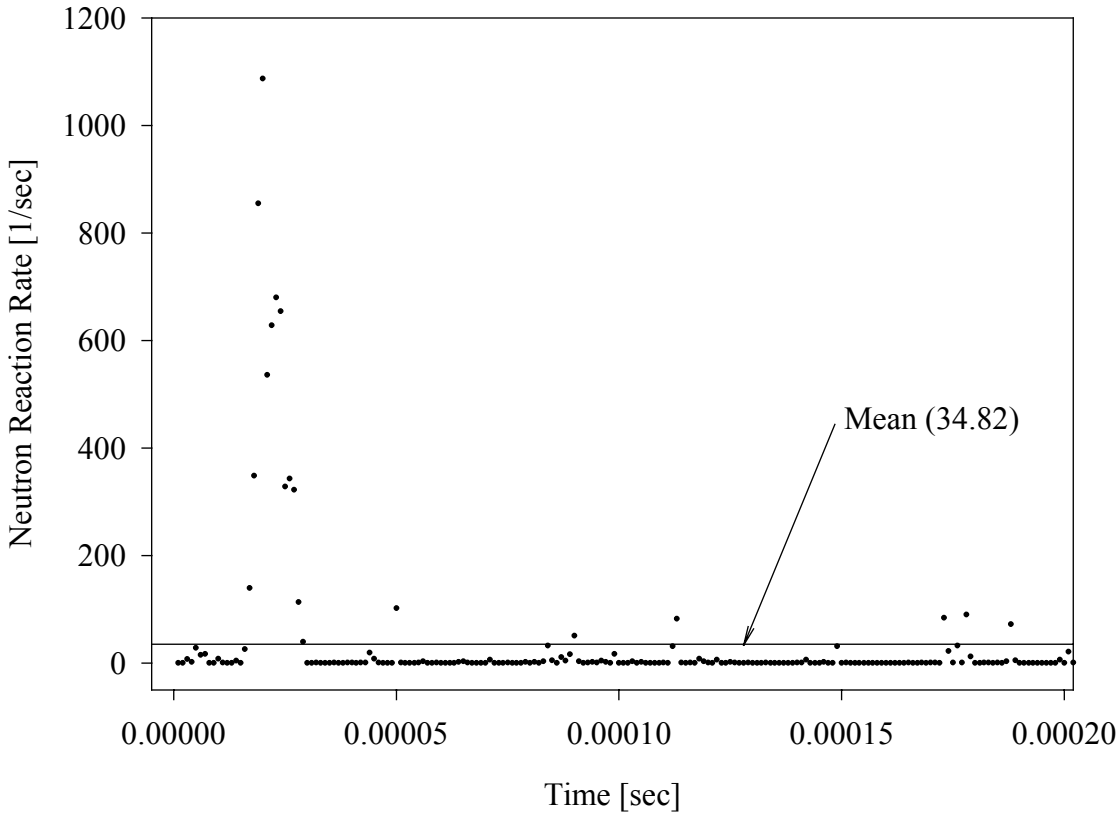

Figure 2. Neutron activity vs. time in a multiplying system.

For comparison, the neutron activity in a non-multiplying system over an identical time interval has also been simulated. Because there are no fissions occurring in this system, the fixed-source used in this simulation was increased to achieve the same average count rate as in the previous example. Otherwise, the sources are identical in behavior. Both simulate an intrinsic neutron source, which is often characterized by a time constant, λ, or a half-life, $T_{1/2}$ because the neutrons are produced in nuclear decay processes. The results for the non-multiplying system (see Figure 3) show that the

counts per 1 μsec channel are randomly distributed about the mean value of 34.82 as expected from a Poisson type distribution. Because there are no fission chains, there is no clustering of neutrons.

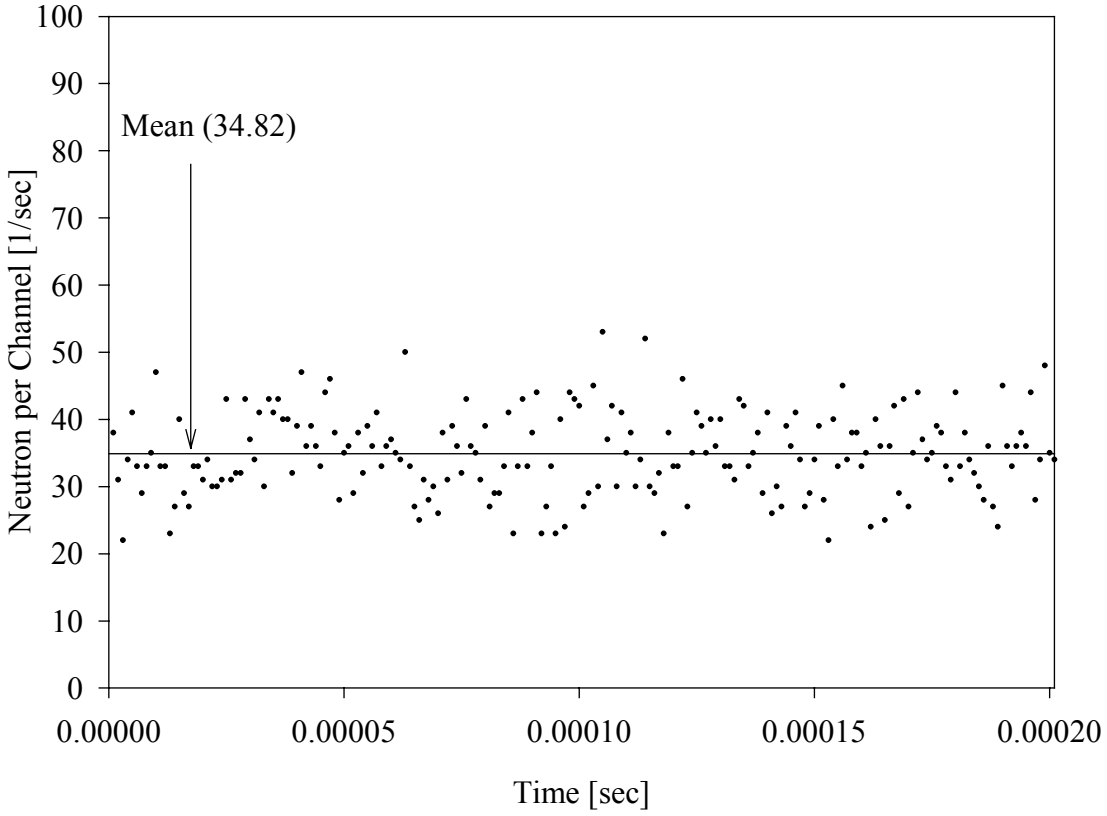

Figure 3. Neutron activity vs. time in a non-multiplying system.

As expected from the results shown in Figures 2 and 3, the variance of the counts per channel is significantly different for the two cases (see Table I). The increase in the variance for the multiplying system is a result of the clustering of the neutrons during the prompt fission chains. For the non-multiplying system shown in Figure 3, the counts per channel reflect the randomness of the source and are distributed about the mean value in

a Poisson fashion. That is, 99.7% of the channel counts should fall within 3 standard deviations about the mean. As can be noted from Table I, 100% of all the counts in this simulation fell within this tolerance. For the multiplying system shown in Figure 2, this is clearly not the case. Over half of the channels contain zero counts, and a select few have a very large number of pulses due the fission chains.

TABLE I

Statistical analysis of neutron population shown in Figures 2 and 3.

K	**Total Neutrons**	**Total Duration μsec**	**Average Channel Counts**	**Variance σ^2**	**Max**	**Min**
0.00	7034	201.57	34.8218	38.9	53	19
0.99	7034	201.35	34.8218	18,765.2	1087	0

The variance of the channel counts clearly indicates a phenomenon that cannot be adequately described using deterministic methods. The stochastic nature of the prompt fission chains has been previously studied by numerous authors who have noted that the average behavior of the neutron population can be a secondary factor as compared to the behavior of the individual neutrons in these systems.[6,28-39] For this reason, each fission chain is propagated independently in energy, angle, and space rather than estimating the chain's behavior based on an approximation of the average chain.

B. Chain-Length Distribution

The evolution of a fission chain can be summarized as follows. Counting the single source neutron (i.e., external, intrinsic, or delayed neutron) that acts as an initiator, the exact number of neutrons spawned within a particular fission chain will be purely a matter of chance. Each neutron in the chain will either induce a fission event in the system, resulting in additional neutrons in the chain's population, or it will disappear from the system due to leakage or parasitic absorption. (Note scattering events do not remove neutrons from the chain because the chain population does not depend on neutron energy or direction in the system.) As might be expected, the conglomeration of random events results in the appearance of chains with varying total neutron populations (i.e. lengths). Furthermore, chains with identical lengths may also differ with respect to the number and types of events occurring within them. Rather than identifying each chain according to the exact series of events that occurs during the chain's evolution, the chains will be classified according to their total neutron population hereafter referred to as their final length, L. Further, $P(L)$ is defined as the probability per source neutron for observing a fission chain of length L. It is also worth emphasizing that L can only

take on discrete values, i.e., integers. The *chain-length distribution* discussed herein, is just a set of lengths, L, and their associated probabilities, $P(L)$, that uniquely characterize the multiplying system.

Provided the multiplying system can be characterized by known or measurable global parameters, such as K and $\overline{\nu}_p$, the corresponding chain-length distribution is highly predictable and can be readily determined using Monte Carlo techniques. An example of a chain-length distribution is shown below in Figure 4. The figure shows the probability that a source neutron will spawn a fission chain of a specified length. As expected from Figure 2, the shortest chain length, comprised of only the source neutron, is the most frequently occurring. With the exception of the shorter chains, the probability decreases almost monotonically with increasing length. Although longer chain lengths may occur, the longest length shown represents a chain containing several hundred thousand neutrons, and it would be expected to occur only once per 10^{14} source neutrons $\left(P\left(L = 5 \cdot 10^5\right) \simeq 10^{-14}\right)$. A more in-depth treatment explaining the shape of the distribution including its tails appears in the following sections.

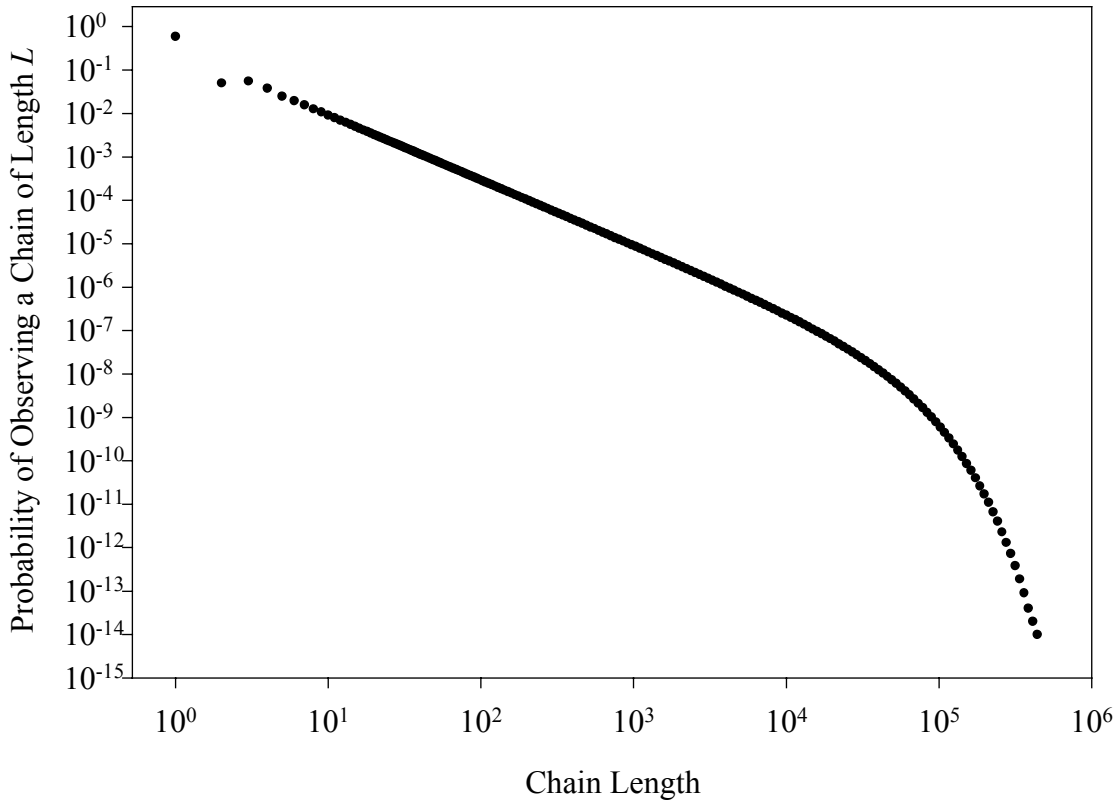

Figure 4. Chain-length distribution for a *K=0.99*.

C. Neutron Number Distribution

To better understand the nature of the chain's behavior, it is useful to begin with an examination of the multiplicity distribution of the fission neutrons, $P(\nu)$. In almost every book on neutron or reactor physics, the only value mentioned in regard to this distribution is its mean value designated as $\overline{\nu}$ or for prompt neutrons $\overline{\nu}_p$. Because $\overline{\nu}$ is the property that commonly appears in deterministic equations used to describe the fission neutron source in a multiplying system, it is also the parameter included in

typical neutron cross section files as the product of $\bar{\nu}\Sigma_f$. The full distribution for the prompt component was first studied by researchers at the Los Alamos Scientific Laboratory, such as Richard Feynman, who were intensely curious about the actual shape of the distribution.[6] Diven and Leachman measured the first $P(\nu)$ distributions for several isotopes basing their work on the kinetic energy of the fission fragments.[20,21] They determined that the distributions appeared to have a binomial form. As the distributions were revised over the years by various investigators for an ever-increasing range of isotopes, the predicted shape began to change as well.[22-27] In 1988, Frehaut proposed a single distribution that sufficiently captured the multiplicity distributions for a number of major isotopes.[27] The distribution, which is expressed as a function of $\bar{\nu}_p$, provides a much better approximation than earlier relationships. In Frehaut's $P(\nu)$ function, the fitting constants, *a* and *b*, are parameters associated with a particular ν. The values associated with these parameters appear in Table II.

$$P(\nu) = \frac{a}{b\sqrt{2\pi}} e^{-\frac{1}{2}\left(\frac{\bar{\nu}_p - \nu}{b}\right)^2} \tag{II.2}$$

TABLE II

Frehaut's fitting parameters

ν	**0**	**1**	**2**	**3**	**4**	**5**	**6**	**>7**
b	0.94	1.13	1.22	1.295	1.16	1.222	1.226	1.235
a	2.827	1.073	1.075	1.095	0.953	0.958	1.048	1.000

While this distribution provides a means to model the multiplicity for a variety of isotopes, there are some caveats. Frehaut mentioned that the fit was unsatisfactory for thorium isotopes. Furthermore, the distribution is not normalized to 1.0, which means that the $\overline{\nu}_p$ used to construct the distribution is not the average value that would be obtained from the final distribution. This lack of consistency can be understood because Frehaut was more interested in matching his curves to the experimental data rather than insuring that they were sufficient for a Monte Carlo type simulation. As an example of these inconsistencies, the neutron number distribution for $\overline{\nu}_p = 2.42$ has been calculated (see Table III). The values appearing in the last column of Table III arise from a modification to Frehaut's original distribution necessitated by the need to normalize the distribution and preserve $\overline{\nu}_p$. The adjustment was performed so as to have the least impact on the most likely portion of the Frehaut distribution's shape.

Besides using the Frehaut distribution, another more common approach for specifying the multiplicity is to assume that the number of prompt neutrons emerging from a fission is limited to the integers bounding $\overline{\nu}_p$. For example, if $\overline{\nu}_p = 2.5$, then it is assumed that 50% of the fissions yield two neutrons, and the other 50% yield three neutrons. This *binary-distribution* approach has proven to be suitable for calculations in which the macroscopic behavior of the system is of primary interest. For example, MCNP uses this technique when it is run in analog mode.[40] To reduce the variance when performing *k*-eigenvalue calculations, however, Monte Carlo packages generally run in a nonanalog mode and use the value of $\overline{\nu}_p$ or $\overline{\nu}$ directly. Figure 5 shows the

Frehaut distribution as compared to the multiplicity distribution associated with binary sampling.

TABLE III

Frehaut's original and corrected distributions.

		Frehaut		
ν	**Binary**	**Original**	**Normalized**	**Corrected**
0	0.0	0.0436	0.0428	0.0425
1	0.0	0.1720	0.1685	0.1685
2	0.58	0.3313	0.3246	0.3246
3	0.42	0.3051	0.2990	0.2990
4	0.0	0.1296	0.1270	0.1270
5	0.0	0.0337	0.0330	0.0330
6	0.0	0.0048	0.0047	0.0047
7	0.0	0.0003	0.0003	0.0006
Total	1.00	1.0205	1.0000	1.0000
	2.42	2.4680	2.4184	2.4200
Correction			0.0016	

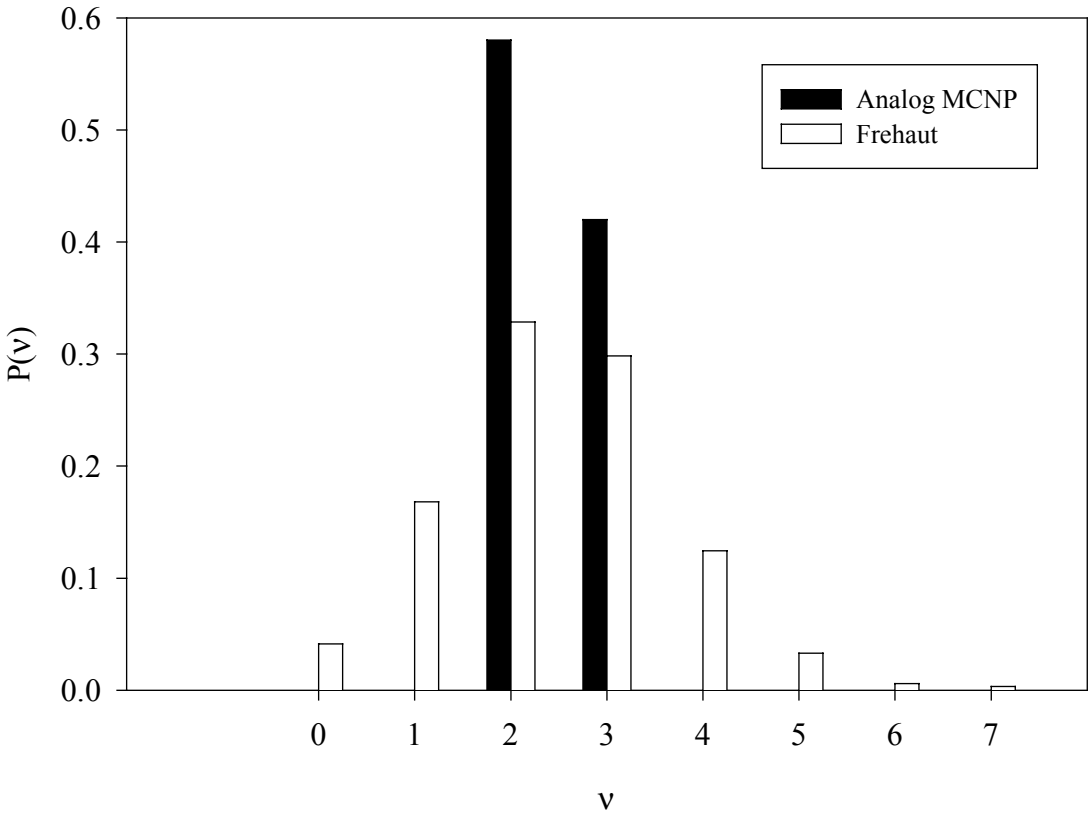

Figure 5. Comparison of Frehaut distribution with binary (analog MCNP) distribution.

D. Probability of Short Chains

The choice of the distribution can have a significant impact on the modeling of a system when the microscopic behavior is important, as when analyzing the neutron noise. The multiplicity distribution directly influences the way the neutrons start a branching process during fission events. Ignoring the time dependence for a moment, a probability tree can be constructed for each source neutron. The terminations, or *leaves* of the probability tree, are comprised of the probability of not causing a fission and the probability of causing a fission that does not release any neutrons. In the same way that

fissions that release zero neutrons terminate a branch; all other fissions create a number of branches equal to the number of neutrons released. Figure 6 shows the beginnings of a probability tree that represents the branching potential of a typical neutron in a multiplying system.

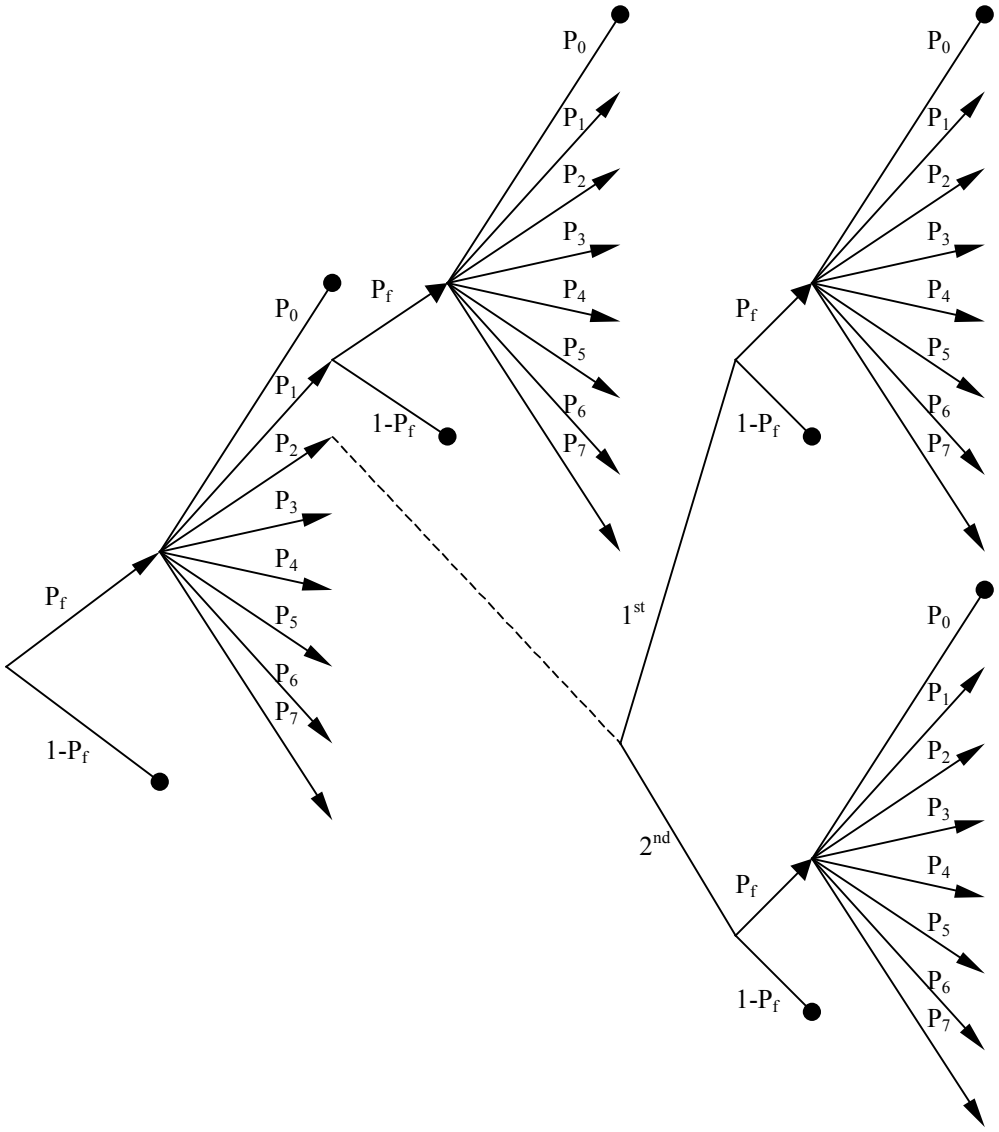

Figure 6. Branching potential for a typical neutron in a multiplying system.

In Figure 6, P_f is the probability that a neutron will cause a fission, and P_n is the probability that a fission event will produce *n* neutrons. Using the probability-tree approach, it is possible to compile the complete set of paths that result in a fission chain of any specified length. While this is straightforward for short chains $(L \leq 7)$, the remaining chain-lengths become increasingly complex to account for as the potential paths increase with increasing length. Tracing the paths for some of the shorter chains has yielded the following observations.

There are actually three ways that a chain can have a length of 1. The most obvious ways in which this may happen occur when the source neutron leaks out of the system or is parasitically absorbed. Noting that either of these *must* happen if the source neutron does *not* induce a fission, the total probability of their occurrence is simply $(1 - P_f)$. A slightly less obvious way to have a chain length of 1 occurs when the source neutron causes a fission from which no neutrons are emitted. In this case, the fission probability must be multiplied by the probability that the fission event produces zero neutrons (i.e., $P_f P_0$). Hence, the probability of obtaining a chain of length equal to 1, $P(1)$, from all three ways is

$$P(1) = (1 - P_f) + P_f P_0 \quad . \tag{II.3}$$

Due to its recurrence in formulating the probabilities for chains with lengths greater than 1, the probability for a non-fission event, $(1 - P_f)$, and the probability for a fission event

producing zero neutrons, $\left(P_f P_0\right)$, are combined into a single probability hereafter denoted as the *loss* probability, P_l. In addition to being the probability of observing a chain with length equal to 1, P_l is also the probability that any branch terminates.

$$P_l = \left(1 - P_f\right) + P_f P_0 \tag{II.4}$$

To further simplify the following notation, it is useful to define the product of the fission probability and the probability for releasing *n* neutrons as

$$P_{fn} = P_f P_n \quad . \tag{II.5}$$

Using this notational convention, the following relations can be used to calculate the probability of a source neutron initiating chains with lengths of 2 through 7.

$$P(2) = P_{f1} P_l \tag{II.6}$$

$$P(3) = P_{f2} P_l^2 + P_{f1}^2 P_l \tag{II.7}$$

$$P(4) = P_{f3} P_l^3 + 3P_{f1} P_{f2} P_l^2 + P_{f1}^3 P_l \tag{II.8}$$

$$P(5) = P_{f4} P_l^4 + \left(4P_{f1} P_{f3} + 2P_{f2}^2\right) P_l^3 + 6P_{f1}^2 P_{f2} P_l^2 + P_{f1}^4 P_l \tag{II.9}$$

$$\begin{aligned} P(6) = {} & P_{f5} P_l^5 + 5\left(P_{f2} P_{f3} + P_{f1} P_{f4}\right) P_l^4 + 10\left(P_{f1}^2 P_{f3} + P_{f1} P_{f2}^2\right) P_l^3 \\ & + 10P_{f1}^3 P_{f2} P_l^2 + P_{f1}^5 P_l \end{aligned} \tag{II.10}$$

$$\begin{aligned} P(7) = {} & P_{f6} P_l^6 + \left(6P_{f2} P_{f4} + 6P_{f1} P_{f5} + 3P_{f3}^2\right) P_l^5 \\ & + \left(30P_{f1} P_{f2} P_{f3} + 15P_{f1}^2 P_{f4} + 5P_{f2}^3\right) P_l^4 + \left(20P_{f1}^3 P_{f3} + 30P_{f1}^2 P_{f2}\right) P_l^3 \\ & + 15P_{f1}^4 P_{f2} P_l^2 + P_{f1}^6 P_l \end{aligned} \tag{II.11}$$

$$P(8) = P_{f7} P_l^7 + \ldots .$$

For even longer chain lengths, similar expressions can be written following the pattern established above although the process becomes increasingly complex. Regardless of the magnitude of *K*, the numerical solution of $P(L)$ obtained using Monte Carlo techniques can be benchmarked against the analytic solutions given above for chain

lengths 1 through 7. As *K* nears 1.0, the numerical solution can also be benchmarked against the asymptotic solution previously obtained for the Galton-Watson problem described in Harris.[41]

E. Galton-Watson Process

When nuclear researchers first began to study the propagation of fission chains in subcritical systems, they recognized that this problem was akin to an older problem that had been studied since the 1800's.[41,42] Around this time, Francis Galton, a mathematician, and the Reverend H. W. Watson, an amateur mathematician and sociologist, were studying the fate of prominent families in Europe. In particular, they were seeking to determine the probability of a particular surname disappearing from a population given that each generation has an equal probability for having a specified number of male progeny. Using census data, Galton and Watson constructed a probability distribution of having 0, 1, 2, etc. sons for each of several generations and found that the distributions were roughly constant across the generations. This type of process later became known as a Markov process and is the predecessor of the mathematics field of branching processes.

As in the Galton-Watson branching study, the choice of multiplicity distributions can have a profound effect on the probability of observing fission chains of certain lengths. Using the binary distribution given in Table III for $\bar{\nu}_p = 2.42$, it follows that a chain length of 2 can never occur. If the original source neutron is parasitically absorbed or leaks from the system, then the chain length will be 1. If, on the other hand, the

source neutron induces a fission, then either 2 or 3 neutrons will be produced, which means the next possible chain contains at least 3 neutrons. Similarly, if $\bar{\nu}_p$=3.5, the lengths of 2, 3 and 6 are prevented. The exclusion of these common fission chains can be seen by observing how a system's chain-length distribution is affected by the two different multiplicity distributions.

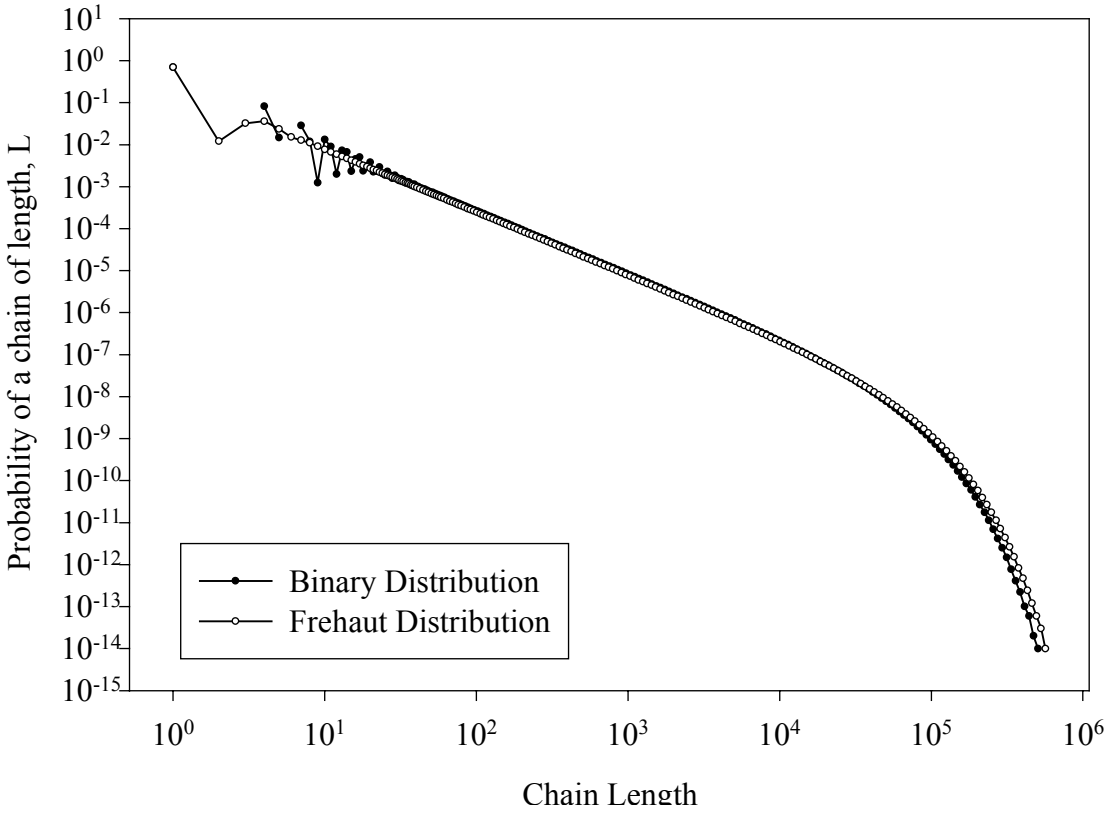

Figure 7. Chain-length distributions for Frehaut and binary distributions at $\bar{\nu}_p = 2.42$.

Using the binary distribution leads to significant differences as compared to the Frehaut distribution at short chain lengths. As the chain lengths increase, the differences

become less noticeable. However, since the area under each chain-length distribution is the same, the probability of observing longer chains is also affected (see Figure 7).

F. Rossi and Feynman

Bruno Rossi has been credited with recognizing that the larger-than-expected oscillations in the neutron count rates observed in the Low-Power Water-Boiler Reactor (LOPO) at Los Alamos were caused by the spawning and dying out of individual, fission chains.[4,8] Evidence for the fission chain theory was further provided by experiments conducted by Wimmett et al. on the research reactor Godiva-II.[43] They performed a series of measurements in which they brought the bare, uranium-fueled reactor to \$0.05 above prompt critical numerous times. The objective was to observe the time that it took to reach a reference power level following the reactivity insertion. Immediately following the reactivity insertion, the system was, of course, super-prompt critical. However, for a measurable time after the reactivity insertion, the power level remained roughly constant at the level of the intrinsic source because the vast majority of the fission chains in the system would spawn and subsequently die out. The reactor power would not increase dramatically until a persistent fission chain emerged. The times that elapsed from insertion to power excursion were tabulated, and it was observed that the scatter in the elapsed times could be explained only by a phenomenon like Rossi's fission chains. This experiment also showed that the system behaved in a stochastic manner prior to the power excursion. Only after a chain reached a sufficiently large size

could a deterministic reactor model adequately represent the time-dependent behavior of the system.

Of course, Rossi provided his own proof, too. He theorized that the random behavior of the fission chains was actually governed by the properties of the multiplying system.[5] Conversely, the key to measuring these properties would depend on the ability to detect and quantify the clumping phenomena (shown earlier in Figure 2). From the power peaks observed in the LOPO, Rossi postulated that the neutrons from a single chain evolved on a faster time scale, and as such, were more highly correlated in time than the intrinsic source neutrons. Rossi's proposal concerning the importance of the fission chains and their time correlation intrigued his associate Feynman, who developed much of the early background theory and equations describing neutron noise analysis.[6] In addition to deriving the Rossi-α formula, Feynman also proposed his variance-to-mean technique. In this technique, the ratio of the signal's variance to its mean is computed. If this ratio is significantly greater than 1.0, it implies that the signal arose from phenomena other than a completely random distribution and that fission chains must be present.

In developing the point-kinetic model for neutron noise, Feynman started with a simple conservation equation,

$$\underbrace{\frac{dN}{dt}}_{\text{Change Rate}} = \underbrace{-\frac{1}{\tau}N}_{\text{Loss Rate}} + \underbrace{\frac{\bar{\nu}_p}{\tau_f}N + S_{eff}}_{\text{Gain Rate}} \quad , \tag{II.12}$$

where τ is the neutron removal lifetime, N is the neutron population, $\bar{\nu}_p$ is the average number of prompt neutrons emitted per fission, and τ_f is the neutron lifetime for fission. As previously discussed, neutrons from external sources, the intrinsic source, and decay of the delayed neutron precursors are considered to be part of the fixed-source term, S_{eff}. Rearranging (II.12) yields

$$\frac{dN}{dt} = \frac{K-1}{\tau} N + S_{eff} \tag{II.13}$$

where K is the prompt neutron multiplication factor defined as

$$K = \frac{\bar{\nu}_p \tau}{\tau_f} \quad . \tag{II.14}$$

The ratio of the two lifetimes is significant since it is identically equal to the probability for fission,

$$\frac{\tau}{\tau_f} = P_f \quad . \tag{II.15}$$

Combining Eqs. (II.14) and (II.15) yields the important result

$$P_f = \frac{K}{\bar{\nu}_p} \quad . \tag{II.16}$$

The solution of the homogeneous portion of Eq. (II.13) is

$$N(t) = N_0 e^{\frac{K-1}{\tau} t} \quad , \tag{II.17}$$

where the coefficient appearing in the exponent is commonly referred to as the prompt decay constant, α, and is defined by the following relationship,

$$\alpha = \frac{K-1}{\tau} \quad . \tag{II.18}$$

The decay constant, α, is one of the fundamental parameters describing the time-dependent behavior of the fission chains. As such, it is one of the primary quantities measured in a neutron noise experiment. Moreover, in a reactor system operating near delayed critical, α measurements are very useful in establishing an independent reactivity scale, as well as for providing a measure of the neutron removal lifetime, and the effective delayed neutron fraction.

G. Definition of Subcritical Multiplication

Another fundamental parameter that has a direct bearing on the prompt fission chains is the subcritical multiplication, *M*. This quantity is the ratio of the neutron production rate per source neutron added to the system. That is,

$$M = \frac{\text{production rate}}{S} \quad , \tag{II.19}$$

where *S* is the external/intrinsic source. As opposed to S_{eff} from earlier, S does not contain the delayed neutron contribution. In a multiplying system, the total neutron production rate is comprised of the external/intrinsic sources and the fission source. Making this substitution yields,

$$M = \frac{S + \iiint \bar{\nu} \Sigma_f \phi dEdV}{S} \quad , \tag{II.20}$$

where $\bar{\nu}$ is the average number of neutrons emerging from fission, Σ_f is the macroscopic cross section for fission, and ϕ is the scalar flux. Another way to

determine M is by the definition of the multiplication factor, k, which is the neutron production rate divided by the neutron loss rate at steady-state. That is,

$$k = \frac{\int\int \bar{\nu}\Sigma_f \phi dEdV}{S + \int\int \bar{\nu}\Sigma_f \phi dEdV} \quad . \tag{II.21}$$

Subtracting 1 from Eq. (II.21) and inverting provides the more common form

$$M = \frac{1}{1-k} \quad . \tag{II.22}$$

Using either of these definitions, the subcritical multiplication factor is interpreted as the average number of neutrons produced per source neutron entering the system. A similar relationship also exists for the subcritical *prompt* multiplication, M_p, where $\bar{\nu}_p$ is specified in place of $\bar{\nu}$ in Eq. (II.21), and K replaces k in Eqs. (II.22) and (II.21). M_p's relation to the prompt fission chains becomes apparent when one looks at the average of the chain-length distribution. Suppose that each chain length, L, has some associated probability for occurring, $P(L)$, where $P(L)$ is normalized such that

$$\sum_{L=1}^{\infty} P(L) = 1 \quad .$$

It is possible to then define the average chain length, $\bar{L}$, as

$$\bar{L} = \frac{\sum_{L=1}^{\infty} L \cdot P(L)}{\sum_{L=1}^{\infty} P(L)} = \sum_{L=1}^{\infty} L \cdot P(L) \quad . \tag{II.23}$$

Since $\bar{L}$ is the average number of neutrons in a chain, it is essentially the average number of prompt neutrons produced per source neutron, and this is also the exact

definition of the subcritical prompt multiplication $\left(\text{i.e., } M_p = \overline{L}\right)$. However, this derivation is strictly true only if the source and fission neutrons are distributed identically in energy, angle, and space.

H. Equivalent Fundamental-Mode Source

The neutron source driving a subcritical experiment is seldom distributed in a fashion that resembles the fission source unless the delayed neutron contribution is quite significant. Generally, the neutron source is either a point source or a uniformly distributed intrinsic source and, as such, differs significantly from the fission source distribution associated with the fundamental-mode flux. (The neutron flux density's shape in a finite sized, neutron multiplying system can be expressed in terms of an infinite series of spatial modes. The *fundamental mode* is the asymptotic flux shape that remains after all higher-order spatial modes have died away.[44]) This difference in distribution can result in a system multiplication that deviates significantly from the value obtained by Eq. (II.22). To obtain the multiplication predicted by that equation, the source neutrons must be distributed identically to the *fundamental-mode fission source*. A source that is distributed as the fundamental mode is called an *equivalent fundamental-mode (EFM) source*, and the multiplication that it produces is called the *fundamental-mode multiplication*, M_{EFM}. For non-fundamental-mode sources (such as point sources or uniformly distributed intrinsic sources, etc.), one would like to retain the ability to express the system subcritical multiplication, M, in terms of the k-eigenvalue.

To accomplish this, a term g^*, is introduced into the source-multiplication equation,

$$M = \frac{g^*}{1-k} \quad , \tag{II.24}$$

which accounts for the difference in the importance of source neutrons and fission source neutrons.[45-46] The factor g^* can be calculated based on a forward and adjoint solution of the transport equation. For the purposes of this dissertation, however, a physical description of g^* should suffice. Given a slab reactor, it is obvious that a neutron born near the center will have a higher probability of causing a fission than a neutron born near the edge. Consequently, a source that only emits neutrons at the center of a reactor will produce more multiplication in the system than a source that emits neutrons uniformly throughout. If the source were several meters away from the reactor, the importance effect would be even more drastic as only a small fraction of the source neutrons would even enter the reactor. Since the magnitude of *M* is directly related to the number of fission neutrons produced, the same number of source neutrons from each source will produce different *M*'s. An EFM source will provide yet another value of *M* according to the following relation.

$$M_{\text{point at center}} \geq M_{\text{EFM}} \geq M_{\text{Uniform}} \tag{II.25}$$

From this and Eq. (II.24), it is possible to provide a simple relation for g^*.

$$g^* = \frac{M}{M_{EFM}} = M\left(1-k\right) \tag{II.26}$$

In the bare, spherical, uranium system studied by Spriggs, the value of g^* varied as a function of *k* and ranged from approximately 1.0 to 1.8 for a point source located in the center of the assembly.

Because of the equivalence between the system subcritical prompt multiplication, M_p, and the average chain length, $\bar{L}$, the g^* factor must also be considered when comparing the chain-length distribution for various source configurations. For example, to compare the chain-length distribution associated with a point source and a uniformly-distributed source in a system operating at the same *K*, it is necessary to divide the prompt system multiplication through by g^*. This, in effect, allows us to compare the chain-length distribution per EFM source (i.e., the area under each curve will be normalized to the same value of M_P).

I. Neutron Noise Analysis

The Rossi-α technique mentioned earlier is only one of many neutron noise techniques that rely on a time-series analysis of the fluctuation in the neutron population density. Others include the variance-to-mean, interval-distribution, zero-probability technique etc.[47-58] All of these techniques depend on quantifying the degree of correlation associated with a stream of pulses generated by a detector. The pulses caused by neutrons originating from a common ancestor are spaced tightly in time and result in some number of correlated counts. Instead of describing each time-series technique in detail, the focus here is on the Rossi-α technique, which is probably the best known. It will be shown how the correlations arise in neutron multiplying system,

how they then lead to an estimate of the subcritical decay constant, α, and other global parameters, and how the detection of correlated pairs depends on the length of the fission chains (i.e., the chain-length distribution). It will also be shown how the detector efficiency and a reactor's background noise negatively effect the estimate of α.

As shown earlier, a neutron multiplying system is marked by the presence of fission chains, whose evolution can be followed by observing the rate at which neutrons from a common chain interact with the underlying system. The characteristic clumping of the fission chains in time is expected to correspond to a proportionate increase in observed events. For example, Figure 8 shows the propagation of two separate chains over an arbitrary span of time. In this figure, the vertical lines represent the lifetimes of the neutrons, the horizontal lines correspond to the occurrence of fission events, and the number of tracks emerging represents the number of neutrons produced. The terminating lines correspond to loss event whether from parasitic absorption or leakage from the system. A fission termination would be represented by a horizontal line from which there are no emerging lines.

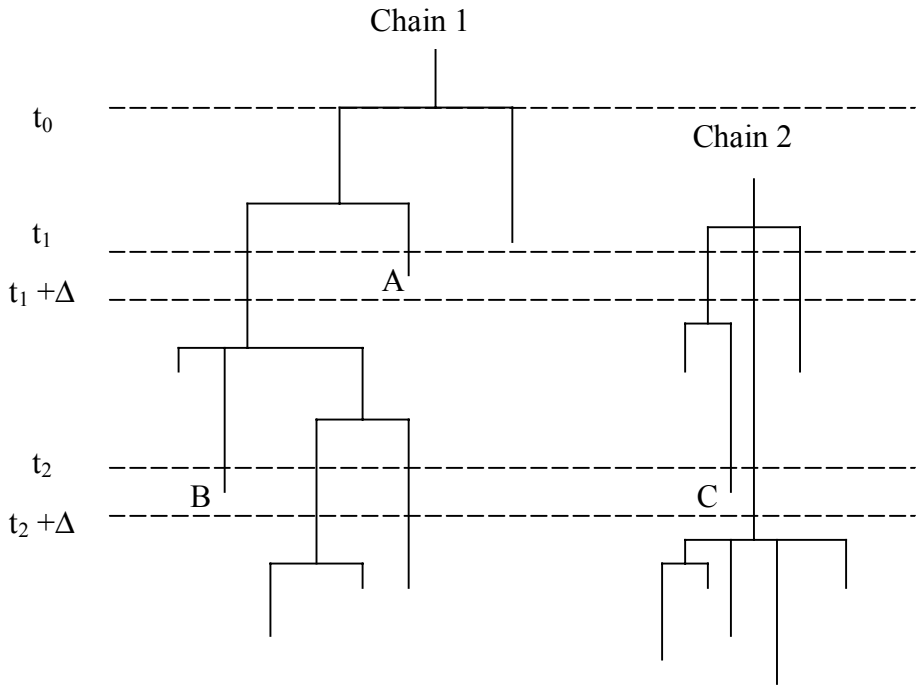

Figure 8. Propagation of two prompt fission chains.

For a Rossi-α measurement to be successful, the algorithm for analyzing the detector's pulse stream must be able to differentiate between the pulses generated by separate chains. In Figure 8, signals or pulses are generated whenever the branches of the chains terminate. The events labeled *A* and *B* are detectable interactions caused by neutrons generated in *Chain 1*. As such, the corresponding detector pulses provide a single, correlated pair for the analysis. The event/pulse labeled *C* occurs within the same time span as *B*, but it arises from a separate chain and should be recognized as an uncorrelated, or accidental, addition to the signal. Although counts such as *C* cannot be altogether eliminated, their contribution must be accounted for by knowing the average count rate in the system. In Figure 8, the uncorrelated counts arise because the two

fission chains overlapped during the observed time interval. Avoiding this in an experiment can reduce the number of accidentally correlated counts. Such a reduction can be achieved by decreasing the rate at which the chains are initiated, by decreasing the average chain length, or by increasing the rate at which the chains propagate.

Ignoring the uncorrelated counts for a moment, the first step towards analyzing a detector signal requires determining the likelihood of detecting two pulses from the same chain. Feynman, de Hoffmann, and Serber first approached this problem in 1944 during their work on the LOPO reactor at Los Alamos.[4-8] They began by assuming that a fission event occurs at t_0 and then by calculating the probability for seeing two neutrons from that fission. After the fission, they follow the remaining ν_p neutrons until one interacts in Δt about t_1. Assuming this neutron is lost from the system, only $\nu_p - 1$ neutrons are then left to interact in Δt about t_2 (see Figure 9).

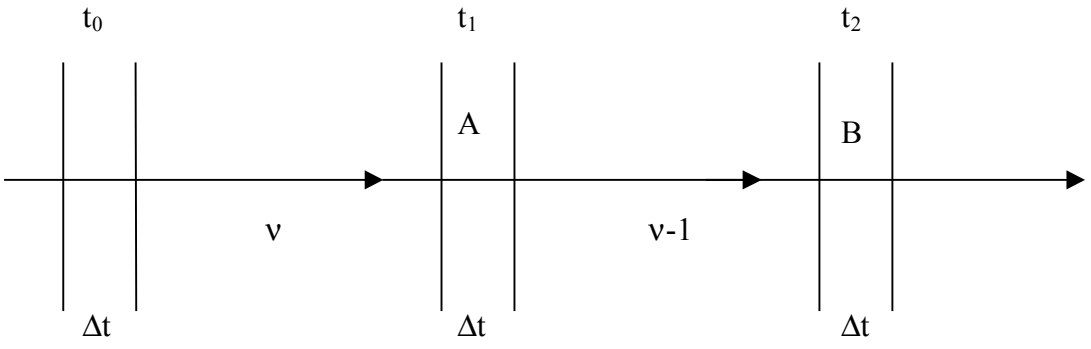

Figure 9. Determining neutron interaction correlations.

Using this approach, they showed that the probability of detecting a correlated count in some *dt* about *t* given a count at $t_0=0$ is,

$$P(t)\,dt = \frac{\varepsilon_f \overline{\nu_p(\nu_p-1)} K^2}{2\bar{\nu}_p^2 \tau (K-1)} e^{-\alpha t} dt \quad , \tag{II.27}$$

where ε_f is the detector efficiency in counts per fission, $\overline{\nu_p(\nu_p-1)}$ is the reduced-second moment of the prompt neutron number distribution, and the other parameters are as defined previously. The terms containing ν_p require a detailed knowledge of the multiplicity distribution, and are often replaced by the Diven factor,

$$\Gamma = \frac{\overline{\nu_p(\nu_p-1)}}{\bar{\nu}_p^2} \quad . \tag{II.28}$$

While this quantity has been measured by a number of investigators for various isotopes, it can also be generically constructed from Frehaut's multiplicity distribution by

$$\bar{\nu}_p = \sum_{\nu_p} \nu_p P(\nu_p), \qquad \overline{\nu_p(\nu_p-1)} = \sum_{\nu_p} \nu_p(\nu_p-1) P(\nu_p) \quad .$$

J. Correlated Pairs

The average chain length is of great importance in neutron noise analysis. It determines the potential number of correlated pairs of neutrons that can be generated at a given subcritical configuration. For example, let us assume that a prompt fission chain produces 20 neutrons that are spaced exactly Δt apart. If every neutron is detected, a time-series analysis would show 19 pairs that were $1 \cdot \Delta t$ apart, 18 that were $2 \cdot \Delta t$ apart,

17 that were $3 \cdot \Delta t$ apart, etc. The total number of correlated pairs would sum to 190. In general, the total number of correlated pairs can be calculated using the expression,

$$\underbrace{n}_{Pulses} \rightarrow \underbrace{\frac{1}{2} n(n-1)}_{Pairs} \quad . \tag{II.29}$$

As will be demonstrated in the results chapter, the coefficient in Eq. (II.27),

$$A = \frac{\varepsilon_f \overline{\nu_p (\nu_p - 1)} K^2}{2 \bar{\nu}_p^2 \tau (K-1)} \quad , \tag{II.30}$$

is proportional to the number of correlated pairs per neutron population, and can be related to $P(L)$ as follows.

$$\frac{\bar{\nu}_p \Gamma}{2} \left(\frac{1}{1-K} \right) \left(\frac{K}{1-K} \right) = \frac{\sum_{L=1}^{\infty} \frac{L(L-1)}{2} P(L)}{\sum_{L=1}^{\infty} L \cdot P(L)} \quad , \tag{II.31}$$

where

$$\bar{L} = \frac{1}{1-K} \quad \text{and} \quad \bar{L} - 1 = \frac{K}{1-K} \quad .$$

This relation was determined heuristically from the numerical analysis. To obtain perfect agreement between the theoretical model and the numerical model, the $\bar{\nu}_p \Gamma$ term in Eq. (II.31) must be included. (At this time, we have no explanation as to why this term must be included. Agreement cannot be obtained otherwise.)

It is most important to recognize that the numerator on the right-hand side of Eq. (II.31) is the number of correlated pairs per *source neutron*. To calculate the number of

correlated pairs per *neutron population*, one simply divides through by the multiplication of the system, which is the denominator on the right-hand side of Eq. (II.31).

The remaining terms contained in the Rossi-α coefficient are related to the rate at which the correlated pairs are expected to be detected and the detector efficiency. Because it is impossible to design an experiment in which one detects every neutron (and hence, every correlated pair), observing the maximum number of correlated pairs can never be achieved. Figure 8 shows a system in which only two of 12 neutrons from the first fission chain are detected. Obviously, the detector efficiency does not change the chain-length distribution, but it will limit the amount of information that a given chain length provides. This will be demonstrated in the following chapter.

CHAPTER III

COMPUTATIONAL APPROACH

Because a generally applicable solution cannot be obtained analytically for modeling the fission chain phenomena, the next best option is to examine the fission chain process as simulated in numerical experiments. In this case, the experiments were carried out on a computer using Monte Carlo-type simulations. The results presented were drawn from the application of two codes that were developed to study different dependencies of the chain-length distribution. The first code, *Chain*, models simple zero-dimensional (i.e., point kinetic) systems, and the second code, MC++, models more complex, three-dimensional systems. The following discussion focuses on the capabilities of the two codes followed by a brief section outlining when one would choose to use one code as opposed to the other.

A. Chain

This section begins with a description of the point-kinetic, Monte Carlo code, *Chain*. To produce a chain-length distribution with this code, a user specifies the global parameters, K and $\overline{\nu}_p$. Using the input global parameters, the code propagates each chain according to a straightforward application of the previous section's equations. Beginning with each source neutron, the code determines a terminating event for each neutron whether it fissions or is lost (via a parasitic absorption or a leakage). This

determination is accomplished by generating a random number and then determining whether that number falls within the interval 0 to P_f, where P_f is defined as,

$$P_f = \frac{K}{\bar{\nu}_p} \quad .$$

If the random number falls within that interval, then a fission event occurs. If, however, the random number falls within the interval P_f to 1.0, then a loss event occurs. The event probabilities are taken to be identical for every neutron because the code assumes that each neutron, including each source neutron, has the same distribution as an EFM neutron. Following each fission event, another random number is generated to determine how many neutrons were released.

The creation of each source neutron is accompanied by the creation of a new queue that stores all of the neutrons in the chain until their terminating events have been determined. If the terminating event is a fission event, the $\bar{\nu}_p$ distribution is sampled, and the resulting fission neutrons are inserted at the end of the queue. Whether the neutron causes a fission or is lost, it is removed from its position at the front of the queue, and the process repeats with the next neutron in the queue. When the queue is empty, the chain has expired and its final length is registered, along with the time interval over which the chain spawned (i.e., its duration). Because *Chain* is a point model, the entire process is very efficient computationally as compared to a more detailed simulation that tracks each neutron in energy, space, and angle. The approach in *Chain* requires, at most, two random numbers per event. The first random number

determines the event type, and the second random number determines the number of neutrons produced by a fission event from sampling the multiplicity distribution.

At the end of the simulation, the chain-length data, which includes the number of neutrons in the chain, its duration, and the number of times it occurred, is written to disk. A separate script sorts the chain length data produced by *Chain* into a series of logarithmically spaced bins. The bin widths are restricted to integer increments to match the purely integer lengths of the chains. The probability that a particular chain length occurs is found by summing the number of chains that fall within a particular bin and then dividing this number by the total number of chains (i.e. the number of source neutrons tracked) and by the width of bin. The chain length associated with each probability is taken to be the midpoint of the bin. The script with its logarithmic binning, also works with the chain length distribution produced by *MC++*.

Although the logarithmic binning increases the complexity of the analysis, it is essential because the long chains appear so infrequently. Moreover, as the chain lengths become increasingly long, the probability of having *multiple* chains of the exactly the same length decreases even faster. Increasing the bin's width at higher values of L increases the potential number of counts per bin by including neighboring lengths. When the total number of counts in a given bin is divided by its width, the resulting probability becomes the probability of seeing a chain with a range of lengths centered about the mid-point of that bin. In addition to smoothing the estimate of observing the long chains, this binning technique also results in the ability to observe probabilities that can be significantly less than the inverse of the number of chains in a simulation.

Chain also provides a means for simultaneously running a number of neutron noise analysis techniques while the chains are evolving. When a particular time-series technique, such as the Rossi-α, is specified in the input file, the code also records the time at which each event in the chain occurs. The addition of time dependent behavior requires the generation of another random number to determine an interaction time, t_{event}. Based on a user-supplied value for the neutron lifetime τ, t_{event} is randomly sampled using

$$t_{event} = t_0 + \left(-\tau \cdot \ln(\xi)\right) \quad , \tag{III.1}$$

where ξ is a uniformly distributed value on the unit interval (0,1). The time of birth, t_0, is either the time at which a source neutron is injected into the system, or the time at which a fission occurred that produced the current neutron. The exponential distribution was chosen because of its close approximation to the actual time behavior of a neutrons propagating in a single material system. All the event times in a chain are elapsed times relative to the birth time of the initiating source neutron. In *Chain*, each source neutron enters the simulation at *t=0* to prevent comparison of pulses from different fission chains. As the last neutron dies out of a chain, the event times generated by that chain are immediately passed to the analysis routines. The event times are effectively converted to detector pulses by applying filters that simulate the detector response. These filters can discriminate based on event type, detector efficiency, and detector dead-time effects. The remaining pulses from a particular chain are then analyzed, and the analysis statistics are accumulated. The result is a very clean signal with a theoretical

background that does not include a contribution from overlapping chains. If the time-series technique is the variance-to-mean, the user supplies a source rate, which is used to space the chains out in time.

Even using the efficient techniques described, the analysis of many individual fission chains can require large amounts of computational time if the user desires to sample chain lengths with low probabilities of occurrence. To expedite the calculation, *Chain* has been written to take advantage of multiple processor machines. *Chain* divides the requested number of source neutrons evenly among the available processors. The chain-length and noise analysis data are only collected after each processor completely propagates its assigned source neutrons. Limiting the communication to the very start and very end provides for an almost perfectly linear speed-up.

B. MC++

The second code presented is the production code, *MC++*,[59-61] which has been modified to generate chain-length distributions and analyze neutron noise signals. *MC++* is a Monte Carlo-based code designed to solve the neutron transport equation in any arbitrary geometry. The ability to model a problem is somewhat limited by the fact that *MC++* only tracks on an Eulerian mesh. One complication encountered with this type of mesh arises when two materials share an interface within a cell. Rather than devising a scheme for averaging the material properties, the interface is modeled by a plane passing through the cell. The original volumes are preserved in the approximation along with the orientation of the materials. The algorithm allows for an indefinite

number of distinct materials within a cell. Even with this correction, a graphical view of the mesh reveals that a spherical object is faceted rather than smooth. As such, most of the test cases run involved slab type geometries since these are represented perfectly with as few or as many cells as are desired.

Unlike *Chain*, a description of *MC++* cannot be separated from its parallelism. The parallel implementation was included in the original design and directly impacts the manner in which it performs the propagation and analysis of the chains. While *Chain*'s design dictates that each chain must initiate and evolve entirely on a single processor, *MC++* does not have this luxury. *MC++* is built upon a generic physics framework called *Tecolote*[62] which is in turn based on the *POOMA*[63,64] framework. One of the early design considerations of these packages was to allow for highly resolved hydrodynamic problems in an Eulerian mesh. Because these types of problems generally involve altering the state of a physical system due to internal and external forces, the problem decomposition for a parallel implementation was chosen such that the mesh cells assigned to a processor corresponded to a contiguous portion of the modeled system. While the scheme works well for hydrodynamic applications, it poses a serious drawback for a Monte Carlo application. For these applications, having the full problem domain split among the processors is counterintuitive as opposed to having an exact copy of the problem on each processor as most Monte Carlo codes attempt to guarantee.

Tecolote's prescribed decomposition scheme limits the efficiency of *MC++* because the neutrons from a specific chain stream through the problem domain and may terminate on processors other than the one from which the source neutron originated.

The spreading is magnified as the chains increase in length and the neutron flux begins to distribute itself in the fundamental mode. Even in an isotropic, one-group problem with all source neutrons starting from a single point in space, the fission neutrons will eventually spread throughout all of the processors as they spread out in space. When a particle moves from the mesh space of one processor to that of another, its attributes must be communicated to the new processor, hampering the parallel efficiency. As might be expected, the problem is exacerbated in modeled systems that are dominated by particle streaming.

The decrease in efficiency, of *MC*++, is more than compensated for by its versatility, and by the ease with which it can be customized. For example, *MC*++ can model several different source configurations. This very important feature allows for a realistic simulation since in most real systems, the initial source distribution rarely resembles the fundamental-mode source. Most systems are driven by an intrinsic source or an external point, both of which can have a significant impact on the chain-length distribution. Hence, the ability to model these real-world distributions is a very important feature of *MC*++.

For this reason, a user of *MC*++ can specify a variety of spatial distributions. These distributions include 1) a point source at any arbitrary location internal or external to the system, 2) a uniformly distributed source bounded within specified geometric surfaces, or 3) a uniformly distributed source within any present fissile material, such as an intrinsic source. The initial energy options for the source configuration include 1) a constant value, 2) sampling from a fission spectrum, or 3) sampling from the

spontaneous fission spectrum for a variety of isotopes. The direction component also provides a few sampling schemes, but the most common is a simple isotropic scheme.

Additional options can be specified for an *MC++* run by setting appropriate input parameters on the input file. For example, if the chain-length distribution is sought during a *MC++* run, each source neutron is tagged with a random number. *MC++* uses this number to identify each fission chain uniquely. As the source neutrons cause fissions in the system, the identifier is passed along to the progeny insuring that each neutron can be traced back to the original source neutron. If a noise analysis is required, the tag is ignored, and instead, each source neutron is assumed to be uniformly spaced in time according to the specified source strength. The tag is not required in this case because each source neutron is associated with a unique "birth time" which simulates the time it appeared in the system relative to the other source neutrons, and a "track time" which stores the amount of time the neutron exists until it leaves the system. The first source neutron on the master processor begins at time, $t=0$ and the last neutron on the last processor will be set to $t=t_{last}$ where

$$t_{last} \simeq \frac{\text{Number of Total Sources}}{S_{eff}\left[\frac{{}^{1}_{0}n}{\text{sec}}\right]} \quad . \tag{III.2}$$

The source strength, S_{eff}, may be specified in the input file or selected from a store of spontaneous fission decay constants for a variety of isotopes. Naturally, the two run types are not mutually exclusive and result in neutrons with unique identifiers and the appropriate birth times.

Once the neutrons have been placed within the simulation environment, they and any fission neutrons they produce will either leave the current cell, leak from the problem, or collide with the cell material during each transport cycle in *MC++*. A transport cycle involves determining which of the events occurs for each of the neutrons that are active in the system. This decision is made after comparing the distances along the particle's flight path to the nearest cell boundary, material interface plane, and collision site. The shortest distance determines the event chosen. If the collision distance happens to be the shortest, the incident neutron is either scattered, parasitically absorbed, or absorbed in a reaction leading to fission. In the first case, the neutron has its energy and angle appropriately adjusted and continues its flight. The second case results in a the neutron being completely removed from the system unless there is the possibility for an *(n,xn)* reaction. The fission event terminates the incident neutron and adds to the neutron population the number of neutrons sampled from the neutron number distribution (i.e., which has been specified to be the modified version of Frehaut's distribution discussed in an earlier chapter).

To remain faithful to the physics of the simulation, all the collisions are treated in an analog Monte Carlo fashion. As such, there are currently no variance reduction techniques employed to improve statistics. However, given the nature of the problem, it is not yet clear how such techniques could be applied while preserving the underlying stochastic phenomena.

Consequently, *Chain* requires system-averaged parameters such as K, $\bar{\nu}_p$, and τ, but in *MC++*, the collision physics are based on the nuclear cross sections requested in

the input file. (For the current version of *MC++* the cross sections must be in a multi-group format as the continuous energy cross sections have not been fully implemented.) During the problem setup stage, the total microscopic cross section for each material is computed from the constituent isotopes. The probability of interaction per unit path length is found by multiplying the microscopic cross section by the material density stored in the local mesh cell. The particular isotope chosen is based on a random number and the relative contribution of each of the individual isotopes to the total cross section. Another step required during the setup is to construct a Frehaut distribution table for each energy group's $\overline{\nu}_p$ for each isotope.

The computational process is slightly different and more complicated if the user desires to produce a chain length distribution for a particular system. In this case, the unique identifier of the source neutron is passed to each neutron that it produces from fission or inelastic scattering. After each event that produces neutrons, the counter associated with the initiating neutron's identifier is incremented. At the end of each transport sweep, the list of chain lengths is passed through. Of course, as nature would have it, as K nears 1.0, the probability for seeing nearly infinite-length chains becomes more distinct. However, the *MC++* simulation is constrained by the memory available on the executing host. For this reason, a maximum chain length is specified. Any chain that exceeds this value is recorded, and the currently present members of this chain are removed from the simulation. This process has been separated from the noise analysis (although they can be run simultaneously) because of the large amount of

communication required after each sweep for the code to know exactly how many neutrons are still "alive" in each chain.

C. Analytic Cross Sections

An important goal of this work is to compare the results from the zero-dimensional and three-dimensional codes. Given the obvious difference in their handling of spatial effects, a valid comparison of results from two such codes hinges on the ability to construct problems that are as physically similar as possible. This objective implies constructing a three-dimensional system for *MC++* that has identical system parameters to those supplied to *Chain*. Of the parameters of interest, the chain-length distribution and the g^* calculation are sensitive to differences in the system's *K*. In C*hain*, this value is supplied directly, but in *MC++*, it must be computed.

As is the case with any Monte Carlo code, *MC++*'s determination of the neutron multiplication factor is actually dependent on many individual collisions and neutron tracks occurring over a series of independent transport cycles. The energy and angular dependence of the solution appear as a result of the nuclear data used to sample the collisions. The data also determines the appropriate interpretation of the multiplication factor. If the data provides $\overline{\nu}_{prompt}$, the factor is the prompt multiplication factor, *K*, whereas $\overline{\nu}_{total}$ yields the traditional *k*. The location of materials within the problem and the density of the collisions determine the spatial dependence. As might be expected, the sampling of the individual events leads to an estimate for the neutron multiplication factor that has an associated uncertainty whose magnitude is determined by the number

of histories compiled. Similar to reducing the variance in the multiplicity, using a single energy group reduces the variance in a *k*-eigenvalue solution, but reducing the variance associated with the spatial effects is considerably harder. As such, it would be difficult, ad hoc, to construct a problem that has a *K* exact to many decimal places.

For this reason, the reference problems have been constructed according to the specifications that accompany a set of analytical cross sections.[65] The analytical cross sections were specifically formulated for use with analytical benchmark problems to be solved using deterministic and stochastic transport codes that compute static *k*-eigenvalues. Based on analytic solutions of the transport equation, these cross sections make it possible to compare the zero-dimensional and three-dimensional codes. In the simple geometries for which they are valid, these cross sections provide *k*-eigenvalues of exactly 1.00000. These problems include both bare and water-reflected systems comprised of infinite cylinders, spheres, and right circular cylinders. Although MC++ is capable of modeling any of these geometries, the infinite slab case has been selected because it can be exactly modeled in the computational mesh available in *MC++*. The curved surfaces associated with the other geometries require a large number of mesh cells to reduce the effects cause by the resulting faceted surfaces. The majority of the *MC++* runs were done with cross sections from the mock plutonium set with the $\bar{\nu}_p$ adjusted as necessary to obtain a range of analytic *K*'s less than 1.0. The plutonium data appears in Table IV.

TABLE IV

Analytic cross section set corresponding to Pu.

$\bar{\nu}$	Σ_f	Σ_c	Σ_s	Σ_t
3.24	0.0816	0.019584	0.225216	0.8264

D. Noise Analysis in MC++

The neutron sources are divided into a series of batches. This option has been adopted to avoid memory limitations encountered when following millions of neutrons through the simulation. By batching, the limitation shifts to how long it takes to run a sufficient number of batches to acquire the required statistical uncertainties. To faithfully reproduce the signal in a detector, the source neutrons in a batch are randomly spaced in time according to the source rate.

When there are no longer any neutrons in the simulation, the processors communicate their pulses to the master processor (Node 0). The pulses represent the simulated detector response to the neutron events that occurred on a processor, and they are stored as a list of times at which the detected events occurred. The events themselves may represent fissions, captures, or escapes depending on the simulated detector type. The master processor sorts the pulses in ascending order in time. It then divides the total number of pulses by the number of processors in the simulation. What happens next depends on the type of noise analysis technique desired. Even in an actual Rossi-α experiment, it is impossible to know beforehand exactly when each chain begins

and ends. If two or more chains happen to overlap, there is no ideal way to differentiate the beginning of a particular chain. For this reason, each processor receives a nearly complete copy of the pulse stream from the master processor. The only difference is that each processor receives a chain that begins farther along the sequence. In this way, all the processors have access to the downstream pulses required to construct the most possible correlated pairs. This elaborate scheme would not be necessary for a simulation of a pulsed neutron experiment since the pulses are only compared against their neighbor. Splitting the pulses across the N-processors would only result in the loss of N-1 pulse comparisons.

E. Handling the Background Noise

Although the conglomeration of each chain's contribution into a single pulse stream is identical to what happens in actual experiments, it adds another element of complexity to interpreting the signal. The resulting pulse stream contains a potentially high number of uncorrelated pulses that arise from comparison of pulses from separate chains. Fortunately, this background noise can be handled by *MC++* in the same fashion that it is handled in an actual experiment. In both cases, its magnitude can be found by taking the total number of counts recorded in the detector and dividing by the total time spent counting.

$$\text{Average Count Rate} = \frac{\text{Number of Pulses}}{\text{Elapsed Counting Time}}$$

This average count rate is the theoretical background signal and must be subtracted from each channel before determining the slope and intercept. A poorly resolved Rossi-α simulation can identified by the large number of channels near this background threshold. Although it takes a large number of counts to accurately resolve this value, it is often many orders of magnitude less than the initial channels of a Rossi-α, so the impact on the intercept and slope may be minimal. Figure 10 shows the simulated output of a multichannel analyzer as it converges to the background in *MC++*. The first hundred channels have been left off to emphasize the oscillations in the background-dominated tail. As the simulation progresses, the tail smooths out as its oscillations about zero decrease.

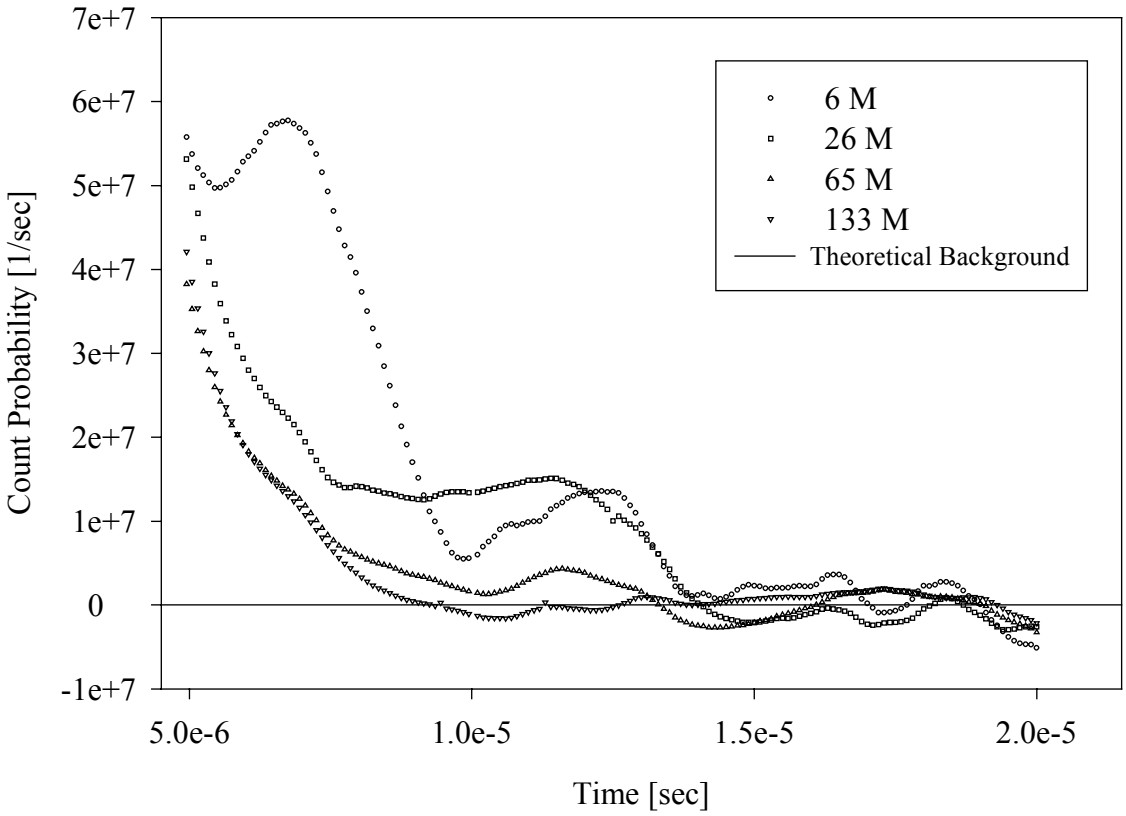

Figure 10. Resolving the background noise threshold.

CHAPTER IV

NUMERICAL RESULTS

The purpose of this chapter is to present the results of some chain-length distribution calculations performed by *Chain* and *MC++* for a variety of prompt neutron multiplication factors and source configurations. However, to lend credence to the results, the point model code is validated by showing that the chain-length distribution produced by *Chain* yields the correct subcritical prompt multiplication, M_p, for a specified prompt multiplication constant, K. Validation of the more complex three-dimensional code, *MC++*, will be performed by making a direct comparison to results from the point model code, *Chain*. Following this validation, it will be shown how the contribution of the longest chain lengths becomes negligible when estimating the subcritical prompt multiplication and when performing neutron noise analysis. A series of chain-length distributions have been generated to identify the factors that have the greatest effect on the distributions. After illustrating the general form and sensitivities of the chain-length distribution to the most important factors, the critical role that the fission chains play in common neutron noise analysis techniques is examined. This chapter concludes by showing how *MC++* reproduces the multiple prompt decay modes that arise because of harmonic effects in highly subcritical systems and because of spatial effects in finite multi-region subcritical systems. It will be shown that detailed information regarding the fission chains is an essential key to understanding and predicting the neutron noise signal that might be observed in subcritical experiments.

A. Code Validation

Although *MC++* has been benchmarked against the widely used Monte Carlo code, *MCNP*, the comparisons have been limited to static k and α eigenvalue problems.[60] The current version of *MCNP* does not follow individual fission chains and, as such, precludes any direct comparison of the chain-length distribution calculated by the two codes. Nevertheless, the chain propagation algorithms in *MC++* have been benchmarked against the chain-length distribution calculated by the zero-dimensional code, *Chain*. Furthermore, the analytic cross sections have been used to verify the particle interaction physics in *MC++* with regards to *k*-eigenvalue calculations.

Because *Chain* is a point model, it is assumed that the source neutrons are distributed as an EFM source, and consequently, they have a common probability for inducing fission. If one follows the branching chains shown in Figure 6, it is possible to construct a family of branches that result in a single chain length. Several of the shorter paths have been combined with the results from Frehaut's multiplicity distribution to construct an analytical benchmark for problems with known chain-length distributions. Tables V and VI show that the chain-length distributions generated by *Chain* are accurate regardless of the initial K or $\bar{\nu}_p$.

TABLE V

Comparison of analytic solution and point model Monte Carlo Solution for K=0.3 with $\bar{\nu}_p$=2.268 for chain lengths 1 through 7.

	***K* = 0.3**	
Probability	**Analytical**	***Chain***
P(1)	0.875607	0.875607
P(2)	0.022522	0.022522
P(3)	0.034638	0.034638
P(4)	0.027241	0.027241
P(5)	0.013217	0.013217
P(6)	0.007995	0.007995
P(7)	0.0056756	0.0056756

TABLE VI

Comparison of analytic solution and point model Monte Carlo solution for K=0.99 with $\bar{\nu}_p$=3.2076 for chain lengths 1 through 7.

	***K*=0.99**	
Probability	**Analytical**	***Chain***
P(1)	0.692995	0.692993
P(2)	0.012044	0.012044
P(3)	0.032204	0.032205
P(4)	0.035953	0.035953
P(5)	0.023561	0.023561
P(6)	0.0151272	0.0151268
P(7)	0.0127485	0.0127484

B. Effects of Prompt Multiplication Factor, K

Besides providing an analytic solution for the probability of obtaining fission chains of a certain length, a Bayesian analysis can also be used to explain the irregular

behavior observed in the chain-length distributions plotted in Figure 11. In this figure, plots are shown for the chain-length distributions associated with a variety of *K* and $\overline{\nu}_p = 2.268$. Although the portion of the distribution associated with the shorter chain lengths appears discontinuous and inconsistent with the remainder of the distribution, the probabilities match exactly with the results predicted by the Bayesian analysis. As predicted, the most probable chain length is 1.0, which corresponds to a source neutron that does not produce any subsequent fission neutrons. Similarly, the dip at *L=2* is expected since a chain length of two can only occur if the source neutron undergoes a fission in which only a single neutron is released. According to Frehaut's multiplicity distribution, the likelihood of this happening is slightly less than a fission event in which 2 or more neutrons are released.

The tails of the distributions are not so easy to describe analytically since the potential number of paths becomes very large, making an analytic solution derived from Bayesian statistics impractical. Nevertheless, there is some confidence that certain characteristics of the chain-length distribution can be inferred without the benefit of an analytic solution. For example, it is noteworthy that as *K* increases, each distribution exhibits an asymptotic behavior at the longer chain lengths. Although the distribution does not indicate the presence of an absolute maximum chain length, it does indicate that that chain lengths farther along the asymptotic tail are highly improbable. For *K=0.3*, the probability of seeing a chain length of 105 neutrons is $1 \cdot 10^{-13}$. For *K=0.999*, this same probability is associated with a much longer chain length of approximately $3 \cdot 10^{7}$ neutrons. Although the probabilities for very long chain lengths are difficult to

determine accurately because of their rarity, this rarity corresponds to a vanishingly small effect on the system performance.

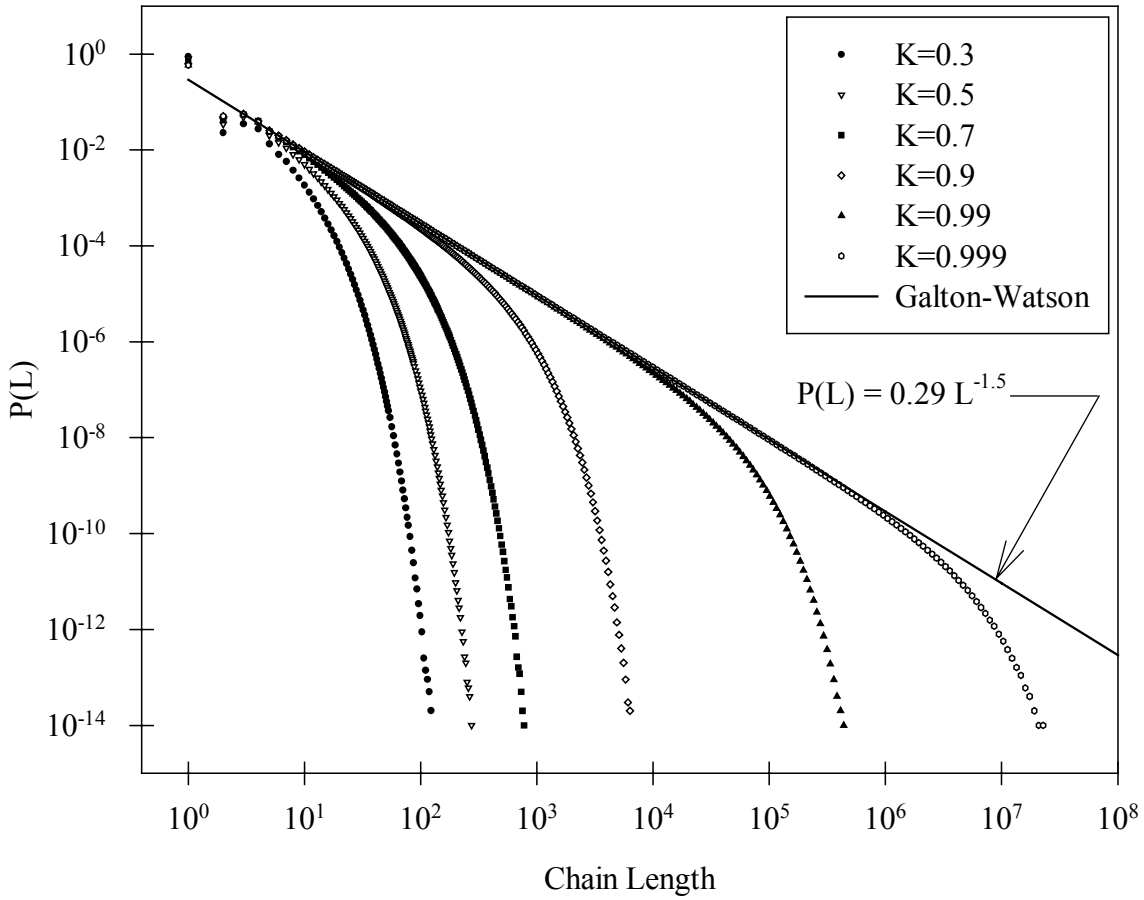

Figure 11. Chain-length distributions for select values of *K*.

Figure 11 also shows that as *K* increases, the probability for observing all chains with lengths greater than 1 increases. As expected, as $K \to 1.0$, the average chain length approaches infinity. The reason why the probability of observing a chain length of *L=1* decreases as *K* increases can be easily seen from the analytical solution for $P(1)$,

$$P(1) = \left(1 - \frac{K}{\bar{\nu}_p}\right) + \frac{K}{\bar{\nu}_p} P_0 \quad .$$

As K increases, it is also apparent from the above Figure 11 that larger portions of each distributions follow the Galton-Watson approximation, which predicts that the probability of obtaining a chain of length L varies as,

$$P(L) = C \cdot L^{-1.5} \quad .$$

The particular solution of the Galton-Watson problem corresponds to the case in which *K=1.00*, and implies that a prompt-critical system will have a finite probability generating a chain of nearly infinite length. As observed in the numerical solutions, the quantity C in this equation is slightly dependent on K. However, to a first approximation, C can be taken to be approximately equal to 0.29.

Unless otherwise noted, the figures in this section are based on results from a series of *Chain* runs that are described in Table VII. The decrease in the number of source neutrons was an unavoidable consequence of the 6-hour *runlimit* imposed on the ASCI Blue Mountain computer at Los Alamos National Laboratory. In *Chain*, the majority of the computation time is expended calling the random number function. Consequently, a limit on the total computation time directly limits the total number of neutrons that can be tracked and not the number in the source itself. With this in mind, each run was designed to last 5 hours running on 1008 processors except for the case with *K=0.5* in which the number of processors was doubled. The 5-hour limit was chosen because the queuing system on the machine terminates any process that exceeds the current 6-hour limit. The limitation on the runtime resulted in chain-length

distributions at higher *K* that are not as thoroughly sampled as are those at lower values of *K*. The lack of resolution in the chain-length distribution is readily apparent in the increasing uncertainty in the estimate for the subcritical prompt multiplication. Even with the just-noted limitations, all of the runs were able to follow a large number of chains revealing much of the structure in the low-probability tail. Later in this chapter, the chain-length distributions resulting from these *Chain* runs will be presented as plots labeled as EFM.

TABLE VII

Multiplication obtained during various *Chain* simulations.

K	**#Sources**	**Tracked**	**Analytic M**	**Computed M**
0.3	1.08e13	1.54e13	1.4285714	1.428571723
0.5	1.50e13	3.00e13	2.0	2.000000157
0.7	5.00e12	1.66e13	$3.\overline{333}$	3.333334098
0.9	1.66e12	1.66e13	10.0	10.00001108
0.99	1.66e11	1.66e13	100.0	100.0016458
0.999	1.66e10	1.66e13	1000.0	1000.135725

As mentioned in the previous section, the chain-length distribution is directly related to the subcritical prompt multiplication of the system. Figure 12 shows that the integral of the chain-length distribution asymptotically becomes equal to M_p of the system. Because of the binning technique used, which was described in a previous chapter, the integration to obtain the integral chain length was performed according to Eq. (IV.1).

$$M_p = \sum_{i=0}^{NumBins} P_i \cdot L_i \cdot BinWidth_i \qquad \text{(IV.1)}$$

Moreover, the subcritical prompt multiplication predicted by the above integral chain length can be compared to the subcritical prompt multiplication computed analytically from the user supplied *K* in order to verify the algorithm performance. For this reason, the *K* values were chosen such that their corresponding *M*'s are whole integers that are easily identifiable on the plots presented in Figure 12.

The plots in Figure 12 also reveal an interesting property related to the importance of the integral contributions of the chain lengths located along the asymptotic tail. Without exception, each of the curves reached the final subcritical prompt multiplication value (to a first approximation) without inclusion of the last decade or so of lengths in the integral. From this observation, it can be concluded that although the longest chains considered had lots of neutrons in them, their presence does not significantly effect the multiplication of the system since they so rarely occur. In addition, inclusion of even longer chain lengths will have negligibly small effects on the computed subcritical prompt multiplication.

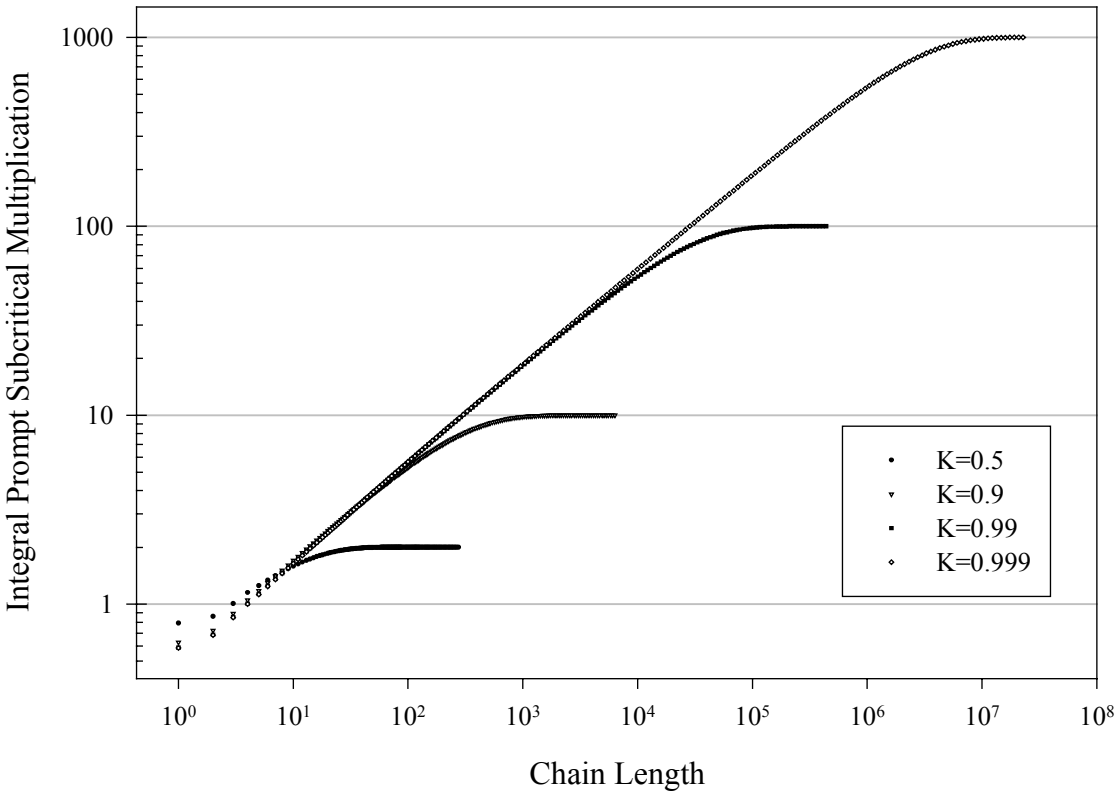

Figure 12. Integral of the chain-length distribution showing its relationship to the subcritical prompt multiplication, M_p.

The lack of importance of the longest chains to these calculations is also apparent in Figure 13, which provides another way to look at the contribution of the longest chain lengths, i.e., those located in the tail of the chain-length distribution. Instead of looking at the integral contribution of all of the chains, in Figure 13 the chain length, L, has been multiplied by the probability of its occurrence. In this figure, it is possible to readily see which chains contribute the most to the subcritical prompt multiplication process. There are two conclusions that can be drawn from Figure 13. First, the vast majority of the

subcritical prompt multiplication of a system is produced by small-to-intermediate length chains that occur with relatively high probability. And, in accordance with previous conclusion, the longest chains in the distribution simply do not affect the subcritical prompt multiplication due to their rarity. Although the chain lengths at *K=0.99* extend past a length of 10^5 neutrons, ignoring the contribution of the chains past a length of 10^4 neutrons would only result in a 2% error in the final estimate of the subcritical prompt multiplication.

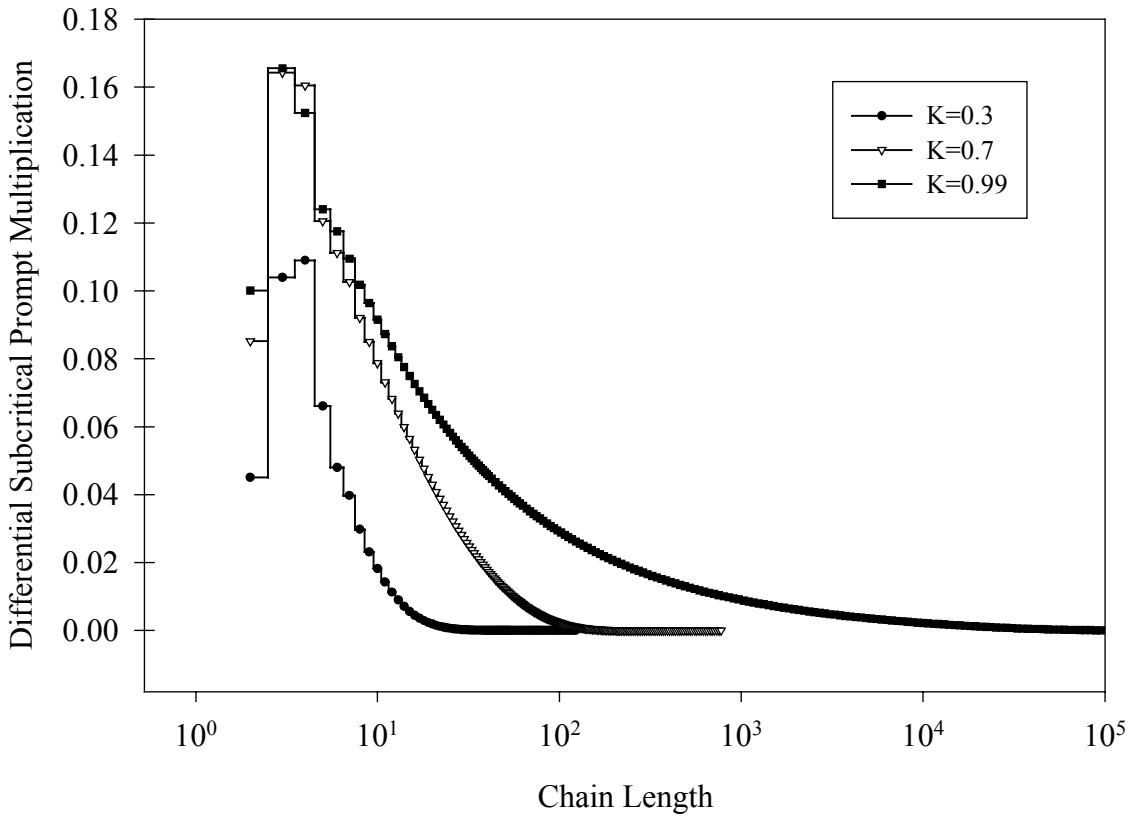

Figure 13. Differential subcritical prompt multiplication contribution of chain lengths $L>1$ for various K.

C. Effects of Multiplicity Distribution

As briefly mentioned earlier, the type of neutron multiplicity employed to generate the fission chains has a significant impact on the chain-length distribution. The influence is most noticeable for the shorter chain lengths because of the limited number of paths a chain may take. Any perturbations at either end of the chain-length distribution must be compensated elsewhere to keep the subcritical prompt multiplication constant. Thus, a non-physical representation of the neutron multiplicity can have an unusual effect, the magnitude of which depends on the value of *K*. In Figure 14, one chain-length distribution was computed using a binary distribution (i.e., either 2 or 3 neutrons are released per fission as assumed in analog *MCNP*), and the other distribution was computed using the more realistic Frehaut distribution. For both cases, *K=0.5* and $\overline{\nu}_p = 2.268$. The former chain-length distribution shows some initial oscillations for the chain lengths around 7-10 neutrons, which are quickly damped. Because the prompt multiplication constant, *K*, of the system was specified to be identical in both cases, the area under the two curves must also be identical. Consequently, an increase in the chain length probabilities at one end of the chain-length distribution must be offset by a decrease in the probabilities at the opposite end. In conclusion, when simulating the evolution of fission chains using Monte Carlo techniques, one should strive to model the neutron multiplicity as accurately as possible in order to avoid skewing the resulting chain-length distribution.

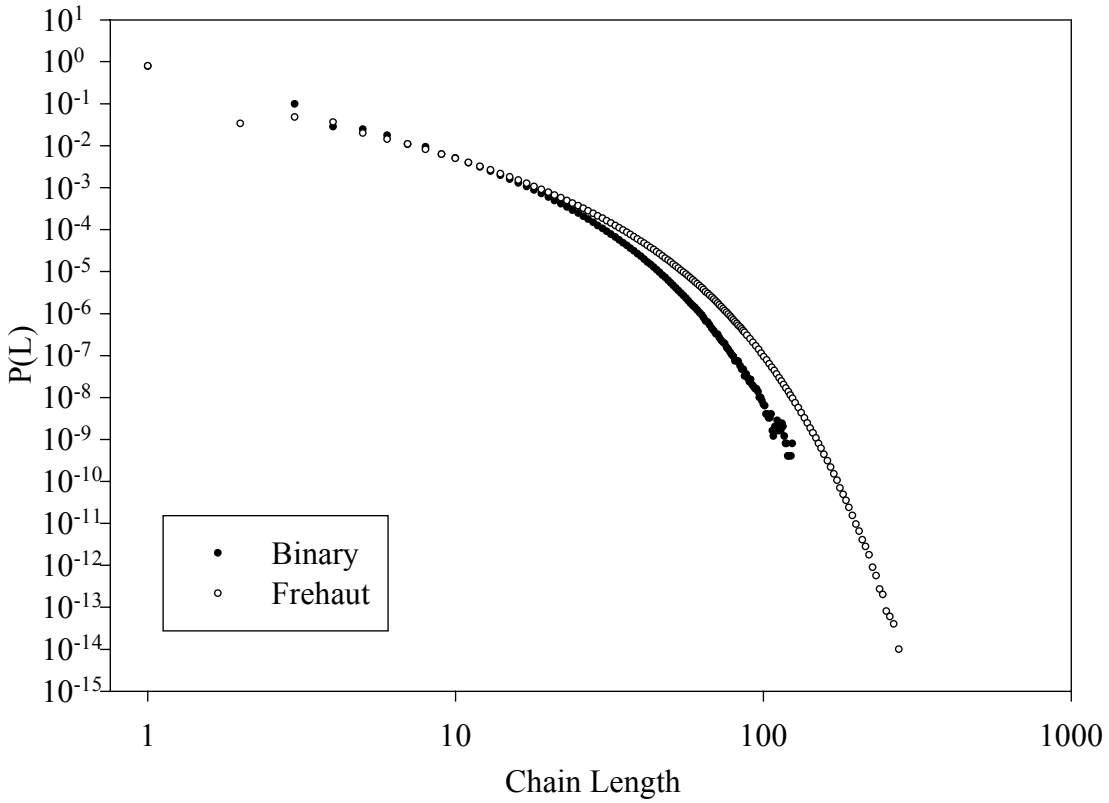

Figure 14. Effect of neutron multiplicity on the chain-length distribution in a highly subcritical system. (K=0.5 and $\bar{\nu}_p$=2.268.)

In the chain-length distributions shown in Figure 15, the value of $\bar{\nu}_p$, i.e., 3.2076, is slightly higher that that used in Figure 14, resulting in even larger oscillations. These oscillations appear to disappear at $L=30$ and $P(L) = 7 \cdot 10^{-3}$. The chain-length distribution generated using the simplified multiplicity overpredicts the probability of observing longer chains when compared to the distribution generated using Frehaut's neutron multiplicity.

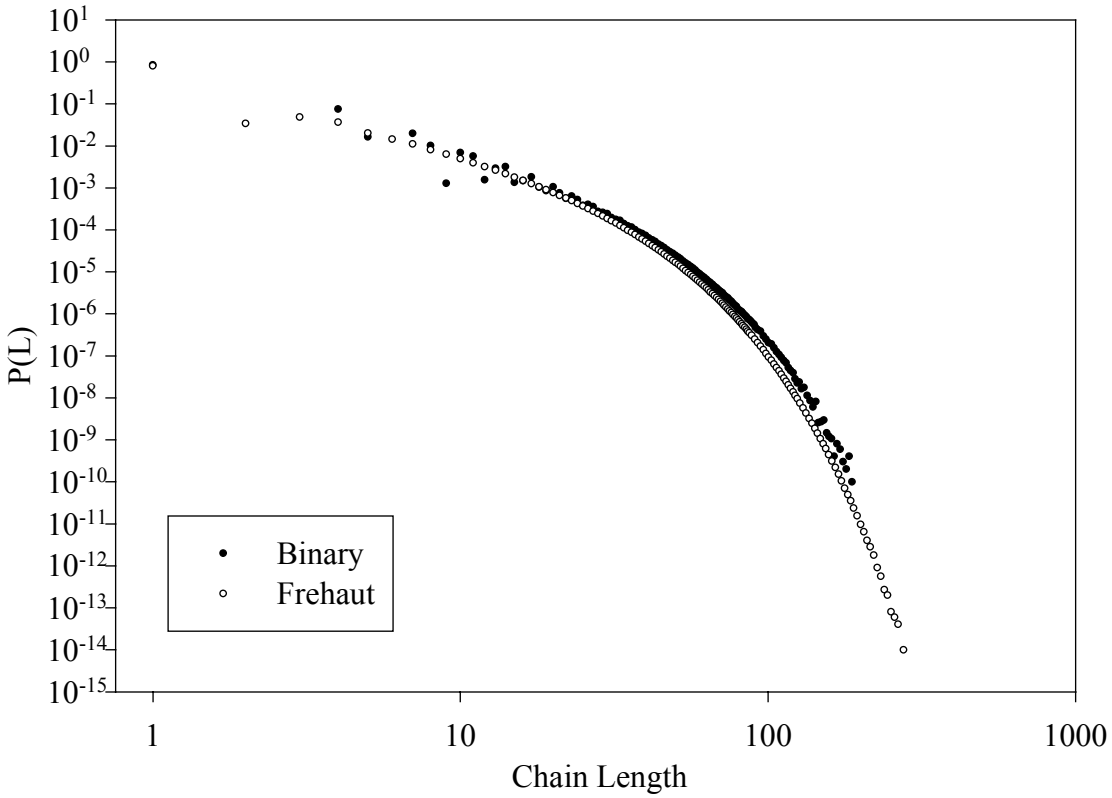

Figure 15. Effect of neutron multiplicity on the chain-length distribution in a highly subcritical system. (K=0.5 and $\bar{\nu}_p$=3.2076)

When the value of K is increased, the effect on the chain-length distribution appears to be minimal though it is nevertheless observable (see Figure 16). In this case, the distribution appears to overpredict the mid-range chain lengths while it under predicts the longest values. Similar to the previous example that used the lower value of $\bar{\nu}_p$, the oscillations die out quickly.

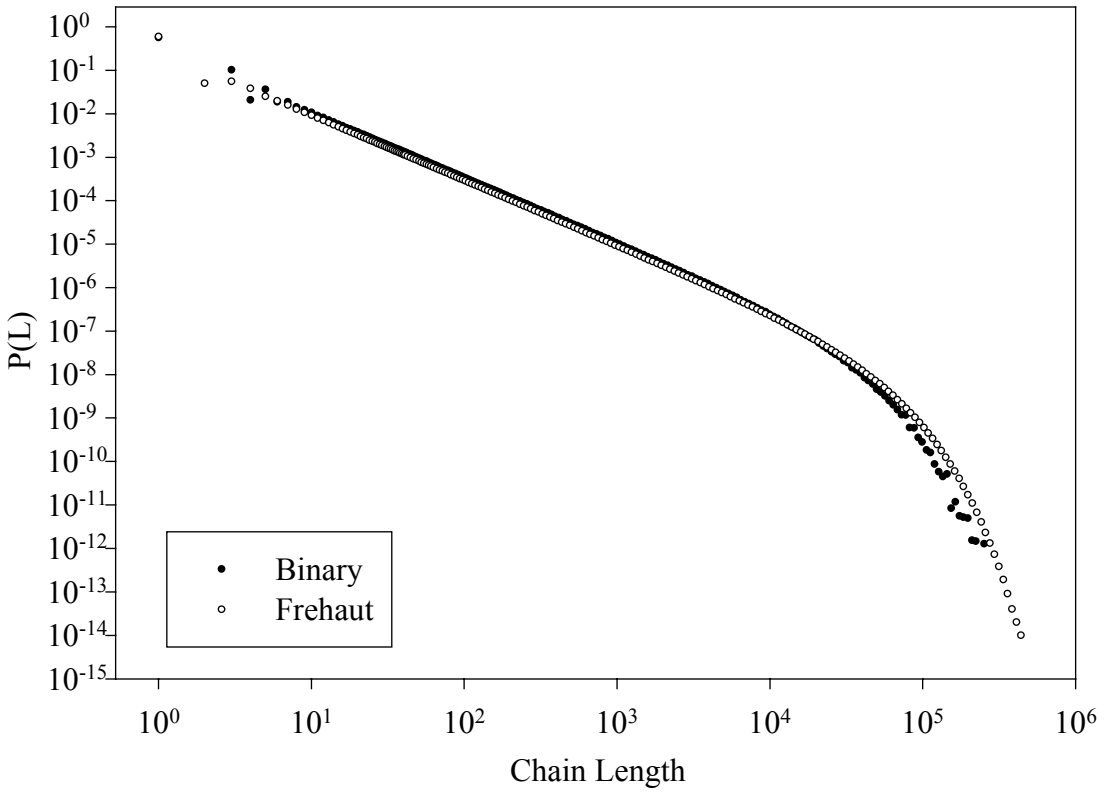

Figure 16. Effect of neutron multiplicity on the chain-length distribution in a slightly subcritical system. (K=0.99 and $\bar{\nu}$ =2.268.)

For the case shown in Figure 17, the value of $\bar{\nu}_p$ is increased. As can be noted there, the oscillations are very noticeable and continue out to about the same lengths as they did for the case in which *K=0.5*. In this example, the distribution appears to overpredict the mid-range chain length probabilities while under-predicting the probability of occurrence of chain lengths in the tail. Although it is unclear how this non-physical behavior would influence a neutron noise analysis, such as a simulation of a Rossi-α

measurement, its alteration of the fission chain length variance may have a noticeable effect in techniques such as the Feynman's variance-to-mean method.

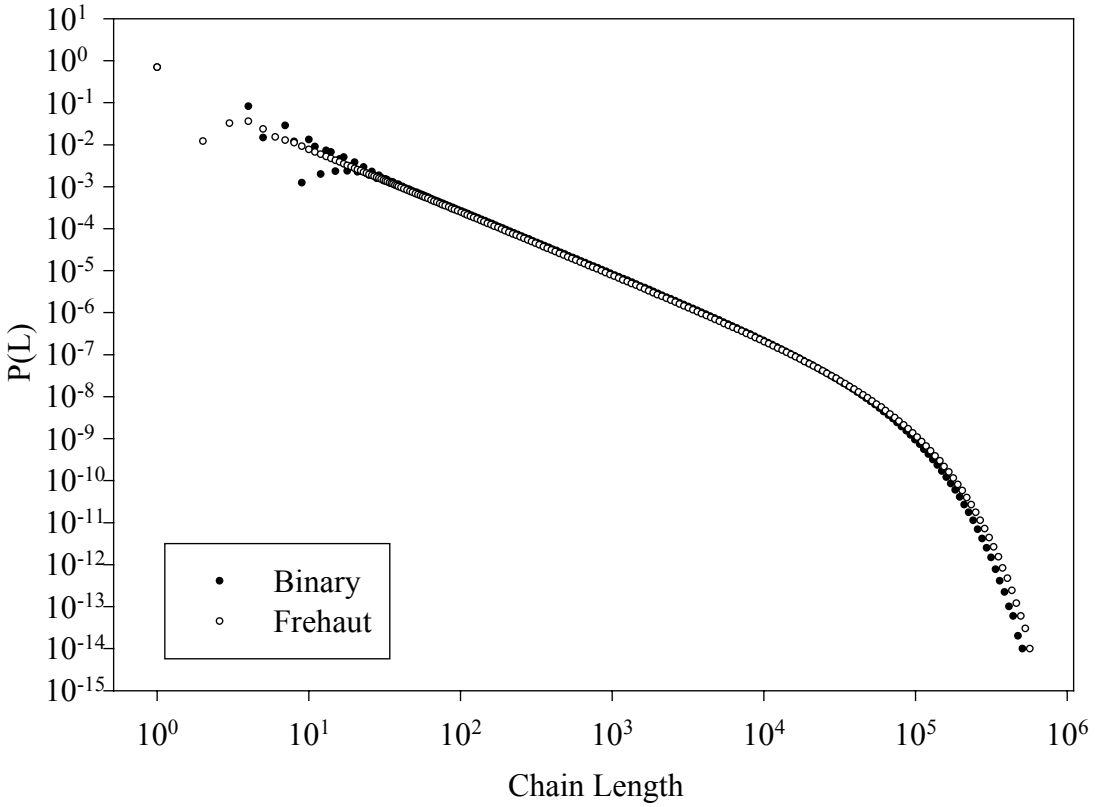

Figure 17. Effect of neutron multiplicity on the chain-length distribution in a slightly subcritical system. (K=0.99 and $\bar{\nu}_p$=3.2076)

D. Effects of Average Prompt Multiplicity, $\bar{\nu}_p$

In addition to the effect on the chain-length distribution resulting from the neutron multiplicity, the magnitude of $\bar{\nu}_p$ has a substantial impact on the chain-length distribution curve. In Figure 18, the resulting chain-length distributions are compared

for a K=0.5 with $\bar{\nu}_p$ equal to 2.268 and 3.2076. As expected, the P_f for each EFM neutron decreases with increasing $\bar{\nu}_p$. That is,

$$P_f = \frac{K}{\bar{\nu}_p} \quad .$$

Because the probability of a neutron loss varies as $\left(1 - P_f\right)$, it then follows that the probability of observing chains with lengths of 1 (L=*1*) will increase with an increase in $\bar{\nu}_p$. Furthermore, while *P(1)* increases, the numerical simulation simultaneously predicts that the probability of seeing short chains (i.e., 2, 3, 4, etc.) decreases as $\bar{\nu}_p$ increases. The longer chains are more likely in this case because the number of neutrons per fission is increasing resulting in slightly longer chains. When the chain-length distributions for the two different values of $\bar{\nu}_p$ are compared, it is noted that for the case with the higher value of $\bar{\nu}_p$ the probability of spawning chains with long lengths is higher than for the case with the lower value of $\bar{\nu}_p$. This increase must occur in order to offset the differences in the chain-length distribution at low values of L (i.e., the areas under both curves are identical). A more physical way of expressing this idea is to see that in both cases the total number of fissions is roughly constant. For a fixed value of K, a higher $\bar{\nu}_p$ results in more neutrons being released per fissions, but this is offset by the decrease in the probability that they will cause other fissions.

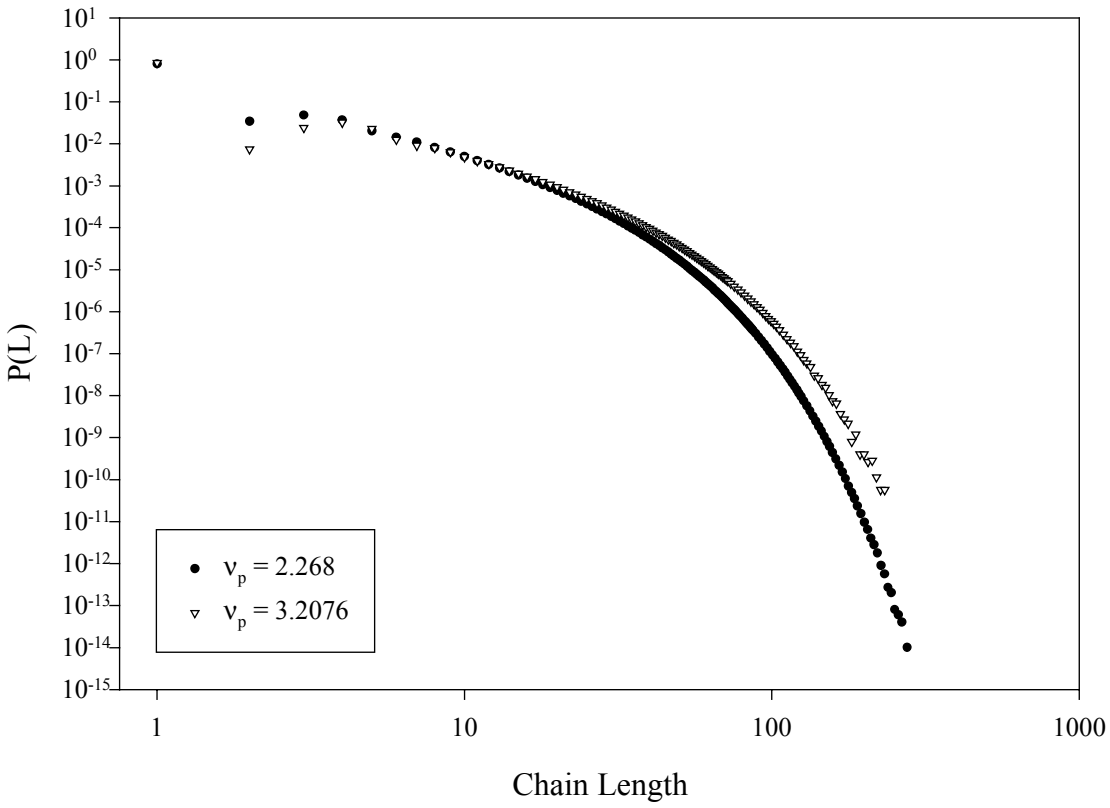

Figure 18. $\overline{\nu}_p$ effects on the chain-length distribution at K=0.5.

When cases with a higher K and the two values of $\overline{\nu}_p$ are considered, it reveals a noteworthy trend in the chain-length distributions at the intermediate lengths (see Figure 19). Keeping in mind that the prompt multiplication, K, is identical for both cases, one might expect that the higher value of $\overline{\nu}_p$ would show higher probabilities for all but the shortest chain lengths. However, Figure 19 shows that for the majority of the chain lengths, the higher $\overline{\nu}_p$ actually results in lower probability of occurrence values, $P(L)$, except near the tail of the distribution at large chain lengths. In this case, the

probabilities of occurrence for the chain lengths in the tail of the distributions are expected to have discernable impacts on the subcritical prompt multiplication calculations.

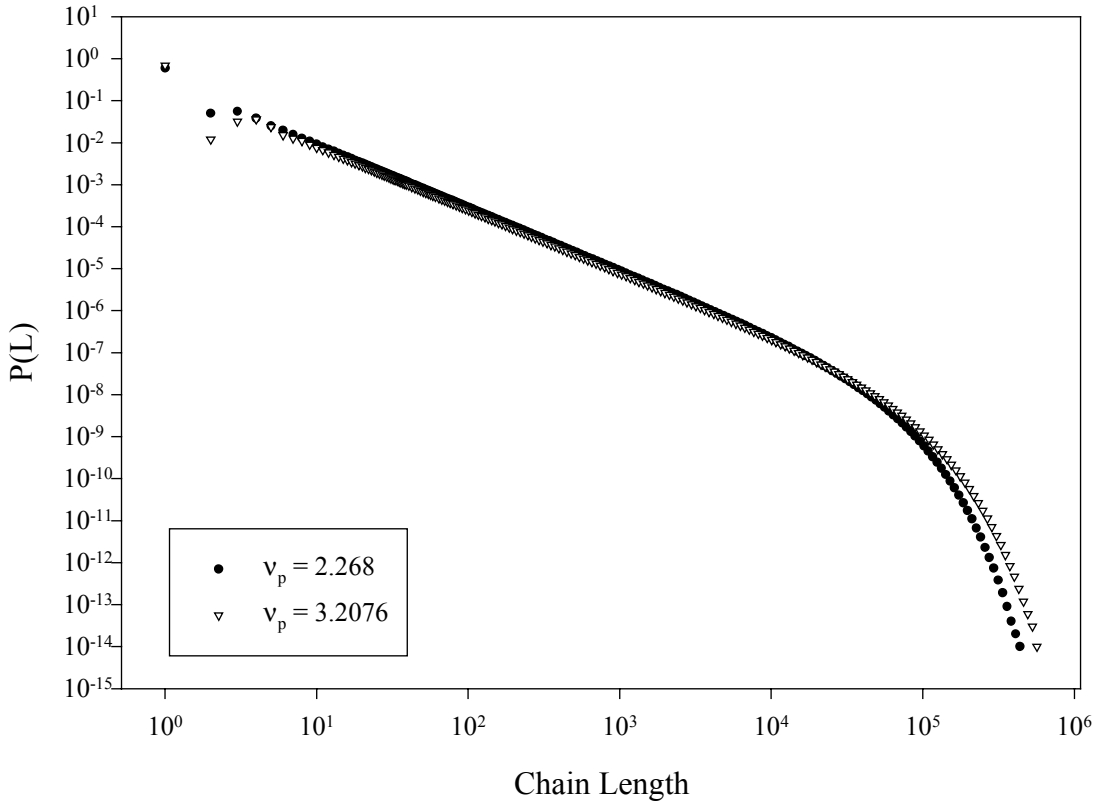

Figure 19. $\bar{\nu}_p$ effects on the chain-length distribution at K=0.99.

Although, it might not be clear from Figure 19 how the tail contribution could be sufficient to guarantee the same subcritical prompt multiplication, the similarity becomes evident in Figure 20. The integral of the distributions is shown there, and it demonstrates that the distribution corresponding to $\bar{\nu}_p = 2.268$ reaches its asymptotic

value sooner than the distribution corresponding to $\bar{\nu}_p = 3.2076$. In this representation, it can be concluded that it is essential to sample the entire chain-length distribution, including the very long chain length values to insure the accuracy of the parameters of interest.

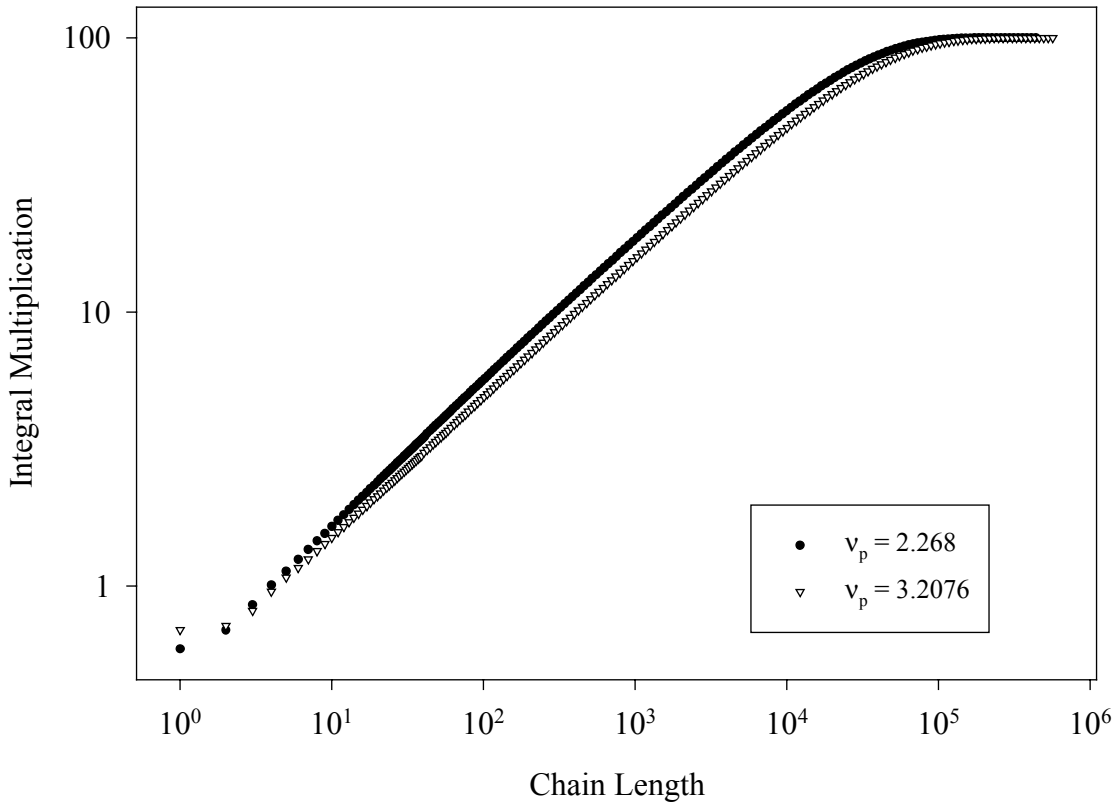

Figure 20. $\bar{\nu}_p$ effects on the integral subcritical prompt multiplication.

E. Effects of the Initial Source

The data appearing in the preceding figures were all produced using *Chain*, which is a zero-dimensional model and, as such, is unable to predict spatial effects.

Nevertheless, spatial effects are always present in any real experiment, and their inclusion is indispensable to accurate computational simulations. In order to study spatial effects on the chain-length distribution, the three-dimensional Monte Carlo code, *MC++*, described in Chapter IV was used. In this section, it is shown how the chain-length distribution changes as a function of the source configuration that drives a multi-dimensional system. Three different source configurations were studied: 1) a point source, 2) a uniformly-distributed, volumetric source, and 3) an equivalent fundamental-mode (EFM) source. The results that are associated with the EFM source generally have smaller statistical uncertainties than the results for the volumetric and point sources since it was possible to sample a greater number of particles in a fixed amount of time when the simpler, EFM model was used. Each of the cases presented in this section was run for a homogeneous, slab reactor. A set of analytical, one-energy group, cross sections was adjusted to match the *K* for the slab to that used in *Chain*.

Figure 21, the first in this series, shows the results for a $K=0.7$ and focuses on a representative portion of the chain-length distribution. This plot shows the $P(L)$ distributions for a point source, EFM source and a volumetric source. The $P(L)$ corresponding to the point source lies above the other two, which is expected since the source neutrons are born at the center of the slab, and, as such, have a higher probability for causing a fission before leaking from the system. The next highest line corresponds to the EFM distribution. Because the fundamental mode in a slab reactor resembles a chopped cosine function, most of the EFM source neutrons are born near the center of the reactor, but there are a significant number of births near the edge of the slab. The

lowest curve belongs to the volumetric source which has even fewer source neutrons started near the center of the slab and more born near the edges.

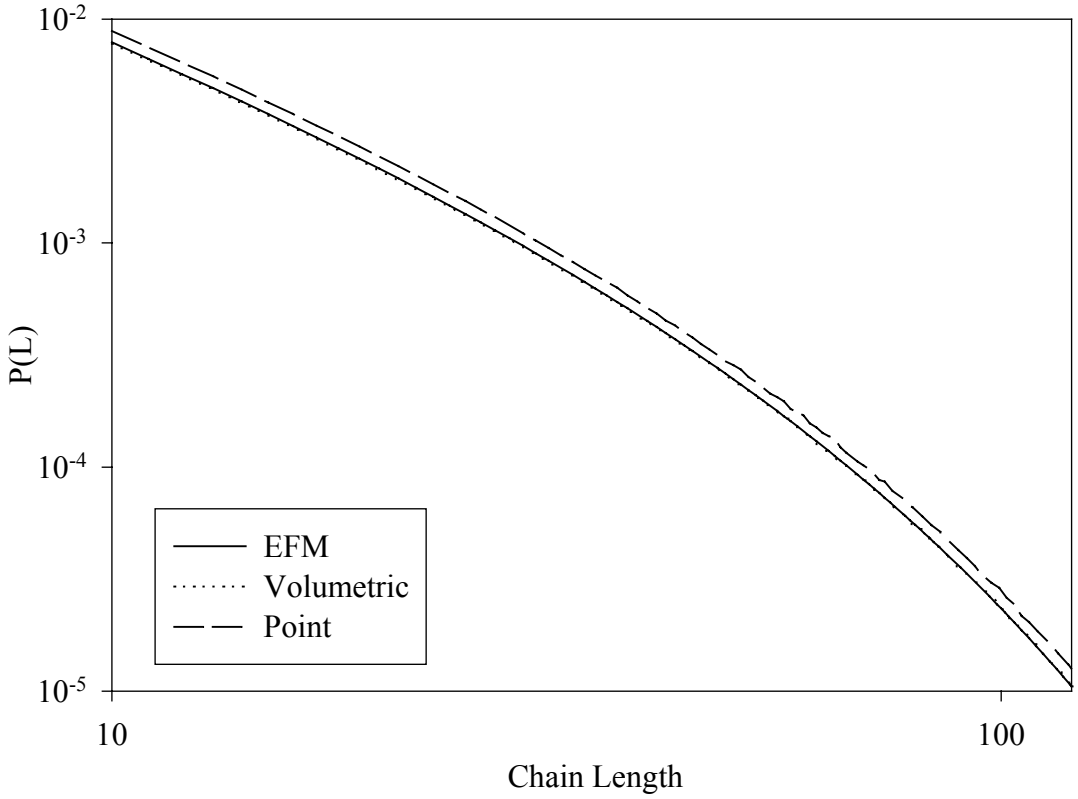

Figure 21. Spatial effects on the chain-length distribution caused by the source configuration. (K=0.7)

When K is increased to 0.99, the same relative positions of the three chain-length distribution are observed (see Figure 22).

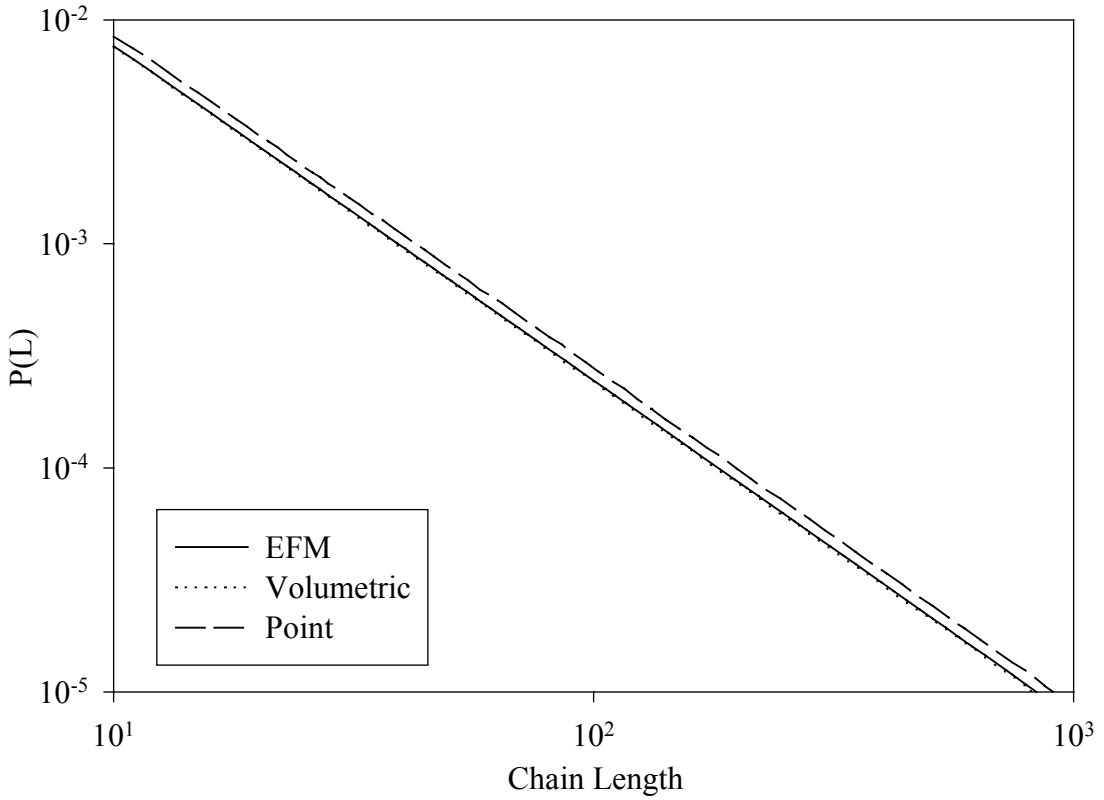

Figure 22. Spatial effects on the chain-length distribution caused by the source configuration (K=0.99)

Unlike the results presented in the previous sections that demonstrated the effects on the chain-length distribution associated with changes in $\bar{\nu}_p$ and the neutron multiplicity, the subcritical prompt multiplication of the slab is not identical for the three different source configurations. This difference is readily apparent when one integrates the chain-length distribution produced by the three source configurations (see Figure 23). As can be seen there, each source distribution leads to a different asymptotic value

for the subcritical prompt multiplication. Only the EFM source agrees with the analytic value, $M_p=3.333\ldots$ predicted by,

$$M_p = \frac{1}{1-K} \quad .$$

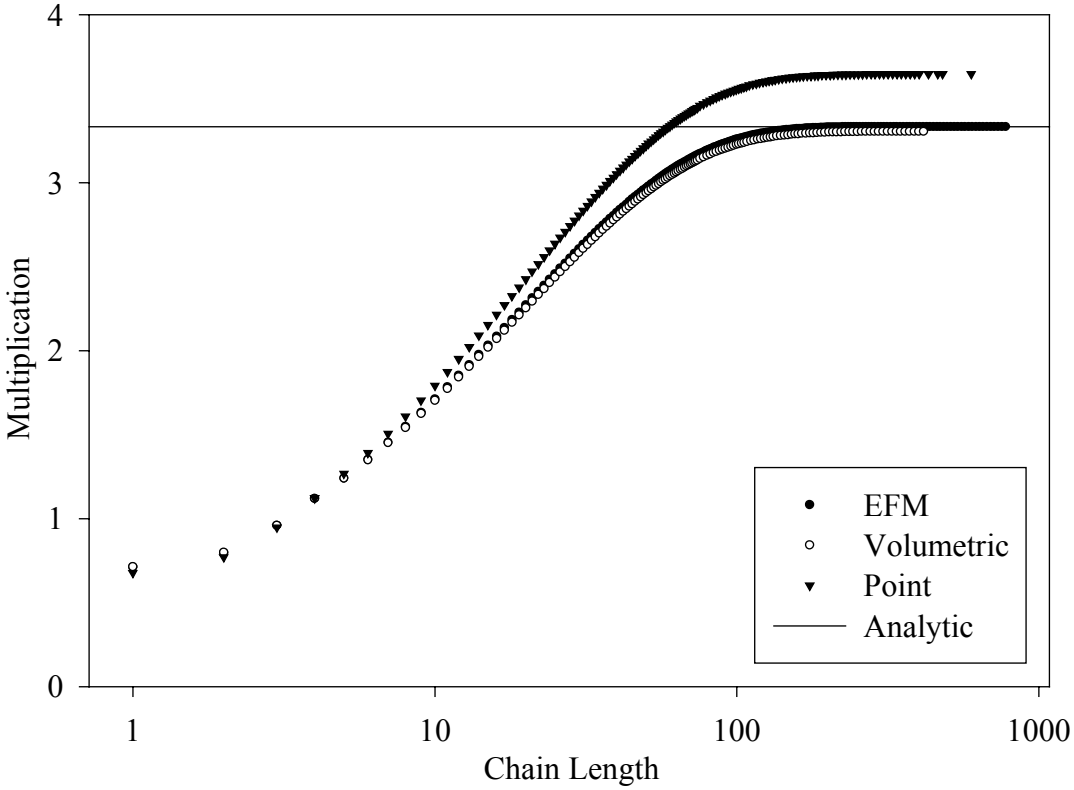

Figure 23. Source configuration effect on system subcritical prompt multiplication calculation (K=0.7).

Furthermore, it should be noted that the same is true in Figure 24 for $K=0.99$. The three asymptotic values for the subcritical prompt multiplication shown there can be used to determine the values of g^* for the both the point source and the uniform volumetric

source. As long as the actual prompt multiplication factor, *K*, is known, this technique can be used to determine g^* from the measured multiplication of the system, *M*.

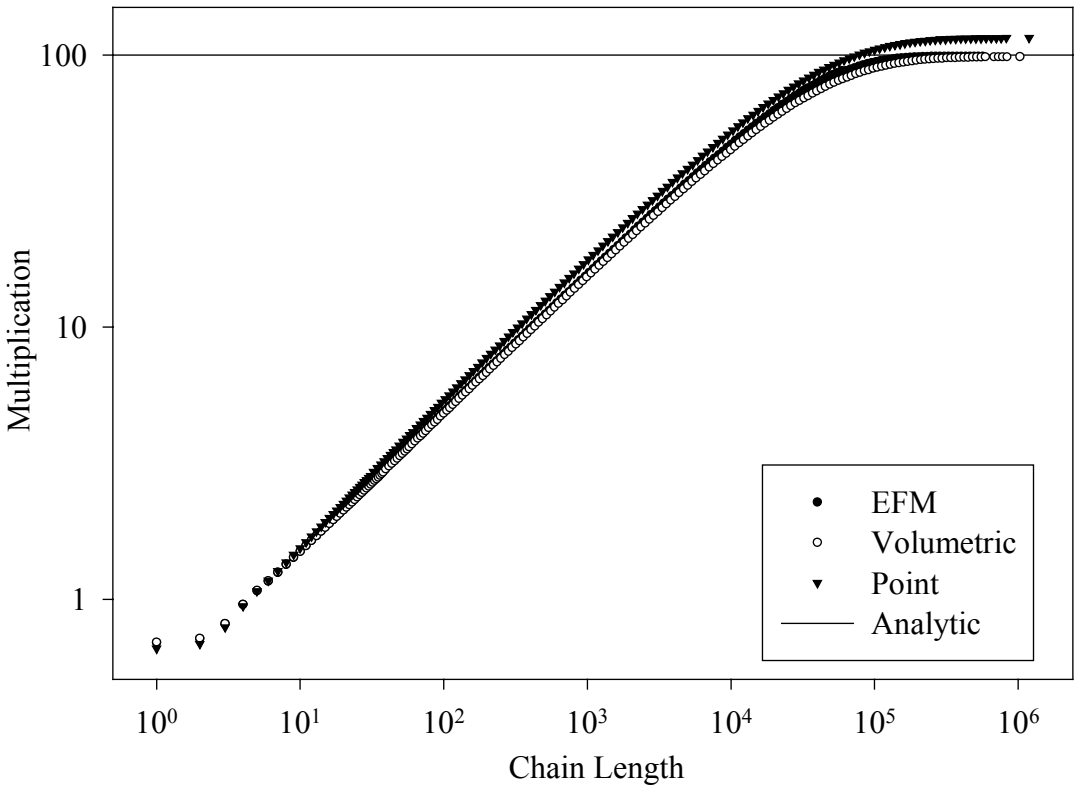

Figure 24. Source configuration effect on the system multiplication calculation (*K*=0.99).

F. Effect on Noise Analysis

As mentioned in the previous chapter, a Rossi-α analysis can provide a great deal of information about the neutronic characteristics of a multiplying system. Because the Rossi-α technique is based on the detection of correlated pairs of counts, it is of interest to determine the maximum number of correlated pairs that can be expected at a certain

value of K. This number can be readily calculated from the chain-length distribution as follows.

$$\text{Num Pairs} = \sum_{i=0}^{NumBins} P_i \cdot \frac{1}{2} L_i \left(L_i - 1 \right) \cdot BinWidth_i \tag{IV.2}$$

Figure 25 shows the integral contribution of different chain lengths to the total number of correlated of pairs for several values of K. The maximum value of attained by each curve corresponds to the actual number of pairs expected per source neutron. However, when performing a Rossi-α experiment, the quantity measured is the number of correlated pairs per neutron population. Consequently, the expected number of pairs is higher than the value from Eq. (IV.2) by a factor of M_p. Further, if one takes the asymptotic value for the number of correlated pairs shown in Figure 25 and multiplies this by the effective source rate driving the system (i.e. the fixed source plus the delayed neutron source), the maximum number of correlated pairs expected per second can be obtained. Similarly to the previous results, it is observed that the contribution from the longest chain lengths is minimal due to their low probability of occurrence.

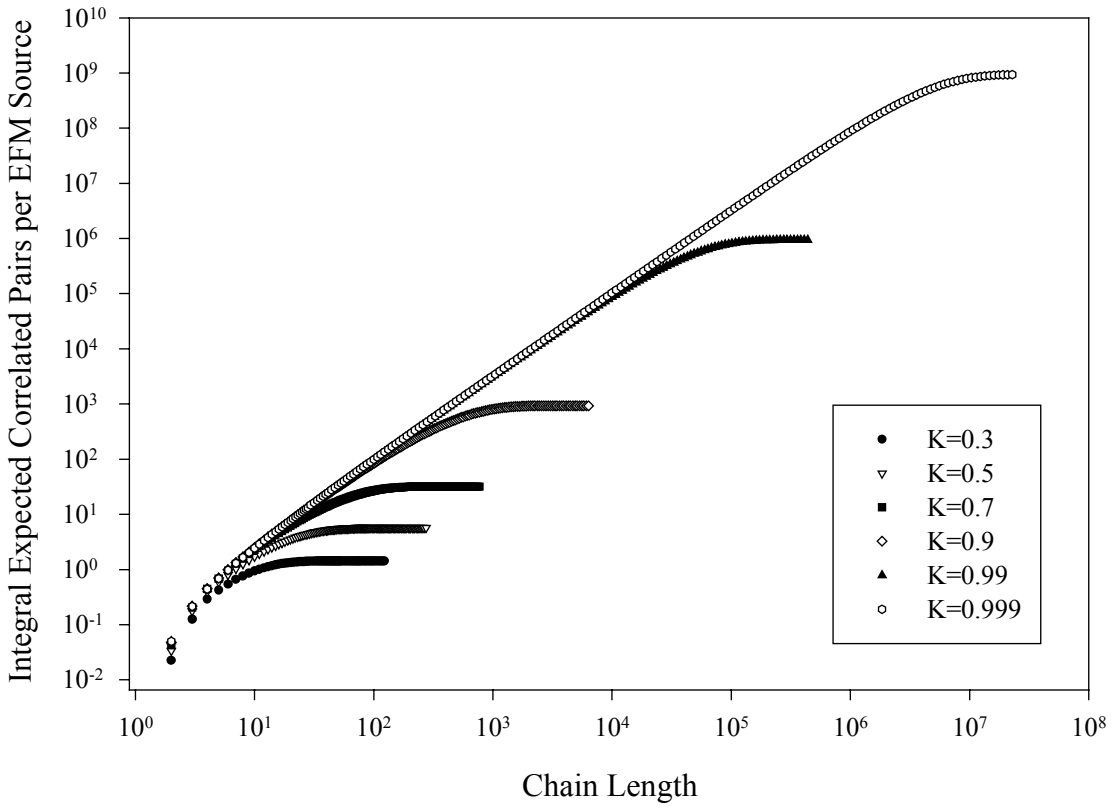

Figure 25. Theoretical maximum number of correlated pairs of neutrons per source neutron from an EFM source.

Because the plots shown in Figure 25 were generated with a numerical simulation, several factors are not accounted for that would affect an actual experimental measurement. When *Chain* and *MC++* tally the neutrons that appear in each chain, the neutrons are counted regardless of their final location, energy, or type of terminating event. In practice, detectors are generally more sensitive to certain types of events or to prescribed energy ranges and their responses are always affected by their location relative to the configuration of the neutron multiplying system. From an experimental

viewpoint, it is always desirable to use a detection system that does not significantly alter the fundamental parameters that are to be measured. For example, placing a plastic scintillation detector in the middle of a small, fast reactor, such as Godiva, would probably result in a significant change in the neutron lifetime. Hence, a measured lifetime obtained by a Rossi-α measurement would not be characteristic of the lifetime in the same system without the detector. Therefore, experiments should be designed and executed in ways that do not unduly influence the natural evolution of fission chain propagation.

Although it is feasible to locate a detector such that it does not induce an unwanted perturbation in the chain-length distribution, location and other factors invariably affect the detector's overall efficiency, which is the efficiency that appears in the analysis equations. These efficiency considerations affect the portion of the fission chain events in the neutron multiplying system that are sampled. Even under the best of circumstances, efficiency considerations must be dealt with for real systems along with their potentially drastic effects on the values derived from a neutron noise analysis. To demonstrate this necessity, the *Chain* code's estimate for the number of correlated pairs per source neutron can be considered again this time when certain events are ignored. The number of expected pairs drops significantly simply by limiting the detector's sensitivity to those neutrons that leak or are parasitically absorbed (~40%). In the real world, a large loss in the number of detectable pulses might need to be offset in some manner such as by using more detectors.

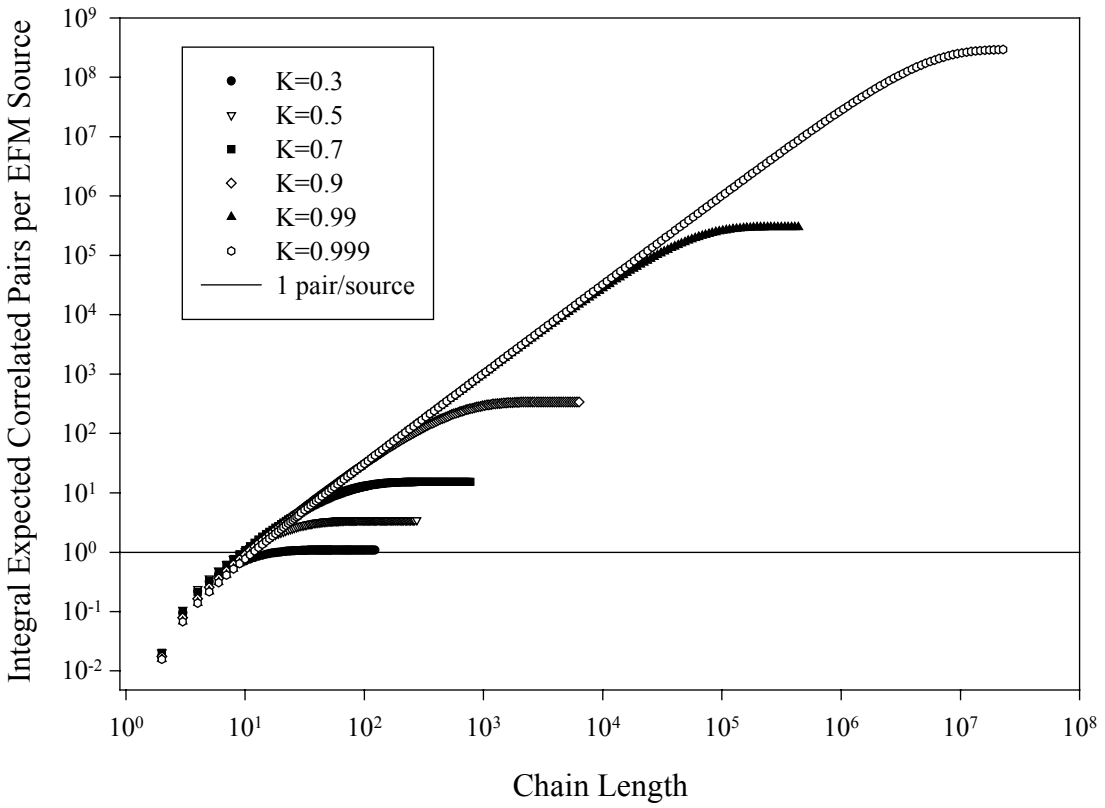

Figure 26. Expected number of correlated pairs from a capture detector with an efficiency of 100% for various *K*.

The horizontal line in Figure 26 shows the level at which the total number of correlated pairs produced per source neutron is less than 1.0. This level is also shown in Figure 27 with the detector efficiency taken into account. In making Figure 27, the efficiency has been arbitrarily set to 10%, and this value reduces the number of expected correlated pairs by a factor of 100. This sensitivity to the detector efficiency arises because the chain length is squared in Eq. (IV.2). Even with these considerations, it is

clear that the higher *K* values will still provide a substantial number of correlated pairs per source neutron.

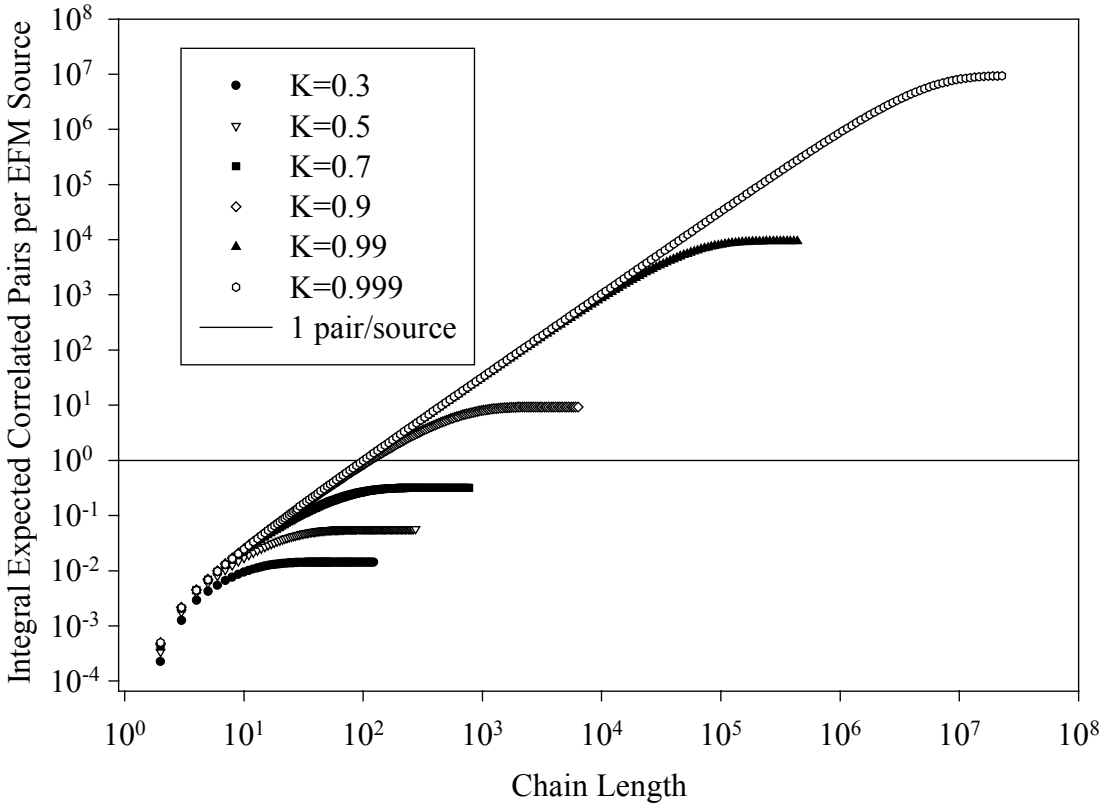

Figure 27. Expected number correlated pairs using a capture detector with an efficiency of 10% for various *K*.

Experience has shown that the decay curve obtained during a Rossi-α experiment cannot be sufficiently resolved without a large number of correlated pulses. The exact number needed is unique to each experiment because it depends on the magnitudes of both α and the background noise. In general, the optimal number of correlated pulses is quite large-being on the order of 10^9. Obviously, for low values of *K*, it would take a

substantial number of source neutrons to produce enough pairs to provide a statistically reliable Rossi-α curve. If the neutron source is relatively weak, the experiment could require a considerable amount of counting time. Although a strong source reduces the counting time required, the allowed strength is limited by the reactor noise threshold.[16]

G. Chain Time Dependence

The reactor noise threshold is essentially a measure of the counting equipment's ability to distinguish between successive prompt fission chains. As such, another factor that influences this value is the average duration of a fission chain. If the average duration is longer than the average time between emission of the source neutrons, a significant fraction of the chains will overlap. The overlapping is particularly problematic for those chains that are longer than the average. As mentioned in Chapter II, the overlapping will appear as an increase in the uncorrelated background. Avoiding this increase requires understanding how the average duration of a fission chain is affected by the prompt neutron lifetime and *K* and comparing the average chain duration to an estimate for the total source rate.

To explore this relationship, a series of runs were executed using *Chain* in which the average duration of the fission chains was measured while the value of the prompt neutron lifetime was increased. Even over several orders of magnitude, it is apparent that the relationship between the average duration of the fission chains and the value of the prompt neutron lifetime is linear (see Figure 28). For *K=0.3*, the average duration of the fission chains is 1.221 times larger than the prompt neutron lifetime, which means

that the average chain only has one event or two events before expiring. Consequently, the average duration of a chain is close to the prompt neutron lifetime.

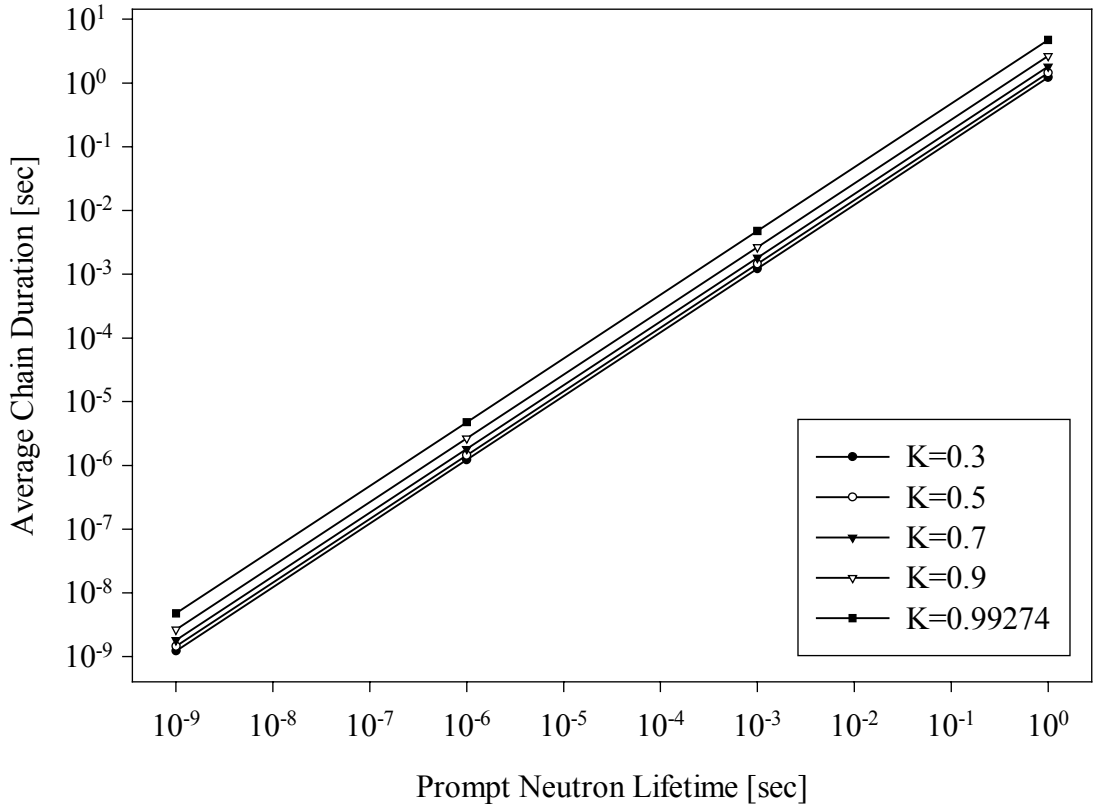

Figure 28. Average duration of a fission chain vs. prompt neutron lifetime.

In Figure 29, the ratio of the fission chain duration to the prompt neutron lifetime is shown for a range of *K*. As *K* increases, the average chain length also increases which results in a longer duration in comparison to the lifetime. Obviously, the most important quantity is the average number of events per chain since this number roughly corresponds to the number of lifetimes involved.

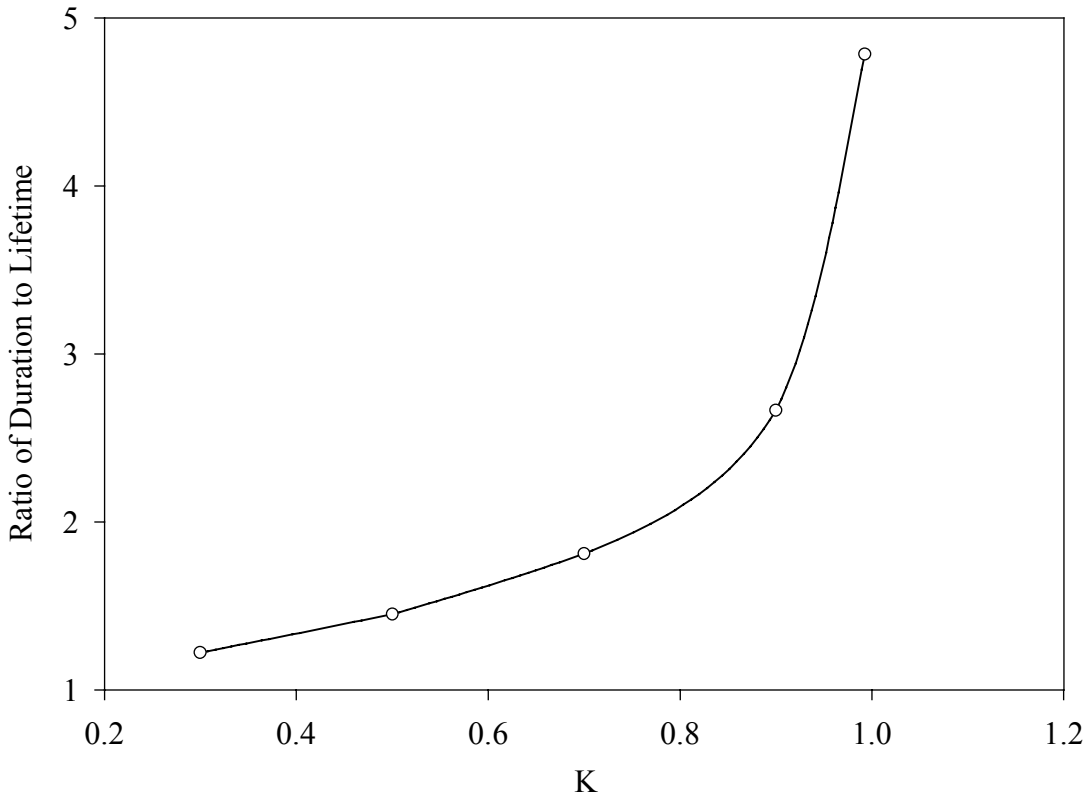

Figure 29. Ratio of fission chain duration to the prompt neutron lifetime vs. *K*.

H. Time Analysis of the Prompt Fission Chains

Besides providing the capability to generate accurate chain-length distributions for any combination of multiplication factors and source configurations, *Chain* and *MC++* can also analyze the time dependence of the fission chains using a variety of neutron noise analysis techniques. In particular, *MC++* with its spatial dependence can be used to simulate actual noise experiments, thus providing a new tool to interpret experimental results. As a demonstration of this capability, *MC++* has been used to model an infinite slab reactor fueled with enriched uranium. Both a bare reactor case

and a reflected reactor case were investigated. The inclusion of the reflected reactor was prompted by the work of Brunson et al., who observed two prompt decay modes in reflected reactors using the Rossi-α technique.[66-68] The neutron source configuration for the two cases was taken to be a point source located at the centerline of the reactor. Figure 30 shows the bare system for which K was computed to be 0.89302 ± 0.00057 using a 30-energy group cross-section set. The enrichment and slab thickness were chosen such that K would remain less than 1.0 even when a water reflector was added. Because the system is bare, all of the neutrons that leak from the slab enter the surrounding void and cannot return to the reactor.

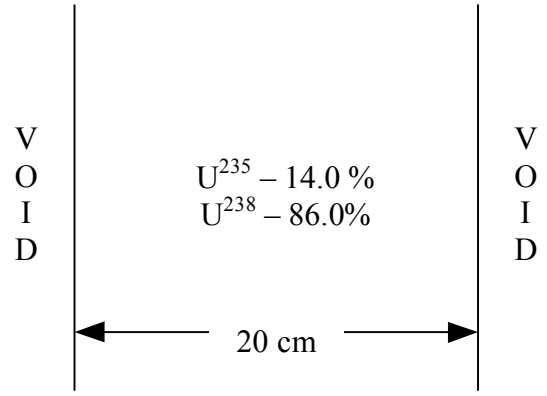

Figure 30. Bare, enriched uranium slab reactor.

The Rossi-α curve that appears in Figure 31 was generated using *MC++* by analyzing $2.0 \cdot 10^7$ prompt fission chains. Although there are some variations due to statistical uncertainties, the plot shows that the system has a single α value. The

measured α corresponds to a prompt neutron lifetime of ~30 nanoseconds which is reasonable for a thin, fast system.

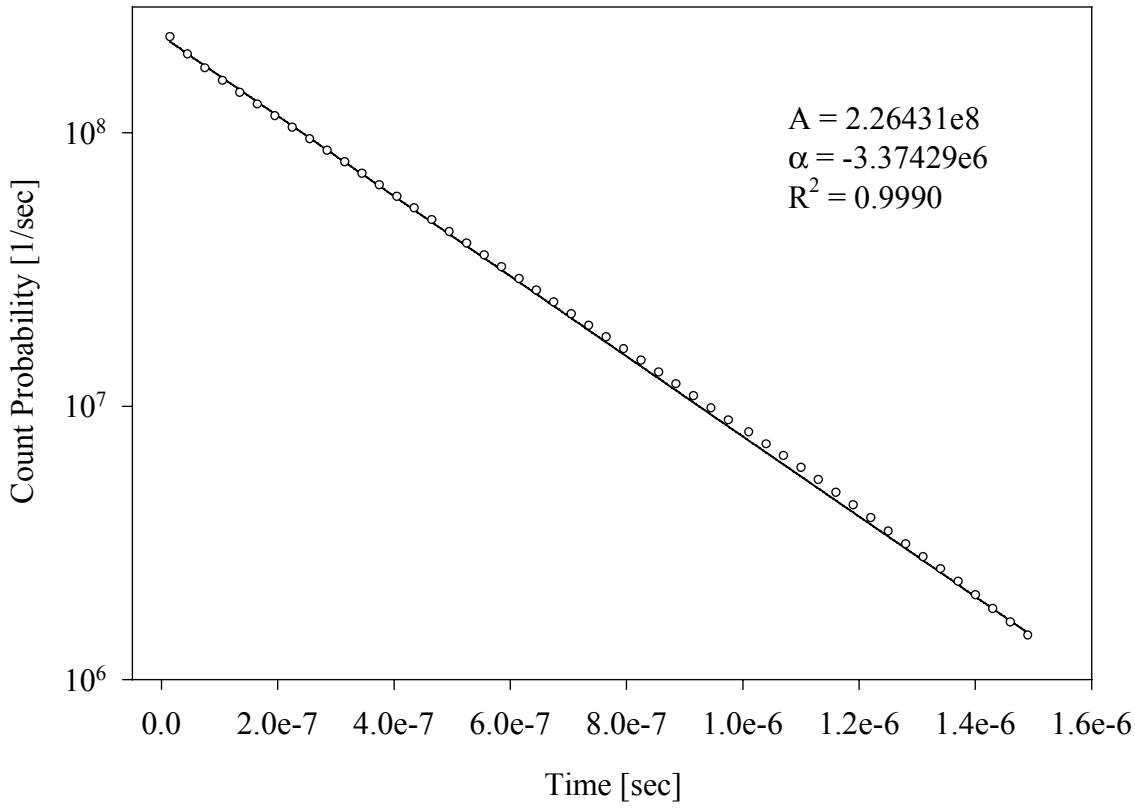

Figure 31. Results for a simulated Rossi-α measurement performed on a bare enriched uranium slab.

In the reflected reactor case, some neutrons re-enter the reactor due to scattering events occurring in a 2.5 cm thick water region on either side of the reactor (see Figure 32). The reflector increases the prompt neutron multiplication factor to K=0.96955 ± 0.00082. Although the addition of the reflectors produces only a modest increase in K,

the effect on the Rossi-α curve is quite significant (see Figure 33). This plot indicates that the fission chains are actually propagating according to two separate time constants. The larger α corresponds to neutrons that are born and then die within the fuel region without having leaked into the reflector regions. The smaller α corresponds to those neutrons that have leaked into the reflector, undergone several collisions, and then returned to the core region to continue propagating their respective fission chains.

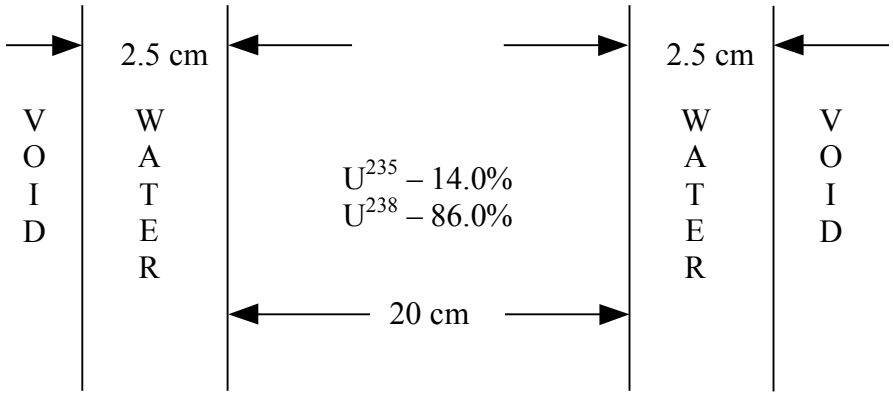

Figure 32. Enriched uranium reactor with water reflector.

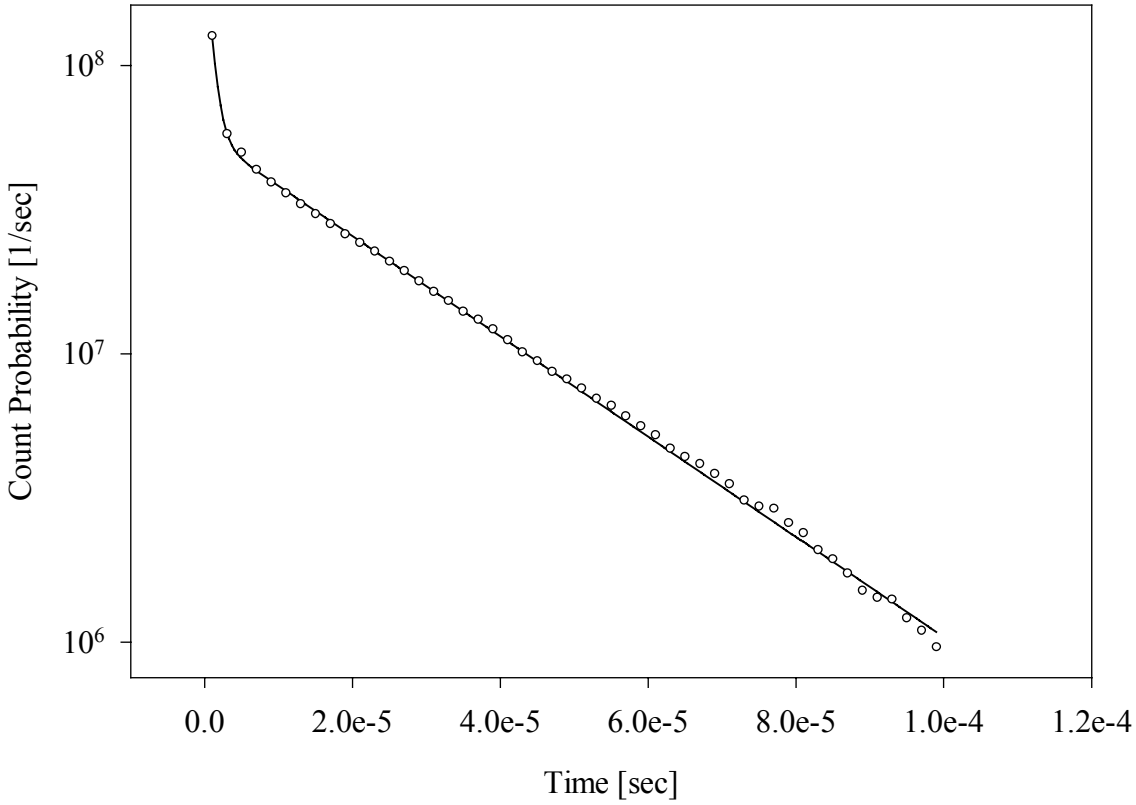

Figure 33. Dual decay mode Rossi-α curve in reflected slab reactor.

The data plotted in Figure 33 can be represented using two exponential terms. The highly curved portion of the plot is shown in more detail in Figure 34. This data is identical to the former except that the channel width has been decreased by a third. The parameters appear in Table VIII.

$$y = A_1 e^{-\alpha_1 t} + A_2 e^{-\alpha_2 t} \qquad \text{(IV.3)}$$

TABLE VIII

Parameters for dual Rossi-α curve fit.

Exponential		**Term 1**	**Term 2**	**R^2**
Dual	A	$2.1667 \cdot 10^8$	$5.7001 \cdot 10^7$	0.999563
	α	$-1.1015 \cdot 10^6$	$-4.0012 \cdot 10^4$	

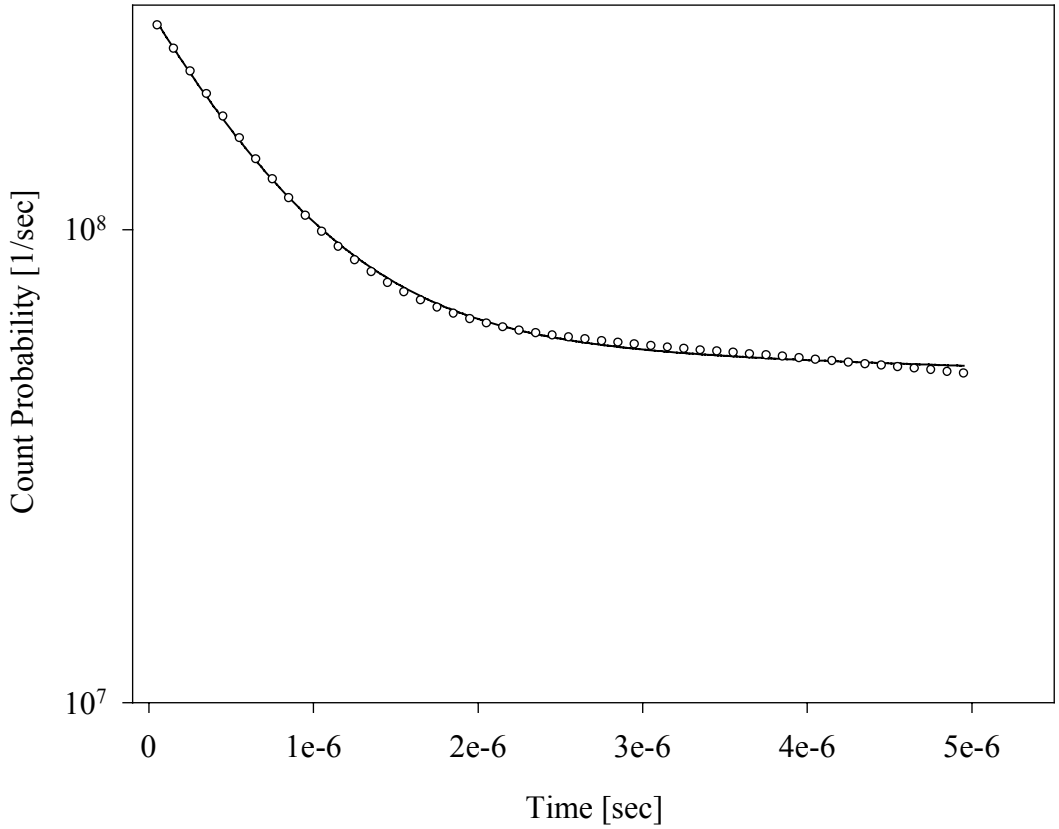

Figure 34. Expanded view of Rossi-α curvature.

I. Spatial Harmonics

Analytic solutions predict that there are an infinite number of α's associated with any given configuration of a multiplying system. However, when the system is very

near delayed critical, the fundamental mode completely dominates the solution, giving the impression that there is only one decay mode. However, as the system becomes increasingly subcritical, other harmonics can be resolved that have their own unique prompt decay modes.[69] For example, if the enriched uranium fuel in the slab reactor shown in Figure 30 is exchanged for natural uranium, K drops to 0.67603 ± 0.00071. Then, as a Rossi-α simulation with *MC++* reveals in Figure 35, other modes become observable.

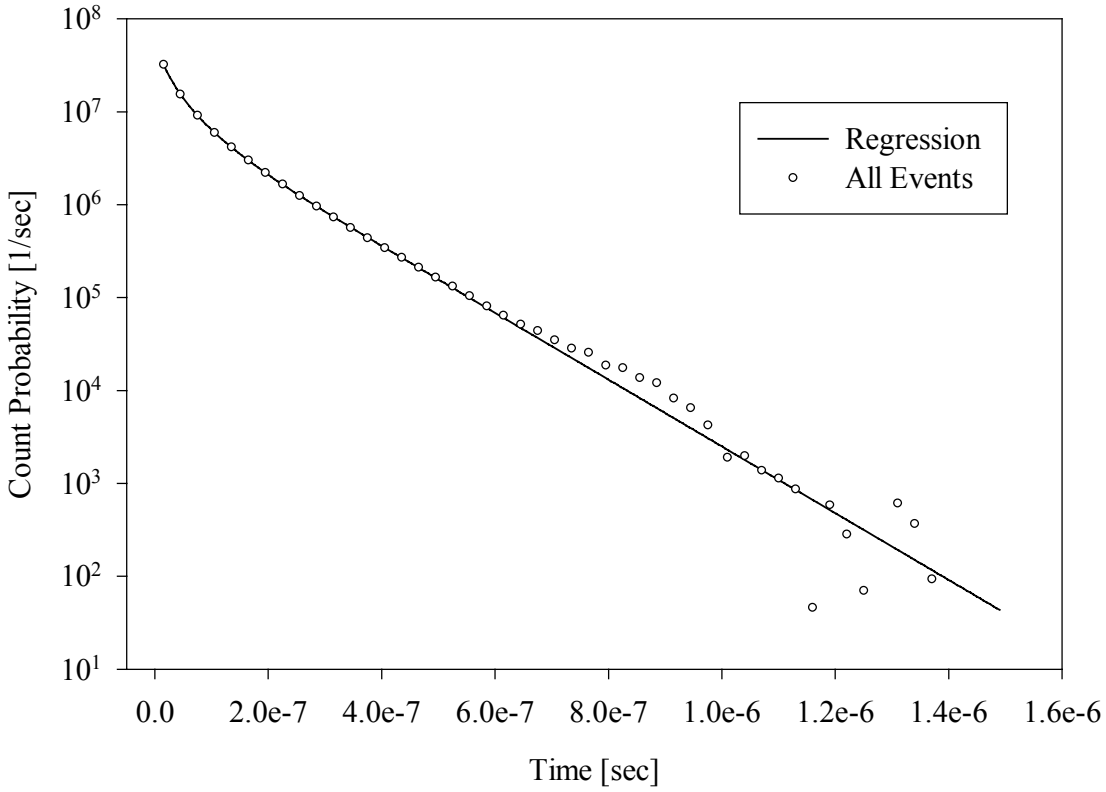

Figure 35. Spatial harmonics appearing in bare slab geometry.

A regression analysis performed on these data suggested that 3 exponential terms are necessary to fit the data. The results appear in Table IX.

$$y = A_1 e^{-\alpha_1 t} + A_2 e^{-\alpha_2 t} + A_3 e^{-\alpha_3 t} \qquad \text{(IV.4)}$$

TABLE IX

Parameters for regression fit of harmonic data.

	Term 1	**Term 2**	**Term 3**	**R^2**
A	2.4621×10^7	1.8068×10^7	9.7697×10^6	0.99999911
α	5.6386×10^7	2.18658×10^7	8.2731×10^6	

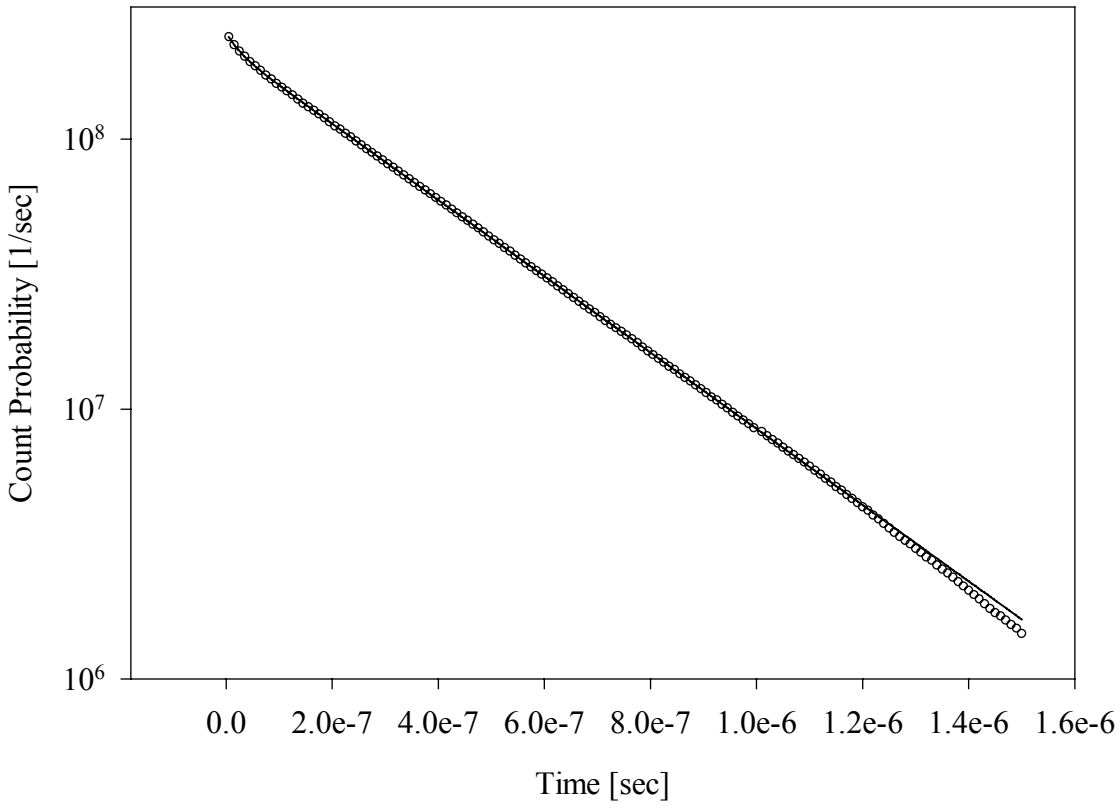

Figure 36. Bare slab with enriched uranium showing harmonics

Harmonics can also be resolved in systems with relatively high values of K. As proof, a Rossi-α experiment has been simulated using the enriched uranium slab. The results are plotted in Figure 36. The significance of this figure is the slight curvature of the data points associated with the shortest bin widths. To verify whether the curve can be attributed to the presence of another decay constant, the data were fit with single and double exponential curves. The results of these fits are presented in Table X. Note that the α's and the amplitudes of the dual-exponential terms differ by an order of

magnitude. The short-lived α term dies out at a faster rate, and it starts at a level that is $1/10^{th}$ the level of the long-lived term. Consequently, the short-lived α is barely noticeable at this *K*, and one obtains a reasonable fit with the single-exponential curve.

TABLE X

Parameters for dual exponential regression fit of bare enriched slab.

Exponential		**Term 1**	**Term 2**	**R^2**
Single	A	$3.3083 \cdot 10^6$	none	0.999753
	α	$-2.2556 \cdot 10^8$	none	
Double	A	$2.9478 \cdot 10^7$	$2.1889 \cdot 10^8$	0.9999898
	α	$-3.9893 \cdot 10^7$	$-3.2535 \cdot 10^6$	

J. Overall Detection Efficiency Considerations

Earlier in this chapter, the maximum expected number of correlated pairs that could be obtained from a given chain-length distribution was calculated. In that calculation, it was assumed that all of the neutrons in every chain could be counted. This assumption is equivalent to modeling detectors that are 100% efficient because the detectors "see" every event in the reactor regardless of event type or location. In reality, it is impossible conduct an experiment with so much sampling. Real neutron detectors are finite in size and are often most sensitive to particular types of events in certain (neutron) energy ranges. As such, their signal only represents a tiny fraction of the total events taking place in the reactor. Factoring in the impact of real detector use, the sampling efficiency for detector systems used in actual reactor noise experiments rarely

exceeds 10^{-4}. Fortunately, this sampling efficiency is adequate for a Rossi-α measurement when the system is operating near delayed critical. In highly subcritical systems, however, low detector efficiencies may preclude any type of analysis within a reasonable counting time. The Rossi-α curves in this section were computed by *MC++* for the natural uranium slab reactor described in the previous section. Table XI shows the effects on the estimate of the fastest decay mode as the detector becomes less sensitive to certain event types. As the sensitivity decreases, the intercept of the curve drops as the amount of data under the curve decreases (see Figure 37). This decrease should be expected because the coefficient of the Rossi-α equation is directly proportional to the detector efficiency. However, the difference no longer appears to be constant when the leakage neutrons alone are available for sampling.

TABLE XI

Detector efficiency effect on fastest decay mode estimate.

	Fission + Loss	**Loss**	**Leakage only**
A	2.447×10^{7}	1.287×10^{7}	1.291×10^{6}
α	5.665×10^{7}	4.473×10^{7}	5.769×10^{6}
R^2	0.99999916	0.99999933	0.99999928

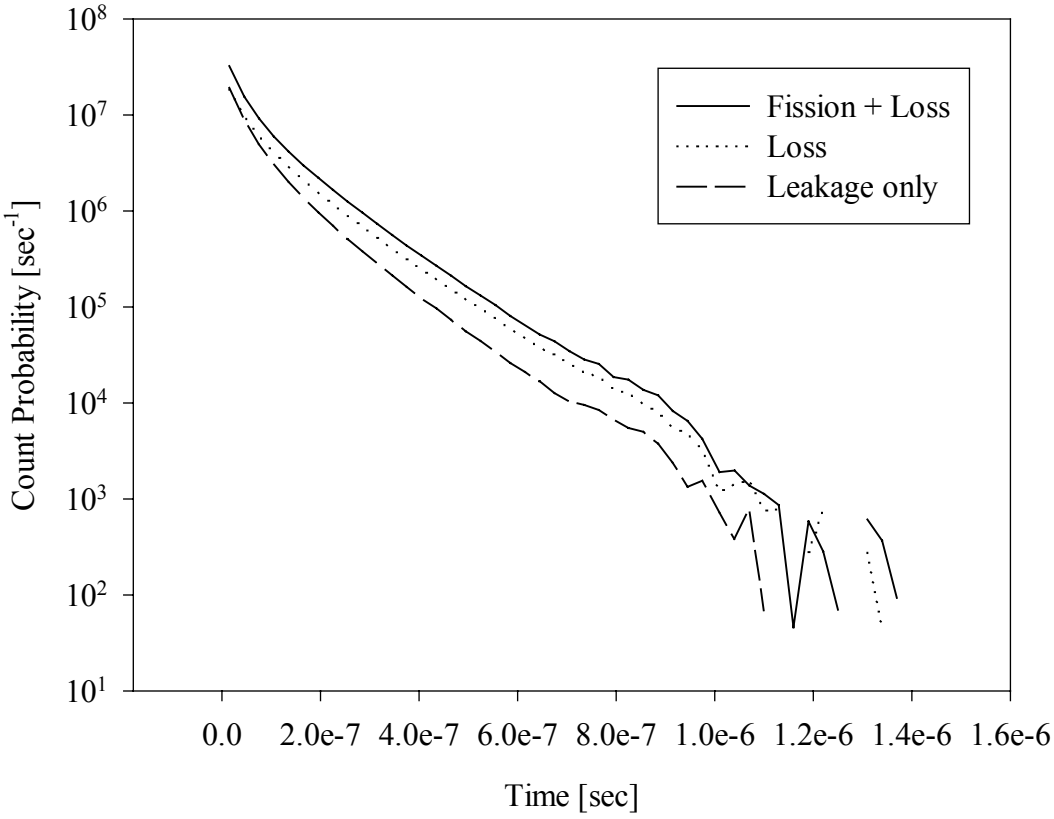

Figure 37. Effect of population type sampled on Rossi-α data.

Figure 38 shows the predicted response of a family of leakage detectors with different detector efficiencies. Leakage detectors (ex-core detector) were selected for simulation since they have the least impact on the natural fission chain propagation. The only difference between the α curves is the amount of data analyzed. The number of neutrons entering the detector is identical, as is the simulated duration of the experiment. It is clear that the detector with the highest efficiency, which captures every leaking neutron, produces the smoothest curve. As the efficiency drops to a more realistic value of 10^{-4},

only one data point appears on the chart as being significantly above the background noise. While the inefficiency of the detector does not preclude eventually obtaining a reasonable α curve, it will take approximately 10,000 times longer to obtain the same accuracy as it would with the detector with the perfect efficiency.

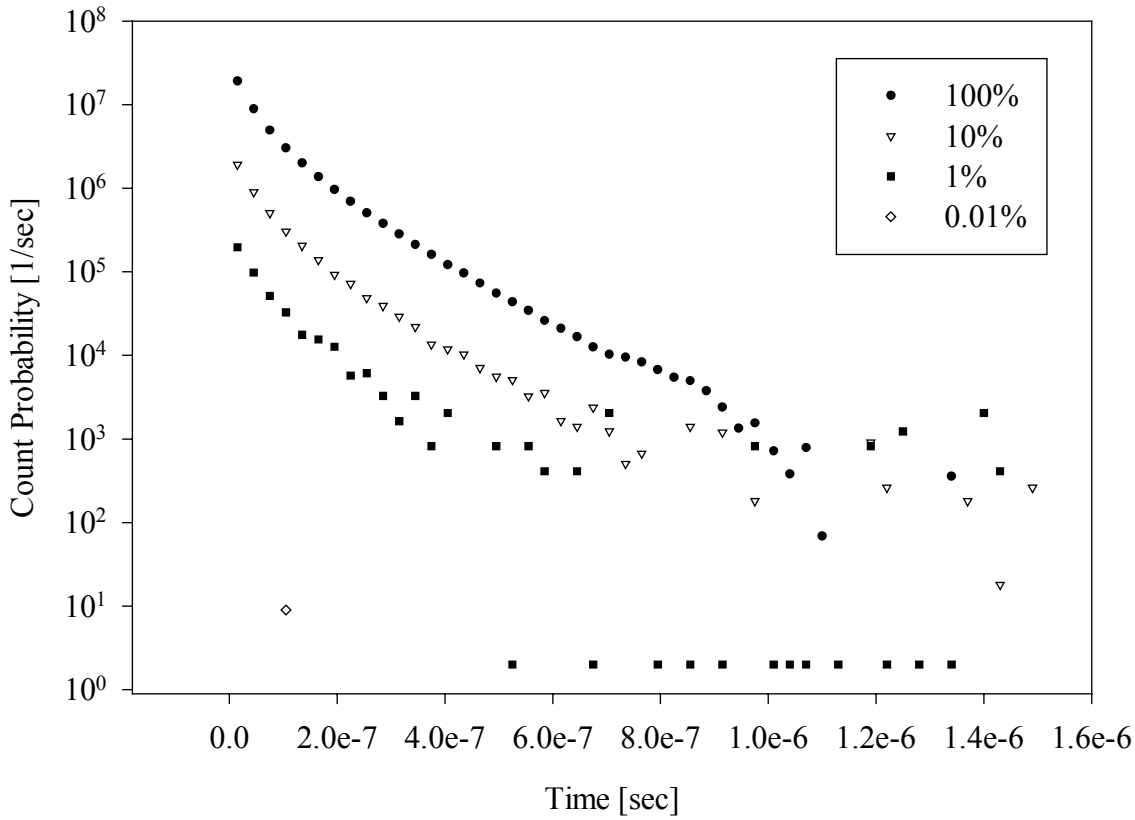

Figure 38. Signal degradation due to decreasing detector efficiency.

CHAPTER V

CONCLUSIONS

A. Summary

Two codes, *MC++* and *Chain*, have been developed that use analog Monte Carlo techniques to simulate the spawning and propagation of fission chains. The codes simulate the stochastic nature of fission chain formation with sufficient detail to provide accurate chain-length distributions. The codes also provide a means for simulating a variety of reactor configurations, source distributions, and detector types with efficiencies. Both codes perform a variety of neutron noise analyses ranging from a straightforward pulse-neutron die-away simulation to the time-series analysis of the Rossi-α technique, and as such, provide a new means for simulating and re-examining previous neutron noise experiments.

From basic theory and the use of these codes, it has been shown that neutron noise analysis techniques are sensitive to the value of the average chain length for a system. Depending on K, the average chain length determines the average number of correlated pairs expected from a source neutron. While the noise signal arising from systems with very low values of K can generally be simulated in a computer environment, the number of source neutrons tracked must be very large to produce a sufficient number of correlated pulses. In similar, real-world systems, it was shown that measurements could require prohibitively long counting times depending on the source rate. As *MC++* demonstrates, the neutron source rate can only be increased until the fission chains begin overlapping. If a detector with a low efficiency is used, the

probability of detecting several neutrons from the same fission chain is significantly reduced. The loss of information must be compensated for with even longer counting times to observe a sufficient number of correlated counts.

In addition to being a function of *K*, it has been shown that the chain-length distribution is also sensitive to the type of multiplicity distribution employed in the simulation and to the properties of the fixed neutron source that drives the problem.

The relationship, $M_p = \overline{L}$, provides an effective means for validating the average chain length calculated with computer codes. Furthermore, it has been shown how this value can be used to find the value of g^* for a multiplying system. Finally, it has been demonstrated that the coefficient that appears in many time-series techniques is directly related to the chain-length distribution through the relationship,

$$\frac{\overline{\nu}\,\Gamma}{2}\left(\frac{1}{1-K}\right)\left(\frac{K}{1-K}\right) = \frac{\sum_{L=1}^{\infty}\frac{L(L-1)}{2}P(L)}{\sum_{L=1}^{\infty}L\cdot P(L)} \quad .$$

B. Future Work

MC++ can provide a means for studying topics that were beyond the scope of this work. Specifically, *MC++* could be used to study spatial-dependent reactor kinetics. A major goal of this effort would be to fully describe the phenomena, which produce the multiple decay modes observed in multi-region systems. Transport models could then be developed to determine the multiple decay constants in terms of more fundamental quantities, such as the neutron lifetimes in the various regions.

Chain, because of its ability to determine the asymptotic behavior of the chain-length distributions, could also have a role in future investigations. Due to its ability to run a much larger number of neutrons in a simulation, this code provides an excellent means for exploring the low-probability portion of the chain-length distribution. Currently, it is not clear whether there exists an absolute maximum chain length for a specified K and $\bar{\nu}$, but there is a definite $\bar{L}$ which approaches infinity as $K \rightarrow 1.0$. What appears more likely is that the tail approaches some asymptotic value that is itself a function of the two parameters.

Both codes would also be useful for evaluating the limitations of existing neutron noise techniques and for developing newer ones that might be better suited to particular applications. Although only a handful of noise analysis techniques have been programmed into the two codes, others could be added in the future. This capability would be most beneficial in studying the sensitivity of various noise analysis techniques to factors like detector dead-time, efficiency, location, etc. Future work should also include a more detailed simulation of the delayed neutron contribution.

Although the current analog Monte Carlo technique used to simulate the prompt fission chains produces realistic results, it greatly reduces the runtime efficiency of the two codes. One way to improve the computational efficiency might be to employ variance reduction techniques such as those employed in other Monte Carlo packages. While implementation of these would require only a modest coding effort, the drawback is that these techniques must not interfere with the truly stochastic nature of the fission chain propagation process. For any variance reduction method applied, it must be

determined whether its reduction of the statistical uncertainty warrants the increased computational time and loss of fidelity in the physical model.

REFERENCES

1. V. L. PUTMAN, "30 September 1999 Criticality Accident, Summary to Date (991130)," INEEL/MIS-1999-1139 update, Idaho National Engineering and Environmental Laboratory (1999).

2. J. THIE, *Power Reactor Noise*, American Nuclear Society, La Grange Park, Illinois (1981).

3. M. M. R. WILLIAMS, *Random Processes in Nuclear Reactors*, Pergamon Press, New York (1974).

4. F. DE HOFFMANN, "Statistical Fluctuations in the Water Boiler and the Dispersion of Neutrons Exited Per Fission," LA-101, Los Alamos Scientific Laboratory (1944).

5. F. DE HOFFMANN, "Intensity Fluctuations of a Neutron Chain Reactor," LA-256, Los Alamos Scientific Laboratory (1944).

6. R. FEYNMAN, "Statistical Behavior of Neutron Chains," LA-591, Los Alamos Scientific Laboratory (1946).

7. F. DE HOFFMANN, *The Science and Engineering of Nuclear Power*, Vol. **II**, pp. 103-109, Addison Wesley Press, Cambridge, Mass. (1949).

8. J. D. ORNDOFF, "Prompt Neutron Periods of Metal Critical Assemblies," *Nucl. Sci. Eng.*, **2**, 450 (1957).

9. E. D. COURANT and P. R. WALLACE, "Fluctuations of the Number of Neutrons in a Pile," *Physical Review*, **72**, 1038 (1947).

10. C. E. COHN, "A Simplified Theory of Pile Noise," *Nucl. Sci. Eng.*, **7**, 472 (1960).

11. W. MATTHES, "Statistical Fluctuations and Their Correlation in Reactor Neutron Distributions," *Nukleonik*, **4**, 213 (1962).

12. G. I. BELL, "Probability Distribution of Neutrons and Precursors in a Multiplying Assembly," *Ann. of Phys.*, **21**, 243 (1963).

13. D. R. HARRIS, "Neutron Fluctuations in a Reactor of Finite Size," *Nucl. Sci. Eng.*, **21**, 369 (1965).

14. H. BORGWALDT and D. STEGMANN, "A Common Theory for Neutronic Noise Analysis Experiments in Nuclear Reactors," *Nukleonik*, **7**, 313 (1965).

15. R. A. RYDIN, J. A. BURKE, W. E. MOORE, and K. W. SEEMANN, "Noise and Transient Kinetics Experiments and Calculations for Loosely Coupled Cores," *Nucl. Sci. Eng.*, **46**, 179 (1971).

16. G. SPRIGGS, "The Reactor Noise Threshold," *Nucl. Sci. Eng.*, **116**, 67 (1994).

17. J. MIHALCZO, V. PARE, and E. BLAKEMAN, "Fission Chain Length Effects on Californium-Source-Driven Subcriticality Measurements," International Conference on Advances in Mathematics, Computation, and Reactor Physics, American Nuclear Society, Pittsburgh, Pennsylvania, April 28 (1991).

18. J. MIHALCZO, E. BLAKEMAN, V. PARE, T. VALENTINE, and D. AUSLANDER, "Subcriticality of Two Uranyl Nitrate Flat Cylindrical Tanks Spaced in Air by ^{252}Cf-Source-Driven Noise Analysis," *Nucl. Tech.*, **103**, 346 (1993).

19. R. FEYNMAN, F. DE HOFFMANN, and R. SERBER, "Dispersion of the Neutron Emission in U-235 Fission," *J. Nucl. Energy*, **3**, 64 (1956).

20. R. B. LEACHMAN, "Emission of Prompt Neutrons from Fission," *Physical Review*, **101**, 1005 (1956).

21. B. C. DIVEN, H. C. MARTIN, R. F. TASCHEK, and J. TERRELL, "Multiplicities of Fission Neutrons," *Physical Review*, **101**, 1012 (1956).

22. J. TERRELL, "Distributions of Fission Neutron Numbers," *Physical Review*, **108**, 783 (1957).

23. J. TERRELL, "Fission Neutron Spectra and Nuclear Temperatures," *Physical Review*, **113**, *2*, 527 (1958).

24. J. TERRELL, "Neutron Yields from Individual Fission Fragments," *Physical Review*, **127**, 880 (1962).

25. N. E. HOLDEN and M. S. ZUCKER, "Prompt Neutron Multiplicities for the Transplutonium Nuclides," BNL-NCS-36379, International Conference on Nuclear Data for Basic and Applied Science, Santa Fe, NM (1985).

26. J. W. BOLDMAN and M. G. HINES, "Prompt Neutron Emission Probabilities Following Spontaneous and Thermal Neutron Fission," *Nucl. Sci. Eng.*, **91**, 114 (1985).

27. J. FREHAUT, "Neutron Multiplicity Distribution in Fast Neutron-Induced Fission," IAEA Consultants Meeting on Physics of Neutron Emission in Fission, May 1988, Mito, Japan (1989).

28. D. HAWKINS and S. ULAM, "Theory of Multiplicative Process, I," LA-171, Los Alamos Scientific Laboratory (1944).

29. G. E. HANSEN, "Assembly of Fissionable Material in the Presence of a Weak Neutron Source," *Nucl. Sci. Eng.*, **8**, 709 (1960).

30. H. HURWITZ, JR., "Kinetics of Low Source Reactor Startups. Part I," *Nucl. Sci. Eng.*, **15**, 166 (1963).

31. H. HURWITZ, JR., "Kinetics of Low Source Reactor Startups. Part II," *Nucl. Sci. Eng.*, **15**, 166 (1963).

32. G. I. BELL, "On the Stochastic Theory of Neutron Transport," *Nucl. Sci. Eng.*, **21**, 369 (1965).

33. G. A. CAMPBELL, V. CHAN, and J. D. LEWINS, "An Exact Special Case Solution of the Neutron Stochastic Equations at Low Power," *Ann. Nucl. Energy*, **8**, 1 (1981).

34. F. C. DIFILIPPO, "Stochastic Processes in a Subcritical Nuclear Reactor in the Presence of a Fission Source," *Nucl. Sci. Eng.*, **90**, 13 (1985).

35. J. D. LEWINS and G. T. PARKS, "An Exact Transient Stochastic Solution for Low-Power Neutron Multiplication," *Ann. Nucl. Energy*, **12**, 65 (1985).

36. L. RUBY and T. L. MCSWINE, "Approximate Solution to the Kolmogorov Equation for a Fission Chain-Reacting System," *Nucl. Sci. Eng.*, **94**, 271 (1986).

37. J. MUNOZ-COBO, R. B. PEREZ, and G. VERDU, "Stochastic Neutron Transport Theory: Neutron Counting Statistics in Nuclear Assemblies," *Nucl. Sci. Eng.*, **95**, 83 (1987).

38. R. SANCHEZ, "An Analysis of the Stochasticity of the Transport Equation," *Trans. Theory Stat. Phys.*, **26**, 469 (1997).

39. I. PAZIT, and Y. YAMANE, "Theory of Neutron Fluctuations in Source-Driven Subcritical Systems," *Nucl. Inst. Meth. in Phys. Res. Sect. A*, **403**, 431 (1998).

40. J. BRIESMEISTER ed., "MCNP-A General Monte Carlo N-Particle Transport Code, Version 4B," LA-12625-M, Version 4B Los Alamos National Laboratory (1997).

41. T. E. HARRIS, *The Theory of Branching Processes*, Dover Publications, Inc., New York (1989).

42. P. GUTTORP, *Statistical Inference for Branching Processes*, John Wiley & Sons, Inc., New York (1991).

43. T. F. WIMMETT, R. H. WHITE, W. R. STRATTON, and D. P. WOOD, "Godiva II—An Unmoderated Pulse-Irradiation Reactor," *Nucl. Sci. Eng.*, **8**, 691 (1960).

44. J. DUDERSTADT and L. HAMILTON, *Nuclear Reactor Analysis*, John Wiley & Sons, New York (1976).

45. G. SPRIGGS, "Two Rossi-α Techniques for Measuring the Effective Delayed Neutron Fraction," *Nucl. Sci. Eng.*, **113**, 161 (1993).

46. G. SPRIGGS, S. OKAJIMA, T. SAKURAI, and R. B. BUSCH, "The Equivalent Fundamental-Mode Source," LA-UR-97-1, Los Alamos National Laboratory (1997).

47. R. E. UHRIG, *Random Noise Techniques in Nuclear Reactor Systems*, Ronald Press Co., New York (1970).

48. C. P. BAKER, "Time Scale Measurements by the Rossi Method," LA-617, Los Alamos Scientific Laboratory (1947).

49. D. H. BRYCE, "Some Comments on the Rossi-α Experiment," *Nukleonik*, **7**, 428 (1965).

50. D. BABALA, "On the Theory of Rossi-Alpha Experiment in Reactor Noise Studies," *Nucl. Sci. Eng.*, **26**, 418 (1966).

51. D. BABALA, "Point-Reactor Theory of Rossi-Alpha Experiment," *Nucl. Sci. Eng.*, **28**, 237 (1967).

52. D. BABALA, "Interval Distributions in Neutron Counting Statistics," *Nucl. Sci. Eng.*, **28**, 243 (1967).

53. T. IIJIMA, "A Remark on the Rossi-α Experiment," *Nukleonik*, **10**, 93 (1967).

54. N. PACILIO, "Reactor Noise Analysis in the Time Domain," *USAEC Critical Review Series*, TID-24512 (1969).

55. T. MISAWA, H. UNESAKI, S. SHIROYA, and Y. YAMANE, "Study on Reactivity Measurement by the Feynman-α Method," PHYSOR 96: International Conference on the Physics of Reactors, 16-20 Sep., Mito, Japan, (1996).

56. G. E. HANSEN, "The Rossi Alpha Method," Workshop on Subcritical Reactivity Measurements, Aug. 1985, Albuquerque, N.M., 148, CONF-8508105 (1985).

57. S. OKAJIMA, M. NARITA, and K. KOBAYASHI, "Simple Determination of Low Power on Reflected Reactors Using the Feynman-α Experiment," *Ann. Nucl. Energy*, **14**, 673 (1987).

58. I. PAZSIT and Y. YAMANE, "The Variance-to-Mean Ratio in Subcritical Systems Driven by a Spallation Source," *Ann. Nucl. Energy*, **25**, 667 (1998).

59. S. R. LEE, "MC++: A Brief Overview of a Work in Progress," LA-MEMO XTM:96-219(U), Los Alamos National Laboratory (1996).

60. S. R. LEE, J. C. CUMMINGS, and S. D. NOLEN, "Preliminary MC++ Timing and Physics Results," *X-Division Research Notes*, XTM-RN(U)96-005, Los Alamos National Laboratory (1996).

61. S. R. LEE, J. C. CUMMINGS, and S. D. NOLEN, "MC++: Parallel, Portable, Monte Carlo Neutron Transport in C++," 8th SIAM Conference on Parallel Processing for Scientific Computing, March 14 Minneapolis, MN (1997).

62. J. MARSHALL, S. CLANCY and L. ANKENY, "Tecolote: An Object-Oriented Framework for Physics Development," European Conference for Object-Oriented Programming, Brussels, Belgium, LA-UR-98-2999, (1998).

63. J. REYNDERS, T. WILLIAMS, J. CUMMINGS, and S. HANEY, "POOMA: A Framework for Scientific Simulations on Parallel Architectures," in G. WILSON and P. LU, eds., *Parallel Programming using C++*, MIT Press, Cambridge, MA, 553 (1996).

64. J. REYNDERS, "POOMA Homepage," online: http://www.acl.lanl.gov/pooma, accessed: March 2000.

65. A. SNOOD, R. A. FORSTER, and D. K. PARSONS, "Analytical Benchmark Test Set for Criticality Code Verification," LA-13511, Los Alamos National Laboratory (1999).

66. G. S. BRUNSON, R. N. CURRAN, J. M. GASIDLO and R. J. HUBER, "Neutron Die-Away Phenomena," *Trans. Amer. Nucl. Soci.*, **6**, 56 (1963).

67. G. S. BRUNSON, R. N. CURRAN, J. M. GASIDLO and R. J. HUBER, "A Survey of Prompt-Neutron Lifetimes in Fast Critical Systems," Argonne National Laboratory, ANL-6681 (1963).

68. G. S. BRUNSON and R. J. HUBER, "Two-Region Analysis of Pulsing Data in Fast Critical Systems," *Nucl. Instr. Methods*, **128**, 379 (1975).

69. T. IIJIMA, T. SUGI, H. EZURE, and M. KASAI, "Space-Dependent Effects in Rossi-Alpha Experiments," *Nucl. Sci. Eng.*, **33**, 344 (1968).

VITA

Steven Douglas Nolen was [redacted] He earned a B.S. in Nuclear Engineering at Texas A&M University in 1994. In December of 1997, he earned a M.S. in Nuclear Engineering. During this time, he began his association with Los Alamos National Laboratory's X-Division which has culminated in the work presented herein. He is currently a post-doctoral researcher at the laboratory. His mailing address in 1990 40th St. Los Alamos, New Mexico 87544.

Los Alamos
NATIONAL LABORATORY
Los Alamos, New Mexico 87545